A STUDY OF SEGMENTED ELECTRODE BOUNDARY LAYERS IN MHD GENERATORS

A THESIS

Presented to

The Faculty of the Graduate Division

by

Samuel Viron Shelton

In Partial Fulfillment

of the Requirements for the Degree

Doctor of Philosophy

in the School of Mechanical Engineering

Georgia Institute of Technology

April, 1969

A STUDY OF SEGMENTED ELECTRODE

BOUNDARY LAYERS IN MHD GENERATORS

Approved:

Chairman

Date approved by Chairman:

30 May 1969

To Sharon

Suzanne and Stacy

ACKNOWLEDGMENTS

The author is indebted to many people who have assisted him both directly and indirectly in preparation for and execution of this work. Among these are his parents who must be acknowledged for their immeasurable love, training, and sacrifice. The understanding and love provided by his wife have also been most generous and appreciated.

Particular gratitude is expressed for the time, encouragement, and professional guidance given by the faculty advisor, Dr. W. O. Carlson. Drs. E. W. McDaniel and J. C. Wu are due a special note of thanks for their sincere interest and constructive comments as readers. The contributions provided by Dr. A. G. Hanson are also noted and particularly appreciated.

The author is very grateful to many others, too numerous to list, who have provided assistance varying in nature from computer programming advice to unyielding confidence and friendship.

TABLE OF CONTENTS

LIST OF TABLES

LIST OF ILLUSTRATIONS

NOMENCLATURE

English
Notation

A	function defined by Equations (115) MHD channel cross sectional area
Ae	function defined by Equation (157)
ae	function defined by Equation (163)
Am	function defined by Equation (153)
am	function defined by Equation (161)
B	magnetic induction function defined by Equations (115)
b	induced magnetic induction by currents in gas
Be	function defined by Equation (158)
be	function defined by Equation (164)
Bm	function defined by Equation (154)
bm	function defined by Equation (162)
C	function defined by Equation (115)
C_d	drag coefficient = $\tau_w/\rho_\infty U$
Ce	function defined by Equation (159)
ce	function defined by Equation (165)
Cm	function defined by Equation (155)
c_p	constant pressure specific heat
c_v	constant volume specific heat
De	function defined by Equation (160)
Dm	function defined by Equation (156)

English Notation

E	imposed electric field on gas
$\bar{E}^*$	effective electric field = $\bar{E} + \bar{U}x\bar{B}$
e	electronic charge energy of molecules due to rotation, vibration, and translation
E_{chem}	average energy per gas molecule required to singly ionize all seed atoms (Equation (213))
e_{chem}	molecular energy due to chemical bonds per unit mass
Ee	function defined by Equations (169) and (173)
$E_{internal}$	average energy per gas mixture molecule due to molecular motion (Equation (214))
Em	function defined by Equations (168) and (172)
F	molar seeding fraction = n_K/n_A
f	arbitrary function
f_A	function defined by Equations (115)
f_K	function defined by Equations (115)
Fe	function defined by Equations (171) and (175)
Fm	function defined by Equations (170) and (174)
G_s	statistical weighing function in Saha's Equation (82)
$\bar{g}_e$	velocity of electron particle relative to mass average velocity $\bar{w}_o$
H	channel height between electrodes
h	Planck's constant
I_e	electron diffusion parameter = $\sigma_\infty BW_A/N_o e\rho_\infty$
$\underline{i}$	unit vector in x direction
J_∞	nondimensionalized current density = $j_\infty/\sigma_\infty U_\infty B$
J	nondimensionalized current density = $j_\infty/\sigma_o U_o B$

English Notation

J_y	nondimensionalized current density = $j_y/\sigma_\infty U_\infty B$
j	current density
$\underline{j}$	unit vector in y direction
j_T	total current density = $\sqrt{j_x^2 + j_y^2}$
K	loading parameter = E_{y_∞}/UB
K_T	function defined by Equation (86)
k	Boltzmann's constant
$\underline{k}$	unit vector in z direction
L	channel length
ℓ	function defined by $\rho\mu/\rho_\infty\mu_\infty$
M	Mach number
m	step number in x direction of finite difference grid
m_e	electron mass
m_s	mass of species s atom
N	value of n at free stream boundary layer
N_o	Avogadro's number
Nu	Nusselt number
n	step number in y direction of finite difference grid
n_s	species s number density
P	nondimensionalized pressure = $p/\rho_o U_o^2$
P_∞	nondimensionalized pressure = $p/\rho_\infty U_\infty^2$
$\bar{\bar{P}}$	pressure tensor defined by Equation (195)
Pr	Prandtl number
p	gas pressure

English Notation

Q_{es}	effective weighted cross section defined by Equation (92)
R	ideal gas constant
Re	Reynolds number = Ux/ν_∞
Re_L	Reynolds number based on L = UL/ν_∞
Re_m	magnetic Reynolds number
Re_x	Reynolds number based on x = Ux/ν_∞
S_o	interaction parameter based on entrance conditions = $\sigma_o B^2 L U_o/p_o$
S_∞	interaction parameter at x = $\sigma_\infty B^2 LU/p_\infty$
T	gas temperature
T_e	electron temperature
T_∞	free stream temperature
T_∞'	nondimensionalized free stream temperature = T_∞/T_o
U	free stream velocity
U_o	free stream entrance velocity
U'	nondimensionalized free stream velocity = U/U_o
u	x component of velocity in boundary layer
u'	nondimensionalized boundary layer velocity in x direction = u/U
V	voltage
V_{is}	first ionization potential of species s
V_{loss}	voltage loss due to boundary layer
VLDT	voltage loss displacement thickness (Equation (80))
V_s	diffusion velocity of species s relative to mass average gas velocity

English Notation

v	y component of velocity in boundary layer
v'	nondimensionalized boundary layer velocity in y direction = v/U
W_A	average atomic weight of gas
$\bar{w}_o$	mass average velocity of gas
$\bar{w}_e$	velocity of electron particle
X_1	dummy variable defined by Equations (139)
X_2	dummy variable defined by Equations (139)
X_3	dummy variable defined by Equations (139)
X_4	dummy variable defined by Equations (139)
X_5	dummy variable defined by Equations (139)
X_n	one of dummy variables X_1, X_2, X_3, X_4, X_5
x	axial coordinate down MHD channel (Figure 1)
y	coordinate normal to electrode wall (Figure 1)
y'	nondimensionalized coordinate normal to electrode wall = y/L
z	coordinate normal to insulator wall (Figure 1)
Z_e	function defined by Equations (98)

Greek Notation

α	constant exponent in Equation (117)
β	Hall parameter = $\sigma B/en_e$
Γ	nondimensionalized pressure = p/p_o
γ	ratio of specific heats = c_p/c_v
Δf	change in function f

Greek
Notation

δ	nondimensionalized boundary layer thickness
$\Delta\xi$	step size in ξ direction of finite difference grid
$\Delta\eta$	step size in η direction of finite difference grid
ε	arbitrarily small constant
ε_o	dielectric constant
η	transformed coordinate normal to the electrode wall (Equation 40)
θ	nondimensionalized boundary layer temperature = T/T_∞
κ	thermal conductivity
κ'	nondimensionalized thermal conductivity = κ/κ_o
μ	viscosity
μ'	nondimensionalized viscosity = μ/μ_o
μ_e	magnetic permeability
ν	kinetic viscosity = μ/ρ
ξ	nondimensionalized axial coordinate = x/L
ρ	gas density
ρ_e	electric charge density
ρ_∞	free stream gas density
ρ_∞'	nondimensionalized free stream gas density = ρ_∞/ρ_o
σ	electrical conductivity
σ_∞'	nondimensionalized free stream electrical conductivity = σ_∞/σ_o
σ'	nondimensionalized boundary layer electrical conductivity = σ/σ_∞
σ_{ms}	momentum transfer cross section (Equation (87))

Greek Notation

σ_{ei}	inverse of the electrical resistivity due to electron-ion collisions
τ	shearing stress
ϕ	arbitrary constant in Equation (119)
ψ	stream function defined by Equations (42) and (43)
Ω	effective cross section quantity in Equation (62)
ω	arbitrary constant exponent in Equation (35)

Subscripts

o	value at entrance of channel
∞	free stream value
e	value for electron unless otherwise listed above
A	value for argon (except W_A--see list above)
c	value due to collisions
s_i	value for ions of species s
s_n	value for neutrals of species s
K	value for potassium
new	new value in iteration sequence
old	old value in iteration sequence
w	value at electrode wall
x	x component
y	y component
δ	value at boundary layer free stream boundary

Special Notation

$(\bar{\ })$	vector quantity
$(\ )^*$	reference quantity except where listed above
$\langle\ \rangle$	quantity averaged over particle velocity distribution
$(\dot{\ })$	derivative with respect to η
$(\ )_m^n$	value at node m,n in finite difference grid

SUMMARY

The details and characteristics of electrode boundary layers in constant velocity, segmented electrode MHD generators, using potassium seeded argon as the working fluid is calculated in this study. A non-equilibrium electrical conductivity model, which has been experimentally verified in electric fields at appropriate current densities, is taken in the free stream flow as well as the boundary layers. Hall currents are included and the two dimensional boundary layer equations are solved by finite difference methods with no similarity assumption. Heat transfer, drag, and electrical losses are evaluated.

The electrical conductivity is calculated from the electron momentum, electron energy, and Saha's equation. This also yields electron temperature and Hall parameter values. Variable collision cross sections are used which produce a relative maximum in the electrical conductivity versus current density curve. This could be advantageous in stabilizing the current density in MHD devices.

Utilizing this electrical conductivity model in the free stream flow shows the electrical conductivity increasing down the channel due to the strong influence of decreasing pressure.

The electrode boundary layers for this free stream are studied by transforming the boundary layer equations and using an implicit finite difference method to solve the coupled momentum differential equation, energy differential equation, and transcendental equations describing the electrical characteristics. These electrical

characteristics. These electrical characteristic equations are the above-mentioned electron energy, momentum, and Saha's equations without simplification.

A new parameter, I_e, is found to be a measure of the relative importance of the energy carried by diffusion of the electrons due to currents. This mode of energy transfer in the boundary layer should not be neglected when I_e is on the same order of magnitude as the nondimensionalized boundary layer thickness, δ. Also, the local interaction parameter appears in the Ohm heating term in the boundary layer energy equation and determines its importance. This gives rise to correlation of the increase in the heat transfer caused by the increased Ohm heating in the boundary layer.

The calculated thermal boundary layer profiles show increasing effects of the MHD terms down the channel, while the viscous boundary layer is essentially unchanged. The resulting boundary layer electrical losses reduce the effective height of the generator (distance between electrodes) on the order of the boundary layer thickness. This demonstrates the desirability of high currents, (30 amperes/cm^2), to heat the electrons.

The heat transfer at the entrance is unchanged by the MHD terms, but increases at the channel exit by as much as 300 per cent.

The increase in the local Nusselt number caused by the MHD effects at all axial positions under varying channel length, Mach number, and other operating conditions is correlated on one plot. The correlation parameter contains only the Reynolds number, the degree of expansion, and the loading parameter. The correlation is accurate to

about 10 per cent when the Mach number, entrance pressure, entrance temperature, seeding fraction, generator length, and loading factor are varied. Varying the wall temperature produces results differing from the correlation curve by up to 20 per cent. Since only the loading factor, Mach number, Reynolds number, and degree of expansion need to be known, this correlation can be helpful in predicting heat transfer rates for any operating condition and axial location. The correlation parameter could possibly lead to a simpler, but more general, analytical solution.

A simple expression for the electrical conductivity, previously used in MHD boundary layer work, is used here in the boundary layer for comparison with the complex expression and found to give heat transfer rates up to a factor of three higher. However, good agreement was found when constants in this expression were changed and Hall currents were neglected.

Hall currents are found to cause negligible changes in the heat transfer, but increase the voltage loss by as much as 300 per cent. However, since this voltage drop is small, it does not appear to be significant in most cases. No shorting of the segmented electrodes is demonstrated by the Hall currents. This suggests that any large electrical losses in non-equilibrium generators due to the electrode would lie in the space charge sheath region.

The relatively high electrical conductivity in the electrode boundary layer calculated in this analysis indicates that when similar electrical characteristics are used in the insulator boundary layer, much higher leakage currents will result than previously found.

CHAPTER I

INTRODUCTION

General Considerations

Among the many new concepts for power generation investigated in the past decade both for space and commercial applications,[1] magneto-hydrodynamic (MHD) power generation with gaseous working fluids has received a great deal of attention. This has been due to its potential for large increases in efficiency and power density over conventional systems.

However, experiments have shown that this potential is not easily realized as performance has been as low as 15 per cent of that expected.[2] The sources of the losses are not well understood or even well identified, but they are usually attributed to boundary layer effects on the MHD channel walls.[2]

The purpose of this work is to analytically investigate the boundary layers on one of these walls, the electrode, by using a mathematical model which resembles the practical device much more closely than any previous investigation. This enables one to calculate the magnitude of the boundary layer losses present and possibly show how they can be reduced. A qualitative description of the problems to be investigated will first be given by considering the fundamental concept.

The MHD concept may be easily presented by comparing its fundamental principles with that of conventional electric machinery. The

essential feature in both is that there is a magnetic field and a conductor which moves through this field and which, if current flows through it, feels a force. Depending upon the direction and relative magnitude of these two quantities, the system acts as a motor or as a generator and the conductor feels an accelerating or retarding force. The primary and important difference between an MHD device and a conventional machine is that the moving conductor is a gas in the former and a solid wire in the latter.

Figure 1 shows a schematic diagram of a simple MHD generator. It consists of a channel through which the gaseous working fluid expands with a velocity, U; a magnetic induction, B, across the channel; and electrodes at the top and bottom across which a voltage exists, creating an electric field, E, in the gas. These electrodes serve much the same purpose as brushes in a conventional generator. The gas, due to its motion through the magnetic field, has an emf generated in it which may drive a current through itself, the electrodes, and the external load. Since a gaseous conductor replaces a metallic conductor, one may immediately note the primary factor that limits the range of applicability and is the fundamental problem of an MHD generator. This factor is electrical conduction in gases.

In order to become an electrical conductor, a gas must become ionized, which normally requires high temperatures. The temperature at which this ionization occurs varies from gas to gas. Analyses of various gases as working fluids[3] have shown noble gases seeded with a small percentage of potassium or cesium, less than 1 per cent, to be the optimum working fluid. The potassium, or cesium, provides

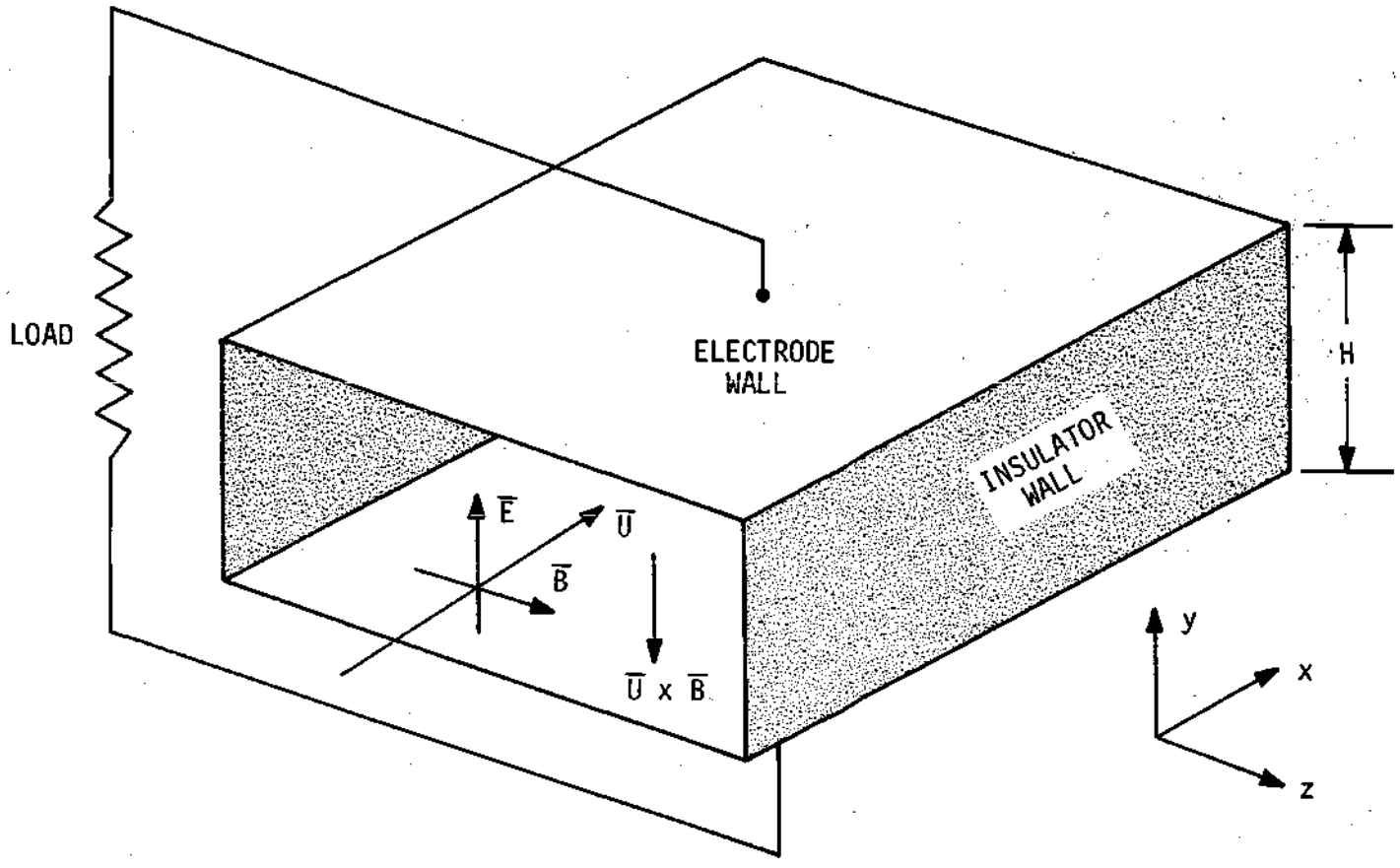

Figure 1. MHD Generator Configuration

ionization at relatively low temperatures and the noble gas atoms provide a small electron-atom collision cross section, the combination of which provides relatively high electrical conductivities. Use of this working fluid in a practical device would normally dictate a closed loop system so that the working fluid could be recirculated.

However, seeded working fluids still require relatively high temperatures. At 3000 degrees K, 3 atmospheres, and small currents, argon seeded with 0.2 per cent potassium has an electrical conductivity of 1/30 that of copper. This would imply an internal volume of an MHD generator 30 times that of copper in a copperwound generator operating at comparable linear velocities.[4] This would not give a power density advantage to the MHD generator. However, this factor can be improved to heavily favor the MHD concept by using higher gas velocities to increase the output voltage and by operating at a condition which allows the electron temperature to rise above the gas temperature, thus increasing the ionization and electrical conductivity.[5,6]

The later condition has been a subject of much study because it offers promise of increasing the electrical conductivity by a factor of one to three orders of magnitude without an increase in the gas temperature.[7,8,9] This is especially important for MHD generator systems using nuclear reactors as a heat source where the temperatures are limited to below 2000 degrees K. The electrons gain their increased energy from the potential through which they fall. When this condition exists, the plasma is termed a nonequilibrium plasma and is similar to electron swarms in drift tube experiments where the Townsend

coefficient appears and is defined as the ratio of the electron mean agitation energy to the mean molecular energy.[10]

In view of the above, high gas temperatures and velocities, seeded noble gases, and nonequilibrium plasmas are seen to be highly desirable, if not necessary in MHD devices.

These conditions dictate channel walls which are cooled and kept at much lower temperatures than the bulk of the gas. This leads to severe temperature and velocity gradients near the walls which produce boundary layers. Many of the major problems which must be solved in MHD applications are directly related to these cool, low velocity boundary layers.

The effects of boundary layers are well known for normal flat plate flow, but in an MHD generator where electric fields, magnetic fields, and currents exist within the gas, many new effects arise.

The MHD boundary layer effects, which do not occur in ordinary boundary layer flow, may be classified as heat transfer effects and electrical effects. The discussion of these effects will be limited to the developing electrode boundary layer in an MHD generator with infinitely segmented electrodes which is the subject of this work. The segmentation of the electrodes perpendicular to the direction of flow inhibits axial currents which degrade a generator's performance. This generator configuration has been shown to be the most favorable for a number of applications.[7,11] For the electrode wall the applied electric field vector is normal to the plate and the magnetic field vector is normal to the free stream gas velocity vector and the electric field vector.

Looking at some of the more important MHD heat transfer effects occurring in the boundary layer, consider a 2000 degree K gas flowing over a 1000 degree K plate. As in non-MHD flow, there must exist a steep temperature gradient in the boundary layer, particularly at the leading edge, resulting in a high heat transfer rate to the plate. When an electrode configuration of an MHD generator is considered, a current is also present in the gas. Joule heating then appears as a heat source. Two effects magnify this Joule heating in the boundary layer over that in the free stream, which significantly increase the heat transfer.

The first is due to the lower temperatures in the boundary layer resulting in a decrease in the electrical conductivity. This tends to increase j_T^2/σ, the joule heating rate per unit volume, where j_T is the total current density and σ the electrical conductivity.

The second effect is due to an increase in the axial current, known as the Hall current, in the boundary layer over that in the free stream. For the segmented electrodes considered here, the Hall current is negligible in the free stream if the boundary layer thickness is thin compared to the channel height H. But in the boundary layer, due again to variable properties, the Hall current, j_x, may be on the same order of magnitude as the current normal to the electrode, j_y. Since j_y is essentially constant in the boundary layer, the additional current leads to increased Joule heating near the wall.

The presence of the current also leads to an electron diffusion velocity normal to the electrode. The thermal energy which these electrons carry produces an additional heat flux normal to the electrode.

Since the electron current flows to an anode and away from a cathode, an antisymmetric channel results.

Considering some of the more important electrical effects, it is seen that the boundary layers inhibit the power output of the generator for several reasons.

First, the increase in Joule heating in the boundary layers noted above extracts energy as heat that would appear as electrical energy in the absence of boundary layers. This effect may also be viewed as a reduction in output voltage due to the increase in the boundary layer electrical resistance.

A second reason for reduction of power results from the velocity boundary layer. A simplified form of Ohm's law for the channel in Figure 1 is:

$$j_y = \sigma(E-UB) \qquad (1)$$

where, for a generator, UB must be larger than E. The current flows against the applied field, E, due to the emf the gas sees, UB, as it moves through the magnetic field. When the velocity decreases in the boundary layer either j_y or E must decrease. This results in a decrease in the local power output density, $j_y E$.

Also, when axial currents flow in the boundary layers they interact with the magnetic field to produce an emf normal to the plate proportional to $j_x B$. Normally, for segmented electrodes j_x flows in the cooler boundary layer in such a manner as to result in an emf in

the opposite direction to UB. This increases the voltage drop in the boundary layer.

From this discussion it is seen that variable properties in the boundary layers, particularly the electrical ones, produce effects in an MHD generator which may have adverse effects on its performance and could be partially responsible for the poor performance previously noted. The importance of these losses and ways to reduce their magnitude need to be known.

Related Work

Due to the complexity created by the coupling of the two-dimensional boundary layers and the effects just discussed, very few investigations have been carried out on MHD boundary layers in the entry region where practical MHD generators operate. Most analyses have assumed fully developed flow as well as constant properties as first carried out by Hartmann.[12] With exception of the reduced velocity effect, none of the effects of interest here are then present. A good bibliography of the literature available on entrance region boundary layers appears in Reference 13.

The entry region investigations which have been carried out on MHD boundary layers may be classified into two groups by the configuration of the plate and magnetic field. These two configurations correspond to the insulator wall and electrode wall of an MHD generator as shown in Figure 1. For the insulator wall, the magnetic field is perpendicular to the plate with currents flowing parallel to it. For the electrode, the magnetic field is perpendicular to both the fluid

velocity and the normal to the plate. The boundary layer effects on the insulator wall[14] differ in many respects from those on the electrode wall which are of interest here; but since the equations and difficulties of both problems are similar, mathematical models and techniques of the insulator wall work will also be discussed. The electrical characteristics assumed in the insulator boundary layers are of particular interest because the same assumptions may possibly be applicable to the electrode wall.

Several entry region analyses have been carried out since 1960 on the insulator wall in MHD channel flow assuming constant properties and incompressibility.[15,16] Both integral and finite difference techniques have been used.

A compressible boundary layer analysis with constant electrical conductivity has recently been carried out by Hwang, et al.[17] Bush[18] assumed compressible flow and variable properties with the electrical conductivity a function of enthalpy. The electrical conductivity was taken to be zero in the free stream which allowed a similar solution. This work is concerned with magnetic field interaction with high temperature boundary layers on re-entry vehicles and not MHD channel flow.

When constant properties are assumed, the electrical conductivity decouples from the boundary layer equations and causes most of the MHD effects to be zero. The incompressibility assumption neglects any coupling between the velocity and temperature profiles and is valid only for Mach numbers, M, such that:[19]

$$\frac{1}{2} M^2 \ll 1 \qquad (2)$$

An incompressible or constant properties solution, therefore, would not be applicable to MHD generators with gaseous working fluids where the boundary layer effects studied here are present.

The insulator wall work of most interest was carried out by Hale and Kerrebrock.[20,21] Compressible MHD accelerator flow with segmented electrodes was considered and, contrary to any other work, included the Hall currents. Two variable electrical conductivity expressions were used and each gave completely different results. One was for an equilibrium plasma and the other for a nonequilibrium plasma. The first is a function of gas temperature only, whereas the latter is a function of gas temperature and current density. These were expressions which over some range approximated theoretically derived values for σ. The variation of the Hall parameter in the boundary layer, which determines the Hall current in the boundary layer, was also an approximation to the derived expression. Also, these theoretically-derived expressions contained many simplifying assumptions, such as slight ionization. A locally similar solution was obtained by taking a free stream flow with constant temperature, Hall parameter, and Mach number. As was pointed out in their work, the errors introduced by the assumptions involved in the electrical conductivity expressions and those required for a similar solution, particularly constant Mach number, could lead to inaccurate results. However, they concluded that the behavior of the boundary layers could be very complex, particularly when compressible flow and nonequilibrium electrical conductivity are considered. This work,[20] as well as others,[22] casts doubts on the applicability of integral

techniques to MHD boundary layers and shows the importance of the electrical conductivity expression in the boundary layers.

Investigations applicable to the electrode boundary layers are much more sparse than for the insulator wall. The only work of interest is by Kerrebrock.[6,23] As stated by Culick,[24] investigation of the detailed effects of MHD boundary layers in channel flow has been done only by Hale and Kerrebrock on accelerators. Kerrebrock[23] obtained a locally similar solution for the electrode boundary layer for variable electrical conductivity and compressible laminar flow neglecting the Hall currents. This work states that the Hall effects are not negligible at pressures less than ten atmospheres. The equilibrium case is assumed where σ is a function of only gas temperature in the boundary layer.

As in Hale's work,[21] the free stream temperature and conductivity were assumed constant. With these assumptions, a similar solution was obtained for the boundary layer profiles which is exact only for a Mach number of zero. This corresponds to the case of no viscous heating. Local similarity is taken for Mach number other than zero which implies a constant Mach number. Profiles were obtained by finite difference techniques for a Mach number of one with various degrees of acceleration.

These calculations show an increase in the input power to the accelerator of 70 per cent due to the boundary layers. Heat transfer rates were ten times that of normal boundary layers.

Following these calculations, Kerrebrock obtained some experimental data for electrode heat transfer in an argon-potassium plasma and found it was less than predicted by his theory.[6] It was also found

that the voltage-current characteristics were not as predicted. These facts lead him to take a nonequilibrium electrical conductivity expressed as a function of the gas temperature and current density which Hale and Kerrebrock used.[20] The same free stream was taken as before,[23] and Hall effects were neglected. This improved the agreement with the experimental voltage-current characteristics, although some constants in the expression were determined from the experimental data. By assuming a quadratic temperature profile and using an integral technique, the increase in heat transfer over normal boundary layer heat transfer was calculated, but it was stated that it did not agree satisfactorily with his data.

In another study, Kerrebrock[25] made some qualitative calculations concerning losses in segmented electrode boundary layers due to an assumed increase in the electrical conductivity near the electrode in a generator. No viscous or thermal boundary layer calculations were made. A form of the electrical conductivity profile was assumed, which increases as the wall is approached, and axial current densities and electrical losses calculated. These qualitative calculations led to the results that with the increase in electrical conductivity near the wall, the boundary layers could under some conditions, severely degrade generator performance by axially shorting the segmented electrodes and making its performance much like a continuous electrode generator.[7,11] It was suggested that Hall currents might produce a profile such as was assumed.

No work which couples the electrical conductivity to the gas boundary layer conditions has shown an electrical conductivity profile

such as Kerrebrock assumed. This could be due to the fact that axial currents have been neglected in any work from which a profile of electrical conductivity could be determined.

Therefore, it is seen that the only significant work on developing compressible boundary layers on MHD electrode walls is Kerrebrock's.[6] This is for an accelerator with no Hall effect (true only for pressures greater than ten atmospheres), a specific free stream with constant electrical conductivity, local similarity which implies constant Mach number and required neglecting a relatively large term, and a simple approximate electrical conductivity expression. The solution was obtained by an integral technique assuming a quadratic temperature profile and gives no detailed information concerning the boundary layer. It has also been shown[25] that if Hall currents could produce an increasing electrical conductivity near the wall, large losses could result.

On the insulator wall, Hall currents have been considered where an assumed local similar solution, which could not be justified, was obtained using the same type of electrical conductivity expression as Kerrebrock.[6] Solutions were obtained by finite differences for various Mach numbers and resulted in very complex profiles.

Present Investigation

In light of the unknown source of the poor performance of experimental MHD generators and the lack of analytical investigations on developing MHD electrode boundary layers, this work theoretically evaluates previously discussed MHD effects in these boundary layers.

An infinitely segmented electrode wall in an MHD generator channel using potassium seeded argon is taken as the model to be studied.

The compressible boundary layer problem is formulated by deriving the continuity, momentum, and energy equations from Boltzmann's equation. An order of magnitude analysis is carried out and typical boundary layer assumptions made. The partial differential equations are then transformed to new independent variables so that the dependent variables vary less rapidly in the new coordinate system. This facilitates a numerical solution of the equations. Variable thermal and electrical conductivity, viscosity, and Hall currents are assumed and expressions derived for them.

Due to the importance of the MHD effects on the electrical properties of the gas, an effort is made to derive an accurate expression for the nonequilibrium electrical conductivity which also yields electron density and electron temperature as a function of pressure, temperature, and total current density. Ionization of both the argon and potassium is considered. Due to the importance of the variable electron-atom collision cross section in argon,[26] this effect is included and yields a relative maximum in the electrical conductivity versus current density curve not before recognized. This could be of significance in preventing current instabilities where the current density rises to very large values.[25,27] A portion of this work has been published in the open literature.[28] This theory has subsequently been modified and experimentally verified by Dowdy.[29]

The free stream solution must be obtained and used as a boundary condition in the boundary layer equatins. The derived electrical

conductivity is used which requires a numerical solution.

The Hall effect is included so that its importance and effects may be shown. This Hall current is closely coupled to the electrical conductivity since each depends on and affect the electron density. Given the gas temperature and pressure and normal current, the electrical conductivity and Hall current must then be obtained by a double trial and error solution.

The finite difference scheme with the variable electrical and thermal properties are all programmed on a Univac 1108 computer and solved simultaneously. The electromagnetic and freestream equations are uncoupled from the boundary layer equations.

This produces profiles of all electrical and thermal properties of the gas. From these profiles, heat transfer and electrical losses may be calculated. Using a constant interaction parameter, which is a measure of the fraction of available energy extracted, significant parameters are varied to determine their effect on the heat transfer and electrical losses.

This provides information on three important aspects of MHD flow which, due to the lack of information revealed in his review, have been recommended by Broadbent in 1968[30] as being needed. These are (1) detailed velocity, temperature, and electrical characteristics in boundary layers, (2) Hall effect in boundary layers, (3) varying electrical conductivity in boundary layers.

CHAPTER II

FREE STREAM FLOW

In order to properly formulate the boundary layer problem, the configuration and free stream flow of the generator must be specified. Proper boundary conditions are then available for the boundary layer solution. For large Reynolds numbers the viscous effects are restricted to thin boundary layers near the wall and the free stream may therefore be treated independently as one-dimensional flow.

The free stream flow is described by the following equations.

Continuity: $$\rho U A = \text{constant} \tag{3}$$

Momentum: $$\rho U \frac{dU}{dx} + \frac{dP}{dx} = (\bar{j} \times \bar{B})_x \tag{4}$$

Energy: $$\rho U \left(c_p \frac{dT}{dx} + U \frac{dU}{dx} \right) = \bar{j} \cdot \bar{E} \tag{5}$$

Equation of State: $$p = \rho R T \tag{6}$$

Ohm's Law: $$\bar{j} = \sigma [\bar{E} + (\bar{w}_o + \bar{V}_e) \times \bar{B}] \tag{7}$$

Constant specific heat and an ideal, neutral gas have been assumed. These assumptions are discussed in Chapter III.

The quantity inside the brackets in Ohm's law is the total effective electric field felt by the electrons. Current due to the ions is neglected because their mobility is approximately 1/1000 of the electron mobility. The quantity $\bar{E}$ is the imposed electric field and $(\bar{w}_o+\bar{V}_e) \times \bar{B}$ is the force felt by the electrons due to their motion through the magnetic field.

The magnetic induction $\bar{B}$ is the sum of the applied induction, $\bar{B}_z$, and the magnetic induction induced by currents flowing in the gas, $\bar{b}$. The induced magnetic induction is negligible for small magnetic Reynolds numbers:

$$Re_m \equiv UL\sigma\mu_e \tag{8}$$

where L is the length of the channel and μ_e is the magnetic permeability. This is shown by Maxwell's relation:

$$\bar{\nabla} \times \bar{B} = \mu_e \bar{j} \tag{9}$$

When it is nondimensionalized with characteristic values and incorporated with the simplified Ohm's law, Equation (1), it leads to:

$$\nabla' \times \bar{B}' = Re_m \sigma'(1-K)\underline{j} \tag{10}$$

where the loading parameter has been used:

$$K \equiv \frac{E_{y_\infty}}{UB_z} \tag{11}$$

and $\underline{j}$ is a unit vector in the y direction. A prime denotes a non-dimensionalized variable. Taking the applied magnetic induction to be constant and equal to $\vec{B}_o$, and defining $\vec{b}$ as the induced field then:

$$\nabla' \times \vec{b}' = Re_m \sigma'(1-K)\underline{j} \tag{12}$$

If

$$Re_m << 1 \tag{13}$$

then compared to the imposed field, only small magnetic fields will be induced by currents in the gas. Equation (13) holds for all cases of interest in this work. This decouples the flow equatins from Equation (9) and the magnetic induction is known and given by:

$$\vec{B} = B\underline{k} \tag{14}$$

since the applied field in an MHD generator is only in the direction normal to $\vec{U}$ and parallel to the electrode wall.

By taking the diffusion velocity of the electrons as that due to the current only:

$$\vec{V}_e = -\vec{j}/en_e \tag{15}$$

Equations (7), (14), and (15) then yield the current components:

$$j_x = \frac{\sigma}{1 + \beta^2} [E_x + vB - \beta(E_y - uB)] \tag{16}$$

$$j_y = \frac{\sigma}{1 + \beta^2} [E_y - uB + \beta(E_x + vB)] \tag{17}$$

where β, known as the Hall parameter, is defined:

$$\beta \equiv \frac{B\sigma}{en_e} \tag{18}$$

Expressions (16) and (17) do not contain a one-dimensional assumption and are therefore valid for two-dimensional boundary layers as well as the free stream. By introducing the one-dimensional restraint, the velocity components are:

$$v = 0 \tag{19}$$

$$u = U \tag{20}$$

which results in:

$$j_x = \frac{\sigma}{1 + \beta^2} [E_x - \beta(E_y - UB)] \tag{21}$$

$$j_y = \frac{\sigma}{1 + \beta^2} [E_y - UB + \beta E_x] \tag{22}$$

For continuous electrodes E_x is zero and an axial current flows in the gas, returning through the electrodes, in such a direction as to decrease the normal current, j_y. Since j_y is the power producing current, the power output is reduced. This appears in Equation (22) as a reduction in the "effective conductivity" due to the $1 + \beta^2$ term.

This reduction in power may be overcome by finely segmenting the electrodes so that no return path for j_x exists. As j_x then attempts to flow, an E_x will be created to exactly balance the Lorentz force on the electrons due to their diffusion velocity across the magnetic field. With j_x zero, Equation (21) gives:

$$E_x = \beta UB(K-1) \tag{23}$$

and from (22):

$$j_y = \sigma UB(K-1). \tag{24}$$

For finely segmented electrodes it is clear that the Hall effect, which tends to create an axial current, does not reduce the power output of the freestream. The segmented electrode generator configuration is taken in this study.

This does not, however, indicate that there are no Hall losses in the boundary layer. Hall currents do flow in the electrode boundary layers in segmented electrode generators creating losses, as will be discussed in Chapter IV. Other studies have neglected these.

The equations relating the freestream variables are now (3), (4), (5), (6), (11), (23), and (24). Taking σ as a known function of pressure, temperature, and current density, there are seven equations and ten unknowns. Three of the dependent variables must be further specified as given functions of x. These are chosen to be U, K, and B. Since there appears to be no strong argument for assuming a more complicated expression, K and B will be taken as specified constants. Constant K will insure a uniform loading and electrical efficiency throughout the free stream and a uniform magnetic induction is relatively easy to produce in an apparatus. The velocity will also be taken as a constant. This simplifies the free stream equations and is close to the optimum, minimum entropy increase, which has been shown to be somewhere between constant velocity and constant Mach number.[30] These two flows are very similar as is shown by the small Mach number variation down the channel in the results of the present study.

Using the results for the segmented electrode configuration:

$$\bar{j}_\infty = j_y \underline{k} \tag{25}$$

and

$$\bar{E} = E_x \underline{i} + E_y \underline{j} \tag{26}$$

in the energy and momentum equations and dividing the energy equation into the momentum equation produces:

$$\frac{\gamma}{\gamma - 1}\frac{1}{K}\frac{d\ln T}{dx} + \gamma M^2 \frac{d\ln U}{dx} - \frac{d\ln p}{dx} = 0 \tag{27}$$

where γ is the ratio of the specific heats. For constant velocity this integrates to:

$$\frac{p}{p_o} = \left(\frac{T}{T_o}\right)^{\frac{\gamma}{(\gamma-1)K}} \tag{28}$$

Putting (28) into the energy equation and using Ohm's law, Equation (24):

$$\frac{\gamma}{\gamma - 1}\frac{p_o}{T}\left(\frac{T}{T_o}\right)^{\frac{\gamma}{(\gamma-1)K}}\frac{dT}{dx} = \sigma KB(E_y - UB) \tag{29}$$

Given the gas properties including σ, Equations (24), (28), and (29) may be solved for p, T, and j_y as functions of x.

These three equations are more suitable for solving if they are put into nondimensionalized form. This is done by using the following nondimensional variables where a $(\ )_o$ denotes the entrance condition.

$$P = \frac{p}{\rho_o U_o^2}, \qquad \xi = \frac{x}{L}, \qquad U' = \frac{U}{U_o}$$

$$\rho'_\infty = \frac{\rho_\infty}{\rho_o}, \qquad J = \frac{j_\infty}{\sigma_o B U_o}, \qquad T'_\infty = \frac{T_\infty}{T_o} \tag{30}$$

$$\sigma'_\infty = \frac{\sigma_\infty}{\sigma_o}, \qquad S_o = \frac{\sigma_o B^2 L U_o}{p_o}$$

The resulting equations are:

$$\frac{d(T'_\infty)^{\frac{\gamma}{(\gamma-1)K}}}{d\xi} = S_o \sigma'_\infty (K-1) \tag{31}$$

$$\frac{P}{P_o} = (T'_\infty)^{\frac{\gamma}{(\gamma-1)K}} \tag{32}$$

$$J = \sigma'_\infty (K-1) \tag{33}$$

The above equations are to be solved for the free stream flow with the following boundary conditions at $\xi = 0$:

$$(T'_\infty)_o = 1$$

$$P_o = \frac{p_o}{\rho_o U_o^2} = \frac{1}{\gamma M_o^2} \tag{34}$$

$$(\sigma'_\infty)_o = 1$$

If σ'_∞ is a function of pressure, temperature, and current density, the three equations will be coupled.

No solutions are available for this coupled condition which is the case for a nonequilibrium electrical conductivity. As pointed out in Chapter I, a constant σ_∞ is customarily taken and has been assumed in all boundary layer work, although Brocher[31] has obtained a one-dimensional solution for the case:

$$\sigma'_\infty = (T'_\infty)^\omega \, p^{-1/2} \tag{35}$$

where ω is a chosen constant.

In Chapter IV, the electrical characteristics of the argon-potassium plasma will be found and a realistic nonequilibrium electrical conductivity expression will be derived and used with Equations (31) through (34) to describe the free stream flow. This is necessary in order to simulate a practical MHD channel flow so that realistic boundary layers may be studied.

CHAPTER III

BOUNDARY LAYER FLOW EQUATIONS

Introduction

The equations describing the flow characteristics in the boundary layer (continuity, momentum, and energy) are derived in Appendix A and the assumptions implicit in them are noted. The continuity, momentum, and energy moments of Boltzmann's equation for a general species s are used as a starting point so that all necessary assumptions to reduce these to a tractable set of boundary layer equations, for this particular configuration, may be noted. A boundary layer order of magnitude analysis is made to determine which terms may be neglected in the boundary layer region of high Reynolds number flow. The resulting equations are (Appendix A):

$$\frac{\partial(\rho' u')}{\partial \xi} + \frac{\partial(\rho' v')}{\partial y'} = 0 \tag{36}$$

$$\rho' \left[u' \frac{\partial u'}{\partial \xi} + v' \frac{\partial v'}{\partial y'} \right] = - \frac{dP_\infty}{d\xi} + \frac{1}{Re_{o_L}} \frac{\partial}{\partial y'} \left[\mu' \frac{\partial u'}{\partial y'} \right] + \frac{S_\infty P_\infty}{\gamma M_o^2 P_o} J_y B \tag{37}$$

$$\rho' \left[u' \frac{\partial \theta}{\partial \xi} + v' \frac{\partial \theta}{\partial y'} \right] = \tag{38}$$

$$+ \frac{1}{Re_{o_L} Pr} \frac{\partial}{\partial y'} \left[\kappa' \frac{\partial \theta}{\partial y'} \right] - \frac{\sigma_\infty B W_A}{N_o e \rho_o} \left[J_y \frac{\partial(\theta_e \theta)}{\partial y'} \right] +$$

$$\frac{\gamma - 1}{Re_{o_L}} M^2 \mu' \left(\frac{\partial u'}{\partial y'}\right)^2 + \frac{S_\infty}{T'_\infty} \frac{P_\infty}{P_o} \left(\frac{\gamma-1}{\gamma}\right) \left(\frac{J_x^2 + J_y^2}{\sigma'} - u'\right)$$

All nondimensional variables are defined in (217).

Controlling Parameters

It is of interest to note here the dimensionless parameters which appear in the momentum and energy equations. These have not been previously pointed out and are shown to be very useful in this study.

One of the additional parameters--other than the customary Reynolds, Mach, and Prandtl numbers--which appears through the MHD terms is the interaction parameter S_∞ defined by $\sigma_\infty UB^2L/p_\infty$. This same type term appears in the free stream equations and is a measure of the fraction of pressure potential energy removed by the generator, but has not in the past been shown to be a controlling parameter in the boundary layer. It determines the importance of the Ohm heating term in the boundary layer energy equation. Its magnitude increases as one moves down the channel due to the decreasing pressure. The increase is due to the Ohmic heating being volume dependent and not density dependent. The Ohmic heating per unit volume does not change with density and as the mass in that unit volume decreases, its heating effect on that mass increases. This parameter is the important one in a constant velocity generator since no gas kinetic energy is removed for this case. In generators which remove primarily gas kinetic energy rather than pressure energy, the interaction is measured by $\sigma_\infty UB^2L/\rho_o U^2$.

Another dimensionless parameter, appearing in front of the electron diffusion term, is $\sigma_\infty BW_A/N_o e\rho_o$ which is denoted by I_{e_o}. It may

be shown to be the ratio of the number of electrons diffusing through a plane of unit area fixed in the gas per unit time with respect to the number of gas molecules moving across a plane of unit area fixed in space per unit time. The electron diffusion is taken as that due to the current flowing in the gas, and the movement of gas molecules is that due to the gas velocity U. These quantities show up by multiplying the numerator and denominator by U giving:

$$I_{e_o} = \left(\frac{\sigma_\infty UB}{e}\right)\left(\frac{W_A}{N_o \rho_o U}\right) \tag{39}$$

The first grouping on the left is the number of electrons flowing relative to the gas per unit area per unit time due to the characteristic current density $\sigma_\infty UB$. The last grouping on the right gives the inverse of the number of gas molecules flowing per unit area per unit time due to the characteristic velocity U.

This dimensionless parameter has not previously been pointed out, but it is a useful measure of the relative magnitude of the energy carried by the movement of the current producing electrons. From the order of magnitude analysis it is seen that this parameter must be smaller than δ in order to neglect this mode of energy transfer. In this study, it is approximately 0.001 which is between δ and δ^2 and will not be neglected. It tends to create dissimilar boundary layers on opposite electrode walls of an MHD generator due to the flow away from one wall and toward the other.

The Mach number also appears in front of the MHD terms and therefore their importance is influenced by this parameter. This may

increase the Mach number's influence on the heat transfer and other characteristics of the boundary layers.

Transformation of Boundary Layer Equations

The continuity, momentum and energy Equations (36), (37), and (38) must be solved simultaneously with the electrical characteristic equations by numerical analysis in which the derivatives are replaced by finite differences as discussed in Chapter V. This assumes a linear variation of the dependent variables over a small distance in the coordinate system. For this reason, the more uniform the flow with respect to the coordinates, the more accurate the numerical solution for the same grid spacing. Since the flow cannot be altered, one then turns to altering the coordinate system which is the subject of this section.

The need for this transformation was made evident in an initial attempt to solve the equations in the x-y coordinate system following Wu's numerical technique.[33] In this technique there is a restriction on the relative size of Δx and Δy, the distances between grid points, for which the solution is stable. With this restriction coupled to the restriction on the maximum size of Δy needed for accuracy in the thin boundary layer region toward the entrance of the channel, the grid spacing became impractically small. This could have been overcome by using a variable grid spacing with a smaller spacing as the plate or entrance is approached, but it was decided to transform the equations to a new coordinate system and use an implicit numerical technique which is always stable. Wu's technique[33] could possibly be used on the

transformed equations with good results also, although their form is somewhat different.

The basic transformation used for y is widespread in its application to boundary layer problems as it results in a rather uniform flow with respect to the axial coordinate. The transformations used are:

$$\eta = \sqrt{\frac{U}{\nu_o x}} \int_0^y \frac{\rho}{\rho_o} dy \tag{40}$$

$$\xi = x/L \tag{41}$$

along with a stream function ψ defined by:

$$\rho u = \frac{\rho_o UL}{\sqrt{Re_{o_L}}} \frac{\partial \sqrt{\xi}\ \psi}{\partial y} \tag{42}$$

$$\rho v = -\frac{\rho_o UL}{\sqrt{Re_{o_L}}} \frac{\partial \sqrt{\xi}\ \psi}{\partial x} \tag{43}$$

The latter two equations satisfy the continuity equation and therefore simplifies solution. The dimensionless variables defined in the previous section are used here also.

The transformation is carried out by use of:

$$\frac{\partial}{\partial y} = \frac{\partial \eta}{\partial y} \frac{\partial}{\partial \eta} + \frac{\partial \xi}{\partial y} \frac{\partial}{\partial \xi} \tag{44}$$

and:

$$\frac{\partial}{\partial x} = \frac{\partial \eta}{\partial x}\frac{\partial}{\partial \eta} + \frac{\partial \xi}{\partial x}\frac{\partial}{\partial \xi} \tag{45}$$

which with (40) and (41) simplify to:

$$\frac{\partial}{\partial y} = \frac{\rho}{\rho_o}\sqrt{\frac{U}{\nu_o x}}\frac{\partial}{\partial \eta} \tag{46}$$

$$\frac{\partial}{\partial x} = \frac{\partial \eta}{\partial x}\frac{\partial}{\partial \eta} + \frac{1}{L}\frac{\partial}{\partial \xi} \tag{47}$$

By use of (46) and (47), the momentum Equation (37) may be transformed to:

$$\xi u' \frac{\partial u'}{\partial \xi} - \left(\xi \frac{\partial \psi}{\partial \xi} + \frac{\psi}{2}\right)\frac{\partial u'}{\partial \eta} = \tag{48}$$

$$\frac{\xi}{U}\left(\frac{\rho_\infty}{\rho} - u'^2\right)\frac{\partial U}{\partial \xi} + \frac{\partial}{\partial \eta}\left(\ell \frac{\partial u'}{\partial \eta}\right)$$

where

$$\ell \equiv \frac{\mu \rho}{\mu_o \rho_o} \tag{49}$$

and j_y in the boundary layer at any x has been taken to be equal to j_y in the free stream at the same x. This later assumption is discussed in Chapter IV. The $J_y B$ term has disappeared due to the substitution of dP_∞/dx from the free stream momentum equation.

The energy equation is transformed by the same methods and assumptions to:

$$\xi u' \frac{\partial \theta}{\partial \xi} - \left(\xi \frac{\partial \psi}{\partial \xi} + \frac{\psi}{2}\right) \frac{\partial \theta}{\partial \eta} = \frac{\partial}{\partial \eta}\left(\frac{\ell}{Pr} \frac{\partial \theta}{\partial \eta}\right) - I_e J_y \xi^{1/2} \sqrt{Re_{o_L}} \frac{\partial(\theta \theta_e)}{\partial \eta} + \quad (50)$$

$$\ell(\gamma-1)M^2\left(\frac{\partial u'}{\partial \eta}\right)^2 + S_\infty \xi \frac{(\gamma-1)}{\gamma} \theta \left(\frac{J_y^2 + J_x^2}{\sigma'} - u'\right)$$

The additional relation needed to relate ψ to other dependent variables is found by operating on ψ with Equation (46) and using (42) to derive:

$$u' = \frac{\partial \psi}{\partial \eta} \quad (51)$$

Equations (48), (50), and (51) are then the flow equations to be solved in conjunction with the electrical characteristic equations derived in the next chapter.

Boundary Conditions

Before a solution of the differential Equations (48) and (50) is attempted, the velocity and temperature must be specified on three sides of the flow region to be solved. These three boundaries are taken to be the wall, free stream, and forward boundary. The specification of the dependent variable ψ on one boundary, the wall, is sufficient to solve the remaining differential Equation (51). The specification of the flow properties at these boundaries makes up the boundary conditions required for the boundary layer differential equations.

The wall boundary conditions consist of the no-slip velocity condition, the wall temperature, and the specification of a constant value for the stream function at the wall. These are written as:

$$\underline{\eta = 0 \; ; \quad 0 < \xi \leq 1}$$

$$u' = 0$$

$$\theta = \frac{T_w}{T_\infty} \tag{52}$$

$$\psi = 0$$

The free stream boundary conditions are approached asymptotically as η increases. The flow conditions are the free stream values given by the solution to Equations (31), (32), (33) and (34) in Chapter II. These values enter the transformed equations through the nondimensionalized parameters. This boundary condition may be expressed as:

$$\underline{\eta = \infty \; ; \quad 0 < \xi \leq 1}$$

$$u' = 1$$

$$\theta = 1 \tag{53}$$

At the forward boundary, the flow conditions are not as straightforward due to the transformation from y to η. In the x-y coordinate system, Figure 2, the velocity and temperature at the leading edge are equal to the free stream conditions for all values of y greater than zero. This follows from the fact that the boundary layer thickness is zero at this point. But in the η-ξ coordinates, Figure 3, the boundary layer thickness is approximately constant with respect to ξ and profiles for u' and θ exist close to the leading edge. These profiles must be specified as a boundary condition and may be found by examining

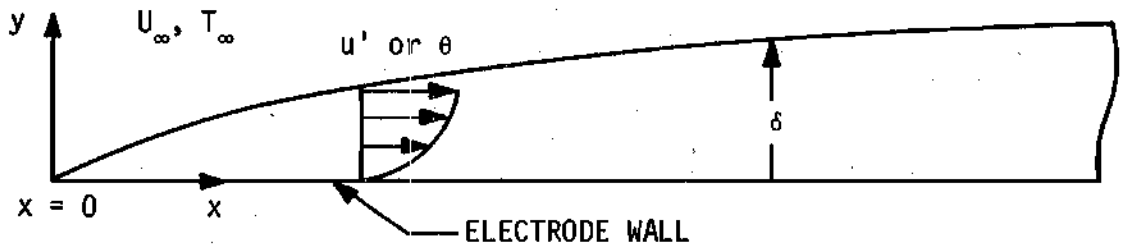

Figure 2. Boundary Layer in x-y Coordinate System

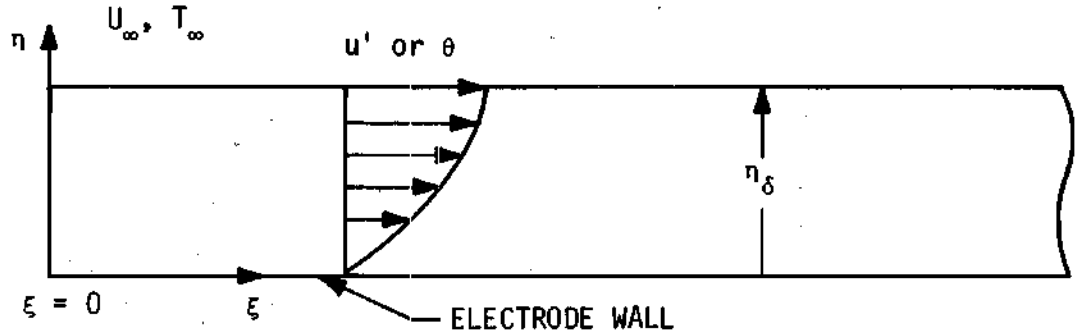

Figure 3. Boundary Layer in η-ξ Coordinate System

Equations (48), (50), and (51) as ξ becomes small. As the leading edge is approached, the terms which are multiplied by ξ become small and may be neglected. This gives the following equations.

$$-\frac{\psi}{2}\frac{du'}{d\eta} = \frac{d}{d\eta}\left[\ell \frac{du'}{d\eta}\right] \tag{54}$$

$$-\frac{\psi}{2}\frac{d\theta}{d\eta} = \frac{d}{d\eta}\left[\frac{\ell}{Pr}\frac{d\theta}{d\eta}\right] + \ell(\gamma-1)M^2\left[\frac{du'}{d\eta}\right]^2 \tag{55}$$

$$u' = \frac{d\psi}{d\eta} \tag{56}$$

The partial derivatives are changed to full derivatives because ξ no longer appears as an independent variable except in conjunction with the free stream flow which is given as a boundary condition. These equations then describe the u' and θ profiles close to the leading edge and may be solved with only the wall and free stream conditions given. These solutions will provide the initial profiles as a boundary condition.

It should also be noted that these initial profiles are the locally similar profiles which exist in conventional non-MHD type boundary layers. This provides the information needed on conventional boundary layers so that a comparison can be made with the MHD boundary layers at the same initial conditions. In this way, the increase in heat transfer due to the MHD effects may be found by comparison with the initial profile results. This coincidence is a result of the MHD terms in the transformed coordinate system becoming negligible close to

the leading edge. The reason for these becoming small is that the MHD terms do not have the same dependence on the derivative $\partial/\partial y$ as the remaining flow terms in Equations (54) and (55). Except for the electron energy convection term, they are independent of this derivative.

Gas Properties

Solution of the momentum and energy Equations (48) and (50) requires specification of gas property parameters containing viscosity, thermal conductivity, specific heat, etc. The electrical properties are also needed and are the subject of Chapter IV.

The gas dealt with in this study is a 0.2 per cent potassium seeded argon mixture and, as has been noted previously, a perfect gas is assumed throughout. This is fully applicable at the relatively low pressures and high temperatures at which MHD devices operate. If a real gas compressibility factor is calculated from the Virial Equation of State[34] at 1 atmosphere and 2000°K:

$$\frac{p}{\rho RT} = 1.00015 \tag{57}$$

The value of R should be the weighted mean, on a mass basis, of the gas constants of the argon and potassium. Since the atomic weight of the two components are 39.944 for argon and 39.100 for potassium, the small percentage of potassium may be neglected which results in:

$$R = 208.141 \ \frac{\text{joules}}{\text{kg } ^\circ\text{K}} \tag{58}$$

Constant specific heats are applicable to about 10,000°K[17,32] which implies constant gamma. These are taken to be:

$$c_p = 520.5 \frac{\text{joules}}{\text{kg } ^\circ\text{K}} \tag{59}$$

$$\gamma = 1.667 \tag{60}$$

For the low pressures dealt with here the viscosity and thermal conductivity are functions of temperature only. This temperature dependence for a Lennard-Jones potential[35] is:

$$\mu = 2.6693 \times 10^{-5} \frac{\sqrt{W_A T}}{\Omega} \frac{\text{gm}}{\text{cm sec}} \tag{61}$$

$$\kappa = 1.9891 \times 10^{-4} \frac{\sqrt{T/W_A}}{\Omega} \frac{\text{calories}}{\text{cm sec } ^\circ\text{K}} \tag{62}$$

where T is in °K and Ω has the units of angstroms^2. The quantity Ω is a very slowly varying function of temperature and will be taken to be the value which exists at 1500°K which is:

$$\Omega = 9.440 \text{ angstroms}^2 \tag{63}$$

The effect of the 0.2 per cent by moles of potassium was calculated in this study by use of relations derived by Chapman and Cowling[36] for gas mixtures. This indicated an error of approximately 10 per cent would result from taking the viscosity and thermal conductivity of the

mixture to be equal to that of argon. This large error for only a small amount of potassium is due to its large cross section.

The parameters Pr and ℓ appearing in the momentum and energy equations may now be found. Since μ and κ have the same temperature dependence and c_p is constant, the Prandtl number becomes a constant or:

$$Pr = 0.667 \tag{64}$$

By use of (61), (62), and the equation of state, the variable ℓ may be expressed as a function of the boundary layer nondimensionalized temperature and free stream nondimensionalized pressure.

$$\ell = \frac{\rho\mu}{\rho_o\mu_o} = \sqrt{\frac{\bar{P}_\infty}{\theta' P_o}} \tag{65}$$

where the fact is used that the pressure in the free stream is equal to that in the boundary layer at the same ξ.

CHAPTER IV

ELECTRICAL CHARACTERISTICS

Introduction

Although it has not been thoroughly investigated, the nature of the electrical characteristics of the gas is the most dominant factor in determining the nature of MHD boundary layers.[6,20,23] The most important quantities are the Hall parameter and electrical conductivity which control the current densities. The effort made here is to derive and use expressions for these quantities which give reasonable accuracy and yet are adaptable to engineering calculations of boundary layers. This has not in the past been done. For example, the only work calculating the Hall currents in the boundary layers has assumed the Hall parameter to be a function of gas temperature only. This is not realistic as this study shows the Hall parameter may vary by a factor of ten or more at a constant gas temperature.

Current Density and Electric Fields

Relationships which must be satisfied by the current density quantities j_x and j_y are given by Ohm's law and current continuity. A decoupling of the current continuity equation:

$$\frac{\partial J_x}{\partial \xi} + \frac{\partial J_y}{\partial y'} = 0 \tag{66}$$

may be accomplished by looking at the magnitude of the deviation of J_y with respect to y' as one moves from the free stream, where J_y is equal to J_∞, through the boundary layer to the wall. This is given by (66) as:

$$J_\infty - J_{y_w} = - \int_0^\delta \frac{\partial J_x}{\partial \xi} \, dy' \tag{67}$$

where δ is the nondimensional boundary layer thickness. The derivative inside the integral is of the order of one or less and $\Delta y'$ is very small, of the order of δ. Therefore:

$$J_\infty - J_y \sim \delta \tag{68}$$

This indicates that the normal current through the boundary layer is essentially constant with respect to y' and may be set equal to the free stream value at the same ξ:

$$J_y(\xi, y') = J_\infty(\xi) \tag{69}$$

This condition, Equation (69), was assumed in deriving the transformed momentum and energy Equations (48) and (50).

A similar decoupling of one of Maxwell's relations, Faraday's law, may be accomplished with the result that the value of E_x may be assumed to be independent of y. The relation is:

$$\frac{\partial}{\partial \xi}\left[\frac{E_y}{UB}\right] - \frac{\partial}{\partial y'}\left[\frac{E_x}{UB}\right] = 0 \tag{70}$$

with the deviation of the axial electric field from its free stream value at the same axial position given by:

$$\left[\frac{E_x}{UB}\right]_\infty - \left[\frac{E_x}{UB}\right]_w = \int_0^\delta \frac{\partial}{\partial \xi}\left[\frac{E_y}{UB}\right] dy' \tag{71}$$

This integral is on the order of δ.

The free stream value of E_x is given by Equation (23) which when utilized with (24) gives:

$$\left[\frac{E_x}{UB}\right]_\infty = \beta_\infty J_\infty \tag{72}$$

This shows E_x/UB to be on the order of one and since it changes only on the order of δ with respect to y':

$$\frac{E_x}{UB} = \beta_\infty J_\infty \tag{73}$$

for all values of y at a given ξ with little loss of accuracy.

It should be noted that the derivatives, $\partial J_y/\partial y'$ and $\partial[E_x/UB]/\partial y'$, are on the order of one and Equations (73) and (69) cannot be used for finding these. But since these derivatives act over a very short distance, the values of J_y and E_x are changed very little from their free stream values.

Ohm's law for two-dimensional current flow is given in Chapter II, Equation (7). This yields the current components:

$$j_x = \sigma\left[E_x + vB - \frac{j_y\beta}{\sigma}\right] \tag{74}$$

$$j_y = \sigma\left[E_y - uB + \frac{j_x\beta}{\sigma}\right] \tag{75}$$

Using (72) in (74) and nondimensionalizing with variables defined by (217):

$$J_x = \sigma'\left[\beta_\infty J_\infty + v' + \frac{J_y\beta}{\sigma'}\right] \tag{76}$$

All these terms are of order one except v' which is very small and may be neglected. With this fact and Equation (69):

$$\frac{J_x}{J_\infty} = -\beta_\infty\left[\frac{\beta}{\beta_\infty} - \sigma'\right] \tag{77}$$

By use of the definition of β, this may be rearranged so that insight into the cause of the J_x may be seen.

$$\frac{J_x}{J_\infty} = \frac{\sigma\beta}{e}\left[\frac{1}{n_{e_\infty}} - \frac{1}{n_e}\right] \tag{78}$$

From this, it is demonstrated that the boundary layer Hall current occurs because of a change in electron density as one passes through the boundary layer. Since j_y is constant at a constant x, a change in n_e causes a change in the diffusion velocity V_e and E_x no longer balances the $(\bar{V}_e \times \bar{B})_x$ force.

Since j_y has been specified without the use of Equation (75), it may be used to yield the electric field E_y. This is needed to find the voltage loss caused by the boundary layer. The loss in generator voltage at any axial location due to the presence of one of the boundary layers is given by:

$$V_{loss} = \int_0^{H/2} (E_{y_\infty} - E_y)dy \tag{79}$$

where H is the channel height. This loss is better expressed as the height of free stream flow needed to make up this loss, i.e. the effective reduction of channel height due to boundary layer losses. This height is given by V_{loss}/E_{y_∞} and will be nondimensionalized with respect to L and termed "voltage loss displacement thickness," or VLDT.

$$VLDT = \int_0^{\delta} \left(1 - \frac{E_y}{E_{y_\infty}}\right) dy' \tag{80}$$

Using (75) for E_y and making a change of variable from y to η by using Equation (40):

$$VLDT = \sqrt{\frac{\xi P_o}{Re_L P_\infty}\sqrt{T'_\infty}} \int_0^{\eta_\delta} \frac{\theta}{K}\left[K - \left[\frac{K-1-\beta J_x}{\sigma'}\right] - u'\right]d\eta \qquad (81)$$

where η_δ is the value of η at the outer edge of the boundary layer. The quantity inside the integral is zero outside of the boundary layer.

Equation (81) demonstrates that if the electrical conductivity and velocity within the boundary layer are lower than their corresponding values in the free stream, a voltage loss is created. Also, if the electron density is lower than the free stream value, Equation (78) gives a positive value for J_x (due to J_∞ being negative) and this Hall current increases the value of the VLDT.

Electrical Conductivity

The working fluid in an MHD device becomes an electrical conductor due to ionization of the atoms caused by collisions of high thermal energy particles. The free electrons present may be accelerated by an electric field. This acceleration continues until a collision occurs with another particle where some of the excess energy may be lost. If this collision occurs with an atom, the energy transfer is inefficient due to the large difference in masses. This causes the electrons to attain a higher energy than the gas atoms and produces a two-temperature, or nonequilibrium, plasma.

The total energy transfer between the free electrons can be shown to be much higher than the transfer between the electrons and atoms.[37] This is due to three factors. The electron densities are large,

approximately 10^{13} cm^{-3}; the electron-electron cross section is larger than the electron-atom collision cross section, approximately $10^{-13}cm^2$ compared to $10^{-15}cm^2$; and the energy transfer in electron-electron collisions is approximately 10^5 times more efficient than electron-atom collisions. This indicates that the electrons may be treated as a separate gas in equilibrium at a higher temperature than the atoms. This electron gas temperature may be found by equating the energy which it receives from the effective electric field, to the energy given to other species through collisions.

This concept of a two-temperature plasma was applied to electron diffusion through gases some time ago, i.e. Reference (38). However, the first application of this model to MHD devices was by Kerrebrock.[39] In his work, Maxwell's energy distribution was taken for the electrons and the important suggestion was made that the electron gas could be considered to be in thermal equilibrium with the population of the excited states. This allows the electron density to be calculated by Saha's relation using the electron temperature, i.e.:

$$\frac{n_e n_{s_i}}{n_{s_n}} = 2G_s \left[\frac{2\pi m_e kT_e}{h^2}\right]^{3/2} \exp\left(-\frac{V_{i_s} e}{kT_e}\right) \qquad (82)$$

where:

G_s - statistical weighting function

h - Planck's constant

m_e - electron mass

T_e - electron temperature

V_i - first ionization potential

n - number density

$( )_e$ - denotes electron

$( )_i$ - denotes ion

$( )_n$ - denotes neutrals

$( )_s$ - species s

The two assumptions, Maxwellian distribution of electron energy and the applicability of Saha's equation evaluated at the electron temperature, are taken in this work. These assumptions have been taken in all two-temperature MHD work and therefore considerable work has been done to demonstrate their validity under typical MHD conditions. Ben Daniel and Tamor[40] show the applicability of Saha's equation evaluated at the electron temperature by solving a set of rate equations which describe the collisional and radiative rates at which the various electron states are populated and depopulated. However, a Maxwellian energy distribution of the electrons is assumed. Since the energy distribution and rate equations are dependent on each other, it is apparent that both assumptions must be investigated simultaneously. This has only recently been done by Shaw, et al.[41] The conclusion of this work is that for typical conditions in an MHD device both assumptions will give good results, particularly if radiation escape is small.

Electron Momentum

The conservation of momentum in the electron gas is carried out by use of the momentum moment of Boltzmann's equation written for the electron species at steady state as:

$$\nabla \cdot [n_e m_e(\bar{w}_o w_{o_j}) + \bar{w}_o V_{e_j} + \bar{V}_e w_{o_j})] + \tag{83}$$

$$(\nabla \cdot \bar{\bar{P}}_e)_j - n_e m_e[E_j^* + (\bar{V}_e x \bar{B})_j] =$$

$$\left[\frac{\partial}{\partial t}(n_e m_e <w_{e_j}>)\right]_c$$

where w_e is the electron velocity and w_o is the mass average velocity of the total gas.

If the asymptotic solution of the preceding equation is approached in distances short compared to the distances over which changes in gas properties occur, a uniform plasma at local conditions may be assumed. All spatial derivatives in Equation (83) may then be set to zero. This may be viewed as a quasi-steady state assumption. As in other work, this assumption must be taken here in order to arrive at a set of equations which are tractable. That it is a reasonable one is demonstrated in calculations by Kerrebrock,[6] where the relaxation length was found to be approximately 10^{-2} centimeters. This is smaller than the typical boundary layer thickness of about one centimeter which indicates that the uniform plasma assumption should be applicable when dealing with the electron gas.

Implementing this quasi-steady assumption into Equation (83):

$$-n_e e[\bar{E}^* + (\bar{V}_e x \bar{B})] = \left[\frac{\partial}{\partial t}(n_e m_e <\bar{w}_e>)\right]_c \tag{84}$$

where the right-hand side represents the rate of loss of the electron

momentum through collisions with other particles, i.e. gas atoms and ions.

The momentum exchange between two Maxwellian gases at different temperatures has been calculated by Morse.[42] Summing his expression over all the species with which the electron gas exchanges momentum gives the values of the collisional term:

$$\left[\frac{\partial}{\partial t}\left(n_e m_e \langle \bar{w}_e \rangle\right)\right]_c = \tag{85}$$

$$\sum_s \frac{\pi(m_e m_s)^{5/2} n_e n_s \bar{V}_e}{K_T^2 V_e^3 (2\pi k)^{3/2}(m_e+m_s)(m_s T_e + m_e T_s)^{3/2}} \cdot$$

$$\int_0^\infty e^{-K_T(w_e^2+V_e^2)} \sigma_{ms}(w_e) w_e^4 [2K_T V_e \cosh(2K_T w_e V_e) -$$

$$\sinh(2K_T w_e V_e)] dw_e$$

where:

$$K_T = \left(\frac{2kT_e}{m_e} + \frac{2kT_s}{m_s}\right) \tag{86}$$

and σ_{ms} is the momentum transfer cross section given by:

$$\sigma_{ms} = \int (1-\cos\theta) I_s(w_e,\theta) d\Omega \tag{87}$$

Here, $I_s(w_e,\theta)$ is the differential collision cross section and $d\Omega$ is the differential solid angle into which scattering occurs.

For MHD conditions, the electron drift velocity, V_e, is approximately 10^{-3} that of the root-mean-square electron particle velocity. Therefore,

$$V_e << w_e \tag{88}$$

By expanding the hyperbolic functions in (85) into series, all the terms except the first may be neglected due to Equation (88). Using this result and the fact that the electron mass, m_e, is much smaller than the species mass, m_s, Equation (85) may be written:

$$\left[\frac{\partial}{\partial t}\left(n_e m_e \langle \bar{w}_e \rangle\right)\right]_c = \left(\frac{2km_e}{\pi}\right)^{1/2} \frac{n_e \bar{V}_e m_e^3}{3k^3 T_e^{5/2}} \cdot \sum_s n_s \int_0^\infty \exp\left(-\frac{m_e w_e^2}{2kT_e}\right) \sigma_{ms} w_e^5 dw_e \tag{89}$$

From (84) and (89):

$$\bar{j} = \frac{3n_e e^2}{8}\left(\frac{\pi}{2kT_e m_e}\right)^{1/2}\left[\sum_s n_s\left(\frac{m_e}{2kT_e}\right)^3 \cdot \int_0^\infty \exp\left(-\frac{m_e w_e^2}{2kT_e}\right)\sigma_{ms} w_e^5 dw_e\right]^{-1}\left[\bar{E}^* + \bar{V}_e \times \bar{B}\right] \tag{90}$$

Comparing Equation (90) with Ohm's law, Equation (7), the electrical conductivity is given as:

$$\frac{1}{\sigma} = \frac{4}{3}\left(\frac{8kT_e}{\pi m_e}\right)^{1/2} \frac{m_e}{n_e e^2} \sum_s n_s Q_{e_s} \tag{91}$$

where:

$$Q_{es}(T_e) = \left(\frac{m_e}{2kT_e}\right)^3 \int_0^\infty w_e^5 \exp\left(-\frac{m_e w_e^2}{2kT_e}\right) \sigma_{ms}\, dw_e \tag{92}$$

This effective cross section, Q_{es}, is a function of only the species and electron temperature. It has been calculated and plotted in Reference (26) for Cs, K, Xe, Kr, He, A, and Ne using total collision cross section data from Massey and Burhop[43] in place of the momentum transfer cross section, σ_{ms}. That this substitution is valid for electron energies below one or two electron-volts is seen in a plot of the two cross sections for argon obtained by Massey and Burhop and shown in Reference (10).

A plot of Q_{es} as a function of electron temperature for argon and potassium is shown in Figure 4.[44]

For potassium seeded argon, the electrical conductivity, Equation (91), becomes:

$$\frac{1}{\sigma} = \frac{4}{3}\left(\frac{8kT_e}{\pi m_e}\right)^{1/2} \frac{m_e}{n_e e^2} \left[n_A Q_{eA} + n_K Q_{eK} + n_i Q_{ei}\right] \tag{93}$$

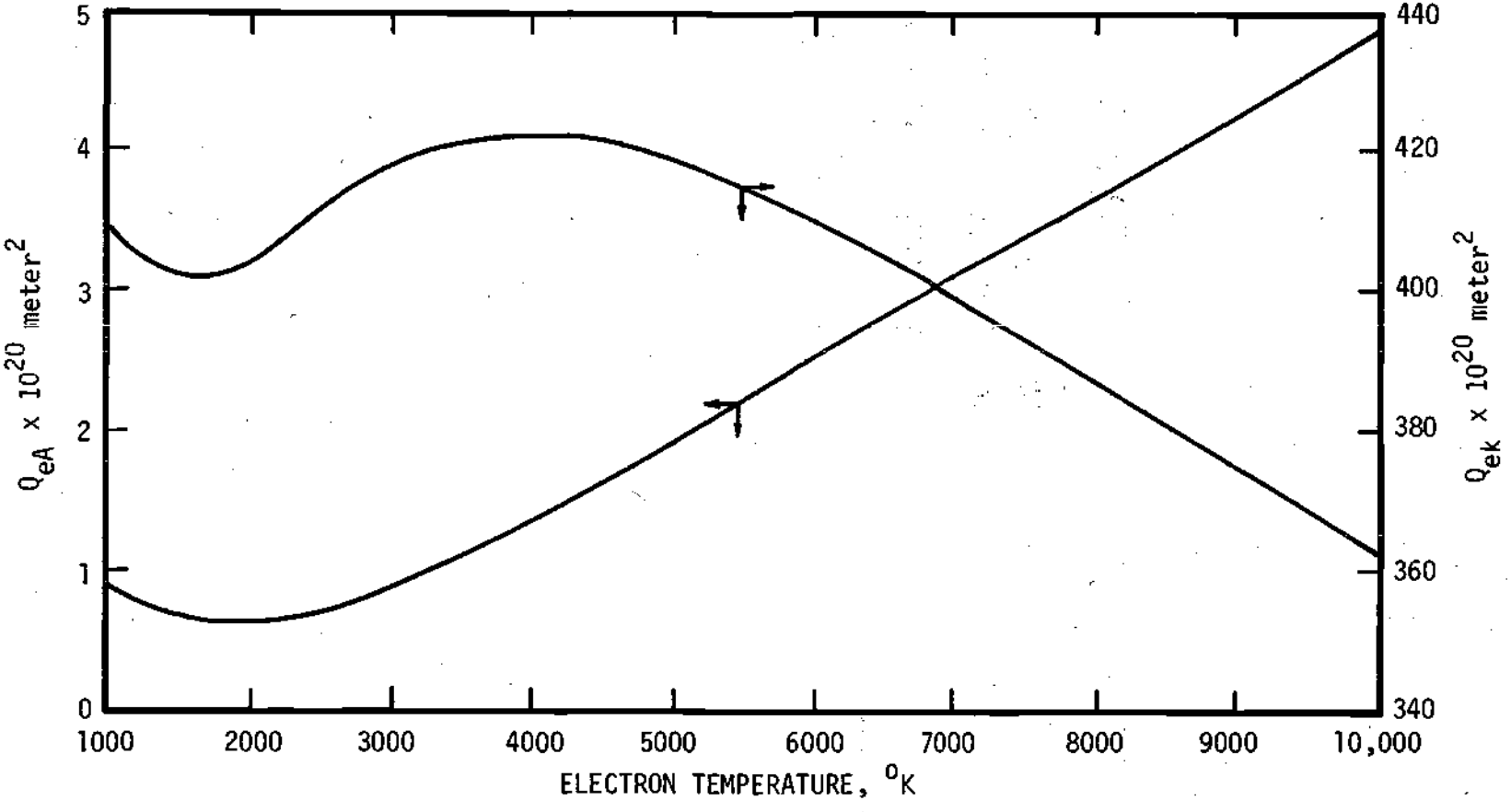

Figure 4. Effective Cross Sections Q_{eK}, Q_{eA} Versus Electron Temperature

where Q_{ei} is the effective cross section for the electron-ion collision.

By defining $1/\sigma_A$, $1/\sigma_K$, and $1/\sigma_{ei}$ as the resistivity due to the electron collisions with argon neutrals, potassium neutrals, and ions, respectively:

$$\frac{1}{\sigma} = \frac{1}{\sigma_A} + \frac{1}{\sigma_K} + \frac{1}{\sigma_{ei}} \tag{94}$$

By comparing (94) with (93):

$$\frac{1}{\sigma_A} = Z_e n_A Q_{eA} \tag{95}$$

$$\frac{1}{\sigma_K} = Z_e n_K Q_{eK} \tag{96}$$

$$\frac{1}{\sigma_{ei}} = Z_e n_i Q_{ei} \tag{97}$$

where:

$$Z_e = \frac{4}{3}\left(\frac{8kT_e}{\pi m_e}\right)^{1/2} \frac{m_e}{n_e e^2} \tag{98}$$

The resistivity due to electron-ion collisions has been calculated by Spitzer and Harm[45] as:

$$\frac{1}{\sigma_{ei}} = \frac{65.3}{T_e^{1/2}} \ln\left[\frac{12\pi}{e^3 n_e^{1/2}} (\varepsilon_o k T_e)^{1/2}\right] \text{ohm-m} \tag{99}$$

where ε_o is the dielectric constant for space.

Utilizing (99) in (94):

$$\frac{1}{\sigma} = \frac{4}{3}\left(\frac{8kT_e}{\pi m_e}\right)^{1/2} \frac{m_e}{n_e e^2}\left[n_A Q_{eA} + n_K Q_{eK}\right] + \qquad (100)$$

$$\frac{65.3}{T_e^{3/2}} \ln\left[\frac{12\pi}{e^3 n_e^{1/2}} (\varepsilon_o kT_e)^{3/2}\right] \text{ohm-meters}$$

which is the expression to be used in this work.

It is of interest to note that the addition of the resistivities in Equation (94) is not an assumption, as has been necessary in other electrical conductivity work,[46,47] but is a direct result of the derivation.

Electron Energy

Equation (100) gives the electrical conductivity as a function of electron density and electron temperature. Saha's equation, (82), gives an expression for electron density but the electron temperature still is not known. This can be found by an energy balance on the electron gas.

The energy moment of Boltzmann's Equation needed in this case is $\frac{1}{2} m_e g_e^2$ where g_e is the electron velocity in the coordinate system moving with the mass average velocity of the gas, w_o.

$$\bar{g}_e = \bar{w}_e - \bar{w}_o \qquad (101)$$

This necessitates transforming Boltzmann's equation from the variable $\bar{w}_e$ to the variable $\bar{g}_e$. This is done by Chapman and Cowling.[36] When the $\frac{1}{2} m_e g_e^2$ moment of Boltzmann's transformed equation is taken and the asymptotic solution is assumed, the justification of which has already been discussed in deriving the electron momentum equation, the result is derived:

$$-\bar{j} \cdot [\bar{E} + \bar{v}_o \times B] = \left[\frac{\partial}{\partial t}\left(n_e \left\langle \frac{1}{2} m_e g_e^2 \right\rangle\right)\right]_c \qquad (102)$$

This equation balances the energy which the electrons receive from the effective electric field to the energy lost in collisions with other particles.

The energy transfer term due to collisions on the right-hand side has been calculated by Morse[42] for Maxwellian gases at different temperatures and is written:

$$\left[\frac{\partial}{\partial t} n_e \left\langle \frac{1}{2} m_e g_e^2 \right\rangle\right] = \sum_s \left[\frac{2\pi (m_e m_s)^{5/2} n_e n_s}{(2\pi k)^{3/2}(m_e+m_s)^2 (m_e T_s + m_s T_e)^{5/2}}\right] \cdot \qquad (103)$$

$$\left\{\frac{m_e m_s (T_s - T_e)}{K_T V_e} \int_o^\infty e^{-K_T(g_e^2+V_e^2)} \sigma_{ms} g_e^4 \sinh(2 g_e K_T V_e dg_e\right.$$

$$\left. + \frac{m_s T_e}{2K_T^2 V_e} \int_o^\infty e^{-K_T(g_e^2+V_e^2)} \sigma_{ms} g_e^2 [2 g_e K_T V_e \cosh(2 g_e K_T V_e) - \right.$$

$$\sinh(2g_e K_T V_e)]dg_e$$

Making the same assumptions as in the electron momentum derivation, i.e.,

$$m_e << m_s$$

$$V_e << g_e$$

expanding the hyperbolic functions into a series and neglecting all terms of order higher than the fourth:

$$\left[\frac{\partial}{\partial t} n_e \left\langle \frac{1}{2} m_e g_e^2 \right\rangle\right]_c = \sum_s \frac{16k m_e^{1/2} n_e n_s T_e^{1/2}}{(2\pi k)^{1/2} m_s} \left[(T_s - T_e)k + \frac{j^2 m_s}{3n_e^2 e^2}\right] Q_{es} \quad (104)$$

Equations (102) and (104) then yield:

$$-\bar{j} \cdot [\bar{E} + \bar{v}_o \times \bar{B}] = 4n_e k^2 \sqrt{\frac{8m_e T_e}{\pi k}} (T_s - T_e) \sum_s \frac{n_s}{m_s} Q_{es} \quad (105)$$

$$+ \frac{j^2 4k}{3n_e e^2} \sqrt{\frac{8m_e T_e}{\pi k}} \sum_s n_s Q_{es}$$

When $\bar{j}$ is dotted with Ohm's law, Equation (7), it is found:

$$-\bar{j} \cdot (\bar{E} + \bar{w}_o \times \bar{B}) = -\frac{j^2}{\sigma} \quad (106)$$

where the vector identity has been used:

$$(\vec{j} \times \vec{B}) \cdot \vec{j} = 0 \tag{107}$$

If the masses of all the species with which the electrons collide are approximately equal, then m_s may be brought outside the summation sign in Equation (105). Since the masses of argon and potassium are 39.955 amu and 39.111 amu, respectively, this may be done for the particular case of potassium seeded argon.

Therefore, taking m_s to be constant and using Equations (106) and (91), Equation (105) is reduced to:

$$j^2 = \frac{3e^2 n_e^2 k(T_e - T)}{2m_A} \tag{108}$$

This simplification arises from the fact that a group of terms, including the summation, in the right-hand side of (105) is equal to the already derived electrical conductivity expression, Equation (91).

Electron Density

As is discussed in the introduction to the electrical conductivity section of this chapter, the electron density is to be obtained from Saha's relation evaluated at the electron temperature. Originally the ionization of only the potassium atoms was considered in this work, which was published by Shelton and Carlson.[28] Subsequently, Dowdy[29] carried out experiments at very high electron temperatures which required the inclusion of the argon ionization. Saha's equation for argon was therefore added by Dowdy to this original work and will be included here also. However, a different method of solution is used here and the argon ionization is only important at current densities

above 100 amps/cm^2, which is higher than is encountered in the MHD generator considered in this study.

From continuity of species and electrical charge:

$$n_{K_i} + n_{A_i} = n_e \tag{109}$$

$$n_{A_n} + n_{A_i} = n_A \tag{110}$$

$$n_{K_n} + n_{K_i} = n_K \tag{111}$$

Also, Dalton's law of partial pressures is needed:

$$p = (n_A + n_K + n_e)kT \tag{112}$$

By definition, the seeding fraction is:

$$F \equiv \frac{n_K}{n_A} \tag{113}$$

Writing Saha's Equation (82) for argon and potassium and using the above five equations, the variables n_{K_i}, n_{A_i}, n_K, n_A, n_{K_n}, and n_{A_n} may be eliminated leaving a cubic equation in n_e:

$$n_e^3 + An_e^2 + Bn_e + C = 0 \tag{114}$$

where:

$$A = f_K + f_A \tag{115}$$

$$B = f_A f_K - \frac{P(f_K F + f_A)}{kT(F + 1)}$$

$$C = - \frac{P f_A f_K}{kT}$$

$$f_K = 2G_k \left(\frac{2\pi m_e kT_e}{h^2} \right)^{3/2} \exp\left(- \frac{V_{i_K} e}{kT_e} \right)$$

$$f_A = 2G_A \left(\frac{2\pi m_e kT_e}{h^2} \right)^{3/2} \exp\left(- \frac{V_{i_A} e}{kT_e} \right)$$

The numerical values of the statistical weighting functions and the ionization potentials which are used here are:

$$\begin{aligned} G_K &= \frac{1}{2} && \text{Reference (32)} \\ G_A &= 5 && \text{Reference (32)} \\ V_{iK} &= 4.318 && \text{Reference (48)} \\ V_{i_A} &= 15.68 && \text{Reference (48)} \end{aligned} \qquad (116)$$

The algebraic solution to the cubic Equation (114) may now be found for a given gas pressure, gas temperature, and electron temperature. Only one root is positive and real.

Solution of Electrical Conductivity Equations

The controlling equations which describe the electrical characteristics of the gas and must be solved are Equations (100), (108), and (114).

The electrical conductivity is usually needed as a function of gas pressure, gas temperature, and current density. However, when these three variables are specified and a solution of the three equations attempted, a trial and error solution is required. This difficulty is overcome if the electron temperature is specified and the current density calculated.

The procedure is to specify pressure, gas temperature, electron temperature, and seeding fraction and calculate:

(1) electron density by (114)

(2) current density by (108)

(3) electrical conductivity by (100) and Figure 4.

The electron temperature may then be varied to produce σ as a function of j. Figures 5 and 6 show the resulting graphs for various temperatures, pressures, and seeding fractions calculated by the Univac 1108 computer program in Appendix B.

The most important aspect of these results is the relative maximum which occurs in the σ vs j curves. This is very important in producing current stability. Previous calculations[37] have shown a continuously increasing electrical conductivity versus current density curve. This leads to current concentrations due to the increasing electrical conductivity producing larger currents and the larger currents in return producing larger electrical conductivities. This is discussed thoroughly by Kerrebrock in Reference (37) using the current relationship:

$$\frac{\sigma}{\sigma^*} \approx \left(\frac{j}{j^*}\right)^{\alpha} \tag{117}$$

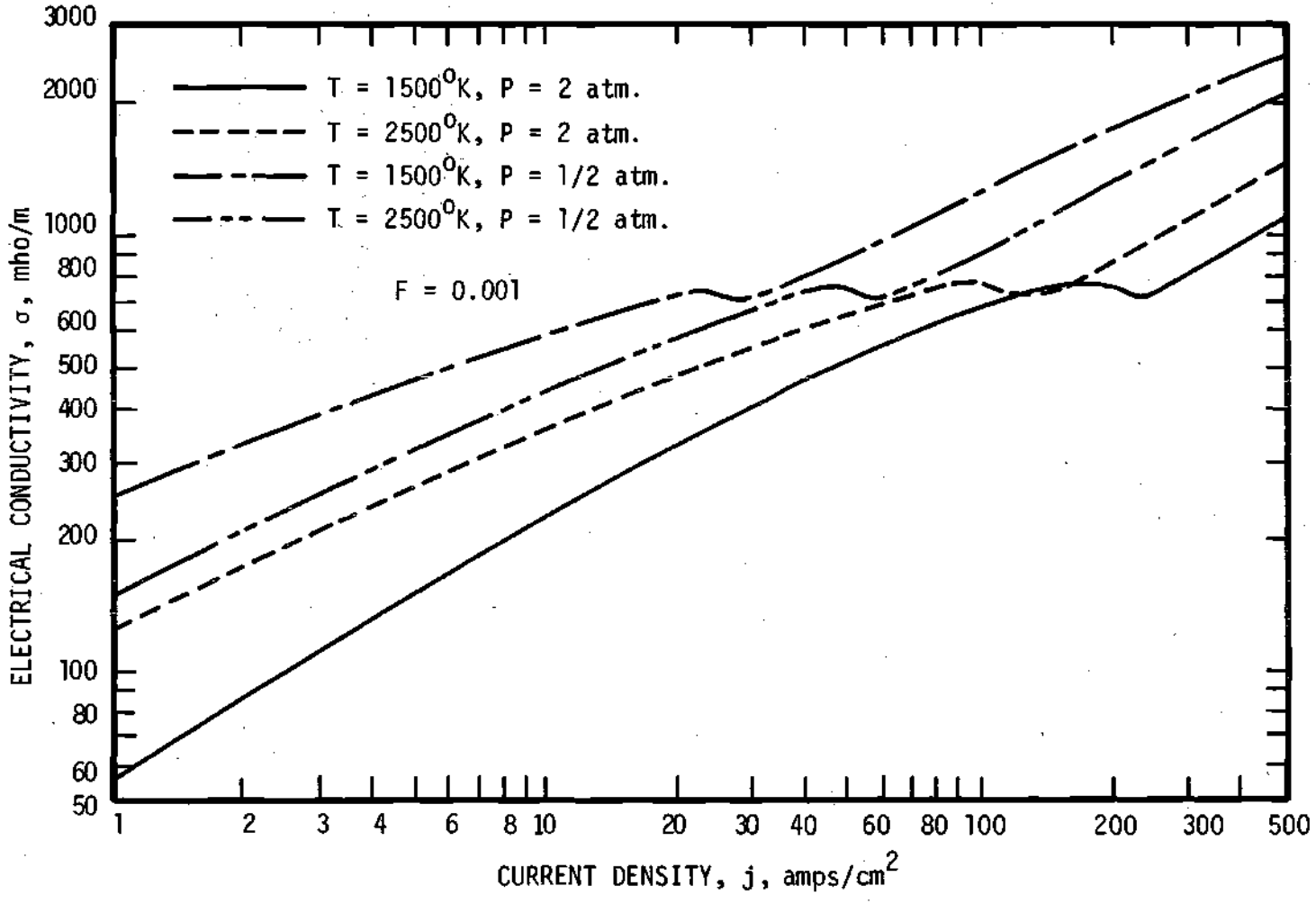

Figure 5. Electrical Conductivity versus Current Density, F=0.1%

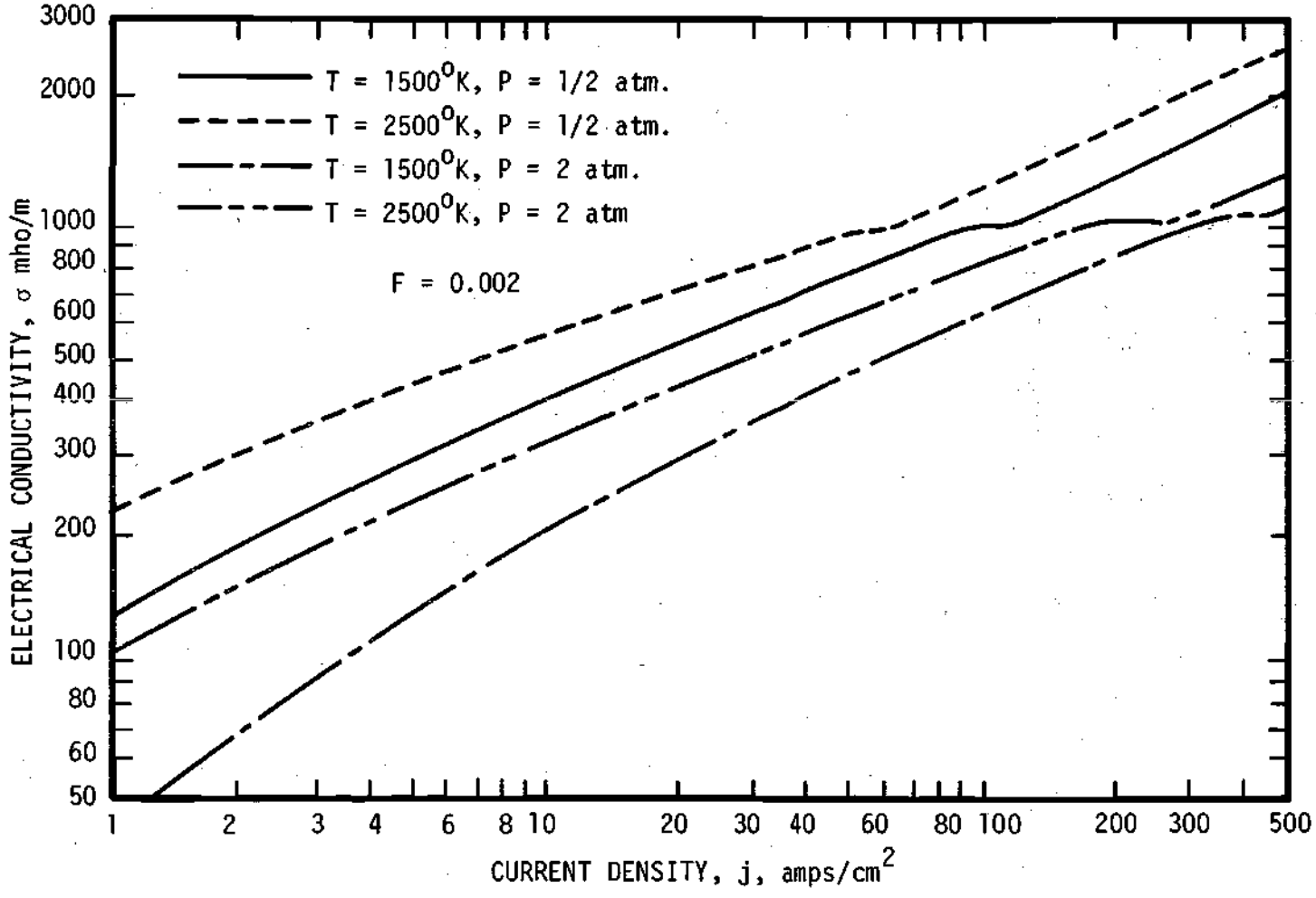

Figure 6. Electrical Conductivity versus Current Density, F=0.2%

Kerrebrock shows that instability should occur in highly ionized gases but states that, even though experiments have been carried out in this region, none have demonstrated it. The relative maximum, or plateau in some cases, would account for the lack of observed instability in potassium seeded argon experiments.

The relative maximum is a result of the Ramsauer effect in the electron-argon cross section. This is seen in Figure 4. At electron temperatures above 2000°K increasing electron temperatures lead to larger electron-argon cross sections, tending to reduce the electrical conductivity. At the same time, increasing electron temperatures create additional electrons which tend to increase the electrical conductivity. At large percentages of potassium ionization, the number of additional electrons produced by increasing electron energies becomes small and the increasing cross section dominates. When the argon ionization becomes significant, sufficient additional electrons are produced by the argon to again increase σ with increasing electron energies.

The lower the seeding fraction, the more pronounced the relative maximum becomes. This is due to the decreasing collision cross section of potassium which tends to offset the Ramsauer effect of argon above electron temperatures of 4000°K.

The existence of this relative maximum has been experimentally demonstrated by Dowdy[29] at a seeding fraction of .002, which was the minimum capacity of his apparatus. After correction for radiation, the experimental data were in excellent quantitative agreement with these theoretical values. This agreement is as good or better than in other

work which includes an arbitrary electron energy loss factor. The present analysis contains no arbitrary constants. This lends substantial validity to the use of these calculations in the present boundary layer work.

Radiation corrections were not attempted here as they are geometry dependent and Dowdy's work predicts a relatively small correction at 30 amps/cm^2, which is the approximate current density in this study.

Hall Parameter

The Hall parameter may be found from values resulting from the electrical conductivity calculations. This is given by:

$$\beta = \frac{\sigma B}{n_e e} \tag{118}$$

The quantity β/B is shown plotted in Figures 7 and 8 for various pressures, temperatures and seeding fractions. This is one of the controlling parameters in determining the axial currents in the boundary layers.

Related Electrical Conductivity Expressions

The only nonequilibrium conductivity expressions used in boundary layer work has been by Kerrebrock,[6] and Hale and Kerrebrock.[14] They utilized the expression:

$$\frac{\sigma}{\sigma^*} = \left(\frac{j}{j^*}\right)^{\alpha} \exp\left[\phi\left(\frac{T}{T^*} - 1\right)\right] \tag{119}$$

where the * superscript denotes a reference condition. In their works

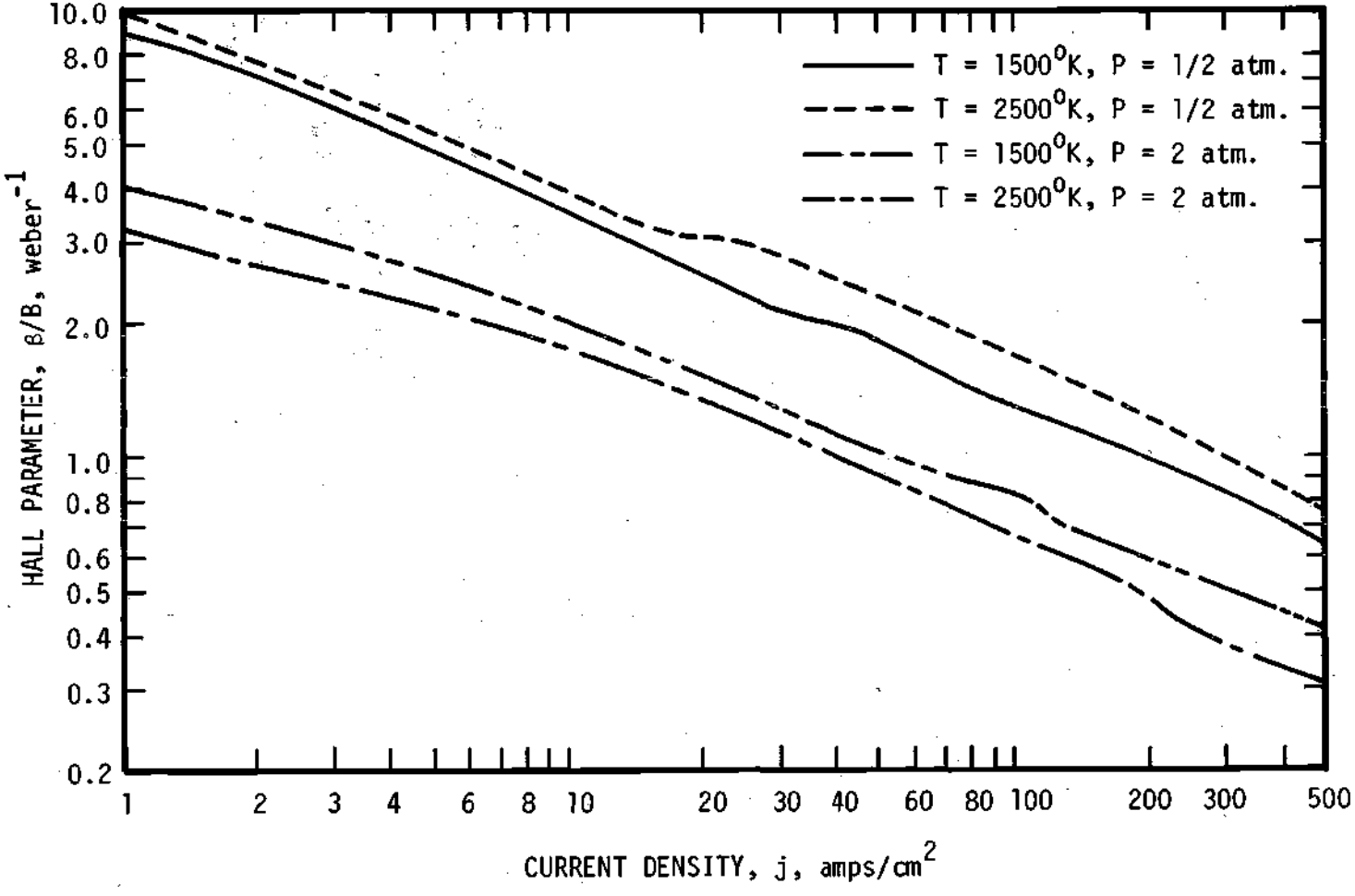

Figure 7. Hall Parameter versus Current Density, F=0.1%

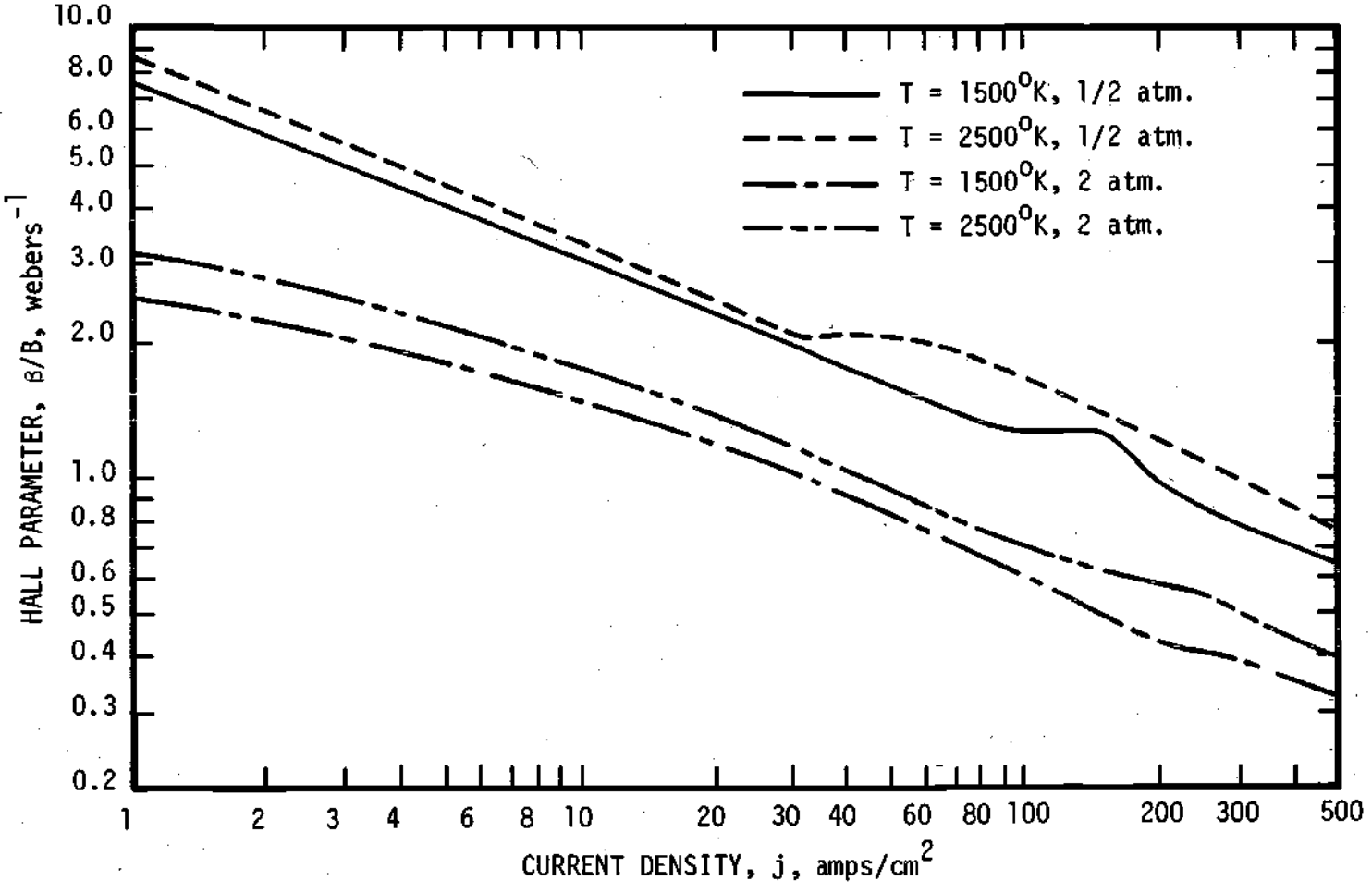

Figure 8. Hall Parameter versus Current Density, F=0.2%

a constant free stream σ was taken and therefore was used as a reference for the boundary layer σ. The parameters α and ϕ are constants, which for potassium seeded argon, are chosen as:[14]

$$\alpha = 0.8$$

$$\phi = 3$$

The only work including Hall currents in boundary layers[14] used the relation:

$$\frac{\beta}{\beta^*} = \frac{T}{T^*} \tag{120}$$

These relations, (119) and (120), are very simple compared to the complex expressions derived in the present work. Therefore, Kerrebrock and Hale's relations, (119) and (120), will be used in the boundary layer equations as well as the results of the present work, (100), (108), (114), and (119), to determine the accuracy of the simple approximations. If the results are not appreciably different, the extra complexity is unwarranted in the boundary layer.

CHAPTER V

SOLUTION OF EQUATIONS

Free Stream

The equations describing the free stream flow are derived in Chapter II, Equations (31) through (33). These may be expressed as one differential equation and four algebraic relations.

$$\frac{\partial \Gamma}{\partial \xi} = S_o \sigma'_\infty (K-1) \tag{121}$$

$$\frac{p}{p_o} = \Gamma \tag{122}$$

$$T'_\infty = \Gamma^{\frac{(\gamma-1)K}{\gamma}} \tag{123}$$

$$J = \sigma'_\infty (K-1) \tag{124}$$

$$\sigma'_\infty = \sigma'_\infty \left(\frac{p}{p_o}, T'_\infty, J \right) \tag{125}$$

where $\sigma_\infty \left(\frac{p}{p_o}, T'_\infty, J \right)$ is a function given by Equations (100), (108), and (114). The value of σ'_∞ for a specified pressure, gas temperature, and current density must be found by a trial and error solution of these three equations. This is done by assuming an electron temperature and solving the equations for the current density and electrical conductivity.

If the current density does not agree with the desired value, a new trial electron temperature is picked. This continues until the desired current density is derived by the calculation.

Since the function σ'_∞ is not known explicitly, these equations must be solved numerically. This is accomplished by using a forward difference approximation to Equation (121):

$$\left.\frac{\partial \Gamma}{\partial \xi}\right|_{\xi_m} = \frac{\Gamma_{m+1} - \Gamma_m}{\Delta\xi} \tag{126}$$

where $(\ )_m$ is the value at $(m-1)\Delta\xi$ and $\Delta\xi$ is the step size desired. Rewriting Equations (121) through (125) in finite difference form:

$$\Gamma_{m+1} = \Delta\xi\ S_o\ \sigma'_{\infty_m}(K-1) + \Gamma_m \tag{127}$$

$$\left(\frac{p}{p_o}\right)_{m+1} = \Gamma_{m+1} \tag{128}$$

$$T'_{\infty_{m+1}} = (\Gamma_{m+1})^{\frac{(\gamma-1)K}{\gamma}} \tag{129}$$

$$J_{m+1} = \sigma'_{\infty_{m+1}}(K-1) \tag{130}$$

$$\sigma'_{\infty_{m+1}} = \sigma'_{\infty_{m+1}}\left(\left(\frac{p}{p_o}\right)_{m+1},\ T'_{\infty_{m+1}},\ J_{m+1}\right) \tag{131}$$

with the boundary conditions given as:

$$\Gamma_1 = 1 \tag{132}$$

$$(\sigma'_\infty)_1 = 1 \tag{133}$$

All equations are solved for m equal to one and then m is increased by one and the process repeated. Equations (127) through (129) present no problem by this method since all values on the left-hand side are given in terms of values at m, all of which are known, or values at m+1 which have already been calculated in previous equations. However, Equations (130) and (131) are expressed in terms of values at m+1 given by the other and must be solved by trial and error. This is carried out by picking a value for J_{m+1} and solving (131). The resulting $\sigma'_{\infty_{m+1}}$ is used to calculate J_{m+1} from (130). If the value picked for $J_{\infty_{m+1}}$ does not agree with the calculated value from (130), then this calculated value for J_{m+1} is used as the new approximation and the routine repeated. This continues until the value of J_{m+1} used in (131) agrees with the value calculated from (130). Since the solution of (131) is a trial and error solution in itself, this routine involves a "double" trial and error technique, where both T_e and J must be iterated simultaneously.

This is programmed in Fortran V language for the Univac 1108 computer at the Rich Electronic Computer Center of Georgia Institute of Technology. The entire program is shown in Appendix C which computes the free stream as well as the boundary layer solution. It is broken up into subroutines such that the free stream equations are solved by subroutine FRST for any values of M_o, S_o, and K input from the main

program. All constants are also input through the main program which calls the subroutine as needed.

Initial Profile

The initial profile in the boundary layer is given by the solution to Equations (54) through (56). For constant freestream velocity, these may be expressed as five first order differential equations:

$$\frac{dX_1}{d\eta} = -\frac{X_1 X_3}{2\ell} = \dot{X}_1(X_1, X_3) \tag{134}$$

$$\frac{dX_2}{d\eta} = \frac{X_1}{\ell} = \dot{X}_2(X_1, \ell) \tag{135}$$

$$\frac{dX_3}{d\eta} = X_2 = \dot{X}_3(X_2) \tag{136}$$

$$\frac{dX_4}{d\eta} = -\frac{PrX_4X_3}{2\ell} - \frac{(\gamma-1)M_o^2X_1^2}{\ell} \tag{137}$$

$$= \dot{X}_4(X_1, X_3, X_4, \ell)$$

$$\frac{dX_5}{d\eta} = \frac{X_4 Pr}{\ell} = \dot{X}_5(X_4, \ell) \tag{138}$$

where:

$$X_1 \equiv \ell \frac{d^2\psi}{d\eta^2}$$

$$X_2 \equiv \frac{d\psi}{d\eta} = u'$$

$$X_3 \equiv \psi$$

$$X_4 \equiv \frac{\ell}{Pr} \frac{d\theta}{d\eta} \tag{139}$$

$$X_5 \equiv \theta$$

$$\ell = \sqrt{X_5^{-1}}$$

The boundary conditions at the wall and free stream are:

$\eta = 0$	$\eta = \infty$
$X_2 = 0$	$X_2 = 1$
$X_3 = 0$	$X_5 = 1$
$X_5 = \theta_w$	

(140)

This set of simultaneous differential Equations (134) through (138) may be solved by the Runga-Kutta method generalized for simultaneous differential equations. Using the Kutta-Simpson one-third rule:[49]

$$X_{n_{m+1}} = X_{n_m} + \frac{1}{6}\left(\Delta^1 X_{n_m} + 2^2 X_{n_m} + 2^3 X_{n_m} + \Delta^4 X_{n_m}\right) \tag{141}$$

$$\Delta^1 X_{n_m} = \Delta\eta \cdot \dot{X}_n\left(X_{1_m}, X_{2_m}, X_{3_m}, X_{4_m}, X_{5_m}, \ell_m\right)$$

$$\Delta^2 X_{n_m} = \Delta\eta \cdot \dot{X}_n\left(X_{1_m} + \frac{1}{2}\Delta^1 X_{1_m},\ X_{2_m} + \frac{1}{2}\Delta^1 X_{2_m},\ \cdots \right. \tag{142}$$

$$\left. \cdots,\ X_{5_m} + \frac{1}{2}\Delta^1 X_{5_m}\right)$$

$$\Delta^3 X_{n_m} = \Delta\eta \cdot \dot{X}_n\left(X_{1_m} + \frac{1}{2}\Delta^2 X_{1_m},\ \cdots,\ X_{5_m} + \frac{1}{2}\Delta^2 X_{5_m}\right)$$

$$\Delta^4 X_{n_m} = \Delta\eta \cdot \dot{X}_\eta\left(X_{1_m} + \Delta^3 X_{1_m},\ X_{2_m} + \Delta^3 X_{2_m},\ \cdots \right.$$

$$\left. \cdots,\ X_{5_m} + \Delta^3 X_{5_m}\right)$$

where n is an integer stepped between one and five to produce five sets of five equations each and $(\ )_m$ is the value at the distance $(m-1)\Delta\eta$ above the plate at ξ equal to zero.

The set of 20 Equations (142) are first calculated for m equal to one and then the five variables at $(\ )_2$ may be calculated by the five equations of set (141). The integer m is stepped up one and the routine repeated. This requires knowledge of all five variables X_1 through X_5 at the wall. The boundary conditions only give X_2, X_3, and X_5 at the wall. Therefore, X_1 and X_4 must be approximated at η equal to zero and the equations solved for increasing m (corresponding to increasing η) until X_2 and X_5 become constant. If the approximations of $X_1(0)$ and $X_4(0)$ were of sufficient accuracy, then $X_2(\infty)$ and $X_5(\infty)$ will become constant at the value of one, which is their proper boundary condition (140). If they are not equal to one, then new initial values of X_1 and X_4, $X_1(0)$ and $X_4(0)$, must be tried until X_2 and X_5 become constant at one for large values of η.

The iteration procedure to arrive at the proper initial values of X_1 and X_4 is as follows. Two closely spaced values for each of the variables $X_1(0)$ and $X_4(0)$ are used and the values at which X_2 and X_5 become constant, $X_2(\infty)$ and $X_5(\infty)$, are found. This requires integrating the equations three times for the three sets of values:

(1) $X_1(0)$; $X_4(0)$

(2) $X_1(0) + \Delta X_1(0)$; $X_4(0)$

(3) $X_1(0)$; $X_4(0) + \Delta X_4(0)$

This yields an approximation of the partial derivatives:

$$\frac{\partial X_2(\infty)}{\partial X_1(0)}, \quad \frac{X_2(\infty)}{\partial X_4(0)}, \quad \frac{X_5(\infty)}{\partial X_1(0)}, \quad \text{and} \quad \frac{X_5(\infty)}{\partial X_4(0)} .$$

The new values to be tried for $X_1(0)$ and $X_4(0)$ are determined by:

$$1 - X_2(\infty)_{old} = \frac{\partial X_2(\infty)}{\partial X_1(0)} [X_1(0)_{new} - X_1(0)_{old}] + \frac{\partial X_2(\infty)}{\partial X_4(0)} [X_4(0)_{new} - X_1(0)_{old}] \tag{143}$$

$$1 - X_5(\infty)_{old} = \frac{\partial X_5(\infty)}{\partial X_1(0)} [X_1(0)_{new} - X_1(0)_{old}] + \frac{X_5(\infty)}{\partial X_4(0)} [X_4(0)_{new} - X_4(0)_{old}] \tag{144}$$

Since all values are known except $X_1(0)_{new}$ and $X_4(0)_{new}$, the equations may be solved for these variables using Cramer's rule. The new initial approximations are tried and the partial derivatives recomputed each time until $X_2(\infty)$ and $X_5(\infty)$ are sufficiently close to one ($\pm$ 0.001).

The subroutine IP of the computer program (Appendix C) carries out this calculation for any values of Pr and M_o which are input from the main program.

Boundary Layer Equations

The energy and momentum boundary layer Equations (48), (50), and (51) for constant U are now to be solved for the velocity and temperature profiles in the boundary layers, from which boundary layer characteristics may be calculated.

Methods for obtaining the proper boundary conditions have been described. The initial profile gives the boundary conditions for ξ equals zero, the free stream solution gives the boundary conditions to which the boundary layer values must approach asymptotically with increasing η, and the zero velocity and wall temperature at the plate produce the remaining necessary boundary conditions at η equals zero.

Summarizing the equations to be solved:

$$\xi u' \frac{\partial u'}{\partial \xi} - \left(\xi \frac{\partial \psi}{\partial \xi} + \frac{\psi}{2}\right) \frac{\partial u'}{\partial \eta} = \frac{\partial}{\partial \eta}\left(\ell \frac{\partial u'}{\partial \eta}\right) \tag{48}$$

$$\xi u' \frac{\partial \theta}{\partial \xi} - \left(\xi \frac{\partial \psi}{\partial \xi} + \frac{\psi}{2}\right) \frac{\partial \theta}{\partial \eta} = \frac{\partial}{\partial \eta}\left(\frac{\ell}{Pr} \frac{\partial \theta}{\partial \eta}\right) \tag{50}$$

$$- I_e J_y \xi^{1/2} \sqrt{Re_{o_L}} \frac{\partial \theta \theta_e}{\partial \eta} + \ell(\gamma-1)M^2 \left(\frac{\partial u'}{\partial \eta}\right)^2 +$$

$$S_\infty \xi \frac{(\gamma-1)}{\gamma} \theta \left(\frac{J_y^2 + J_x^2}{\sigma'} - u' \right)$$

$$\frac{\partial \psi}{\partial \eta} = u' \tag{51}$$

$$\ell = \sqrt{\frac{P_\infty}{\theta' P_o}} \tag{65}$$

$$\frac{J_x}{J_\infty} = -\beta_\infty \left(\frac{\beta}{\beta_\infty} - \sigma' \right) \tag{77}$$

$$\frac{\beta}{\beta_\infty} = \frac{\sigma' n_{e_\infty}}{n_e} \tag{145}$$

$$n_e^3 + A n_e^2 + B n_e + C = 0 \tag{114}$$

$$\theta_e = \theta_e (J_T^2, n_e) \tag{146}$$

$$\sigma' = \sigma'(P, \theta, \theta_e) \tag{147}$$

where the last two are the functional relations given by (108) and (100), respectively. These three simultaneous partial differential equations and six algebraic relations are all coupled and must be solved simultaneously by numerical methods.

Many finite difference methods are available for solving partial

differential equations. Most of the methods have stability restrictions which dictate the relative size of $\Delta\eta$ and $\Delta\xi$ as they approach zero. An accuracy requirement also places a restriction on the maximum size of these increments. The combination of these two restrictions, stability and convergence, may dictate a very small grid. This may lead to very large computing times, making an accurate solution unfeasible even on high speed digital computers. This condition arose in this work in an initial attempt to use an explicit technique.

In order to prevent this occurrence, an implicit finite difference technique is used which appears to have no stability restrictions on the relative size of $\Delta\eta$ and $\Delta\xi$. Also, the transformation from y' to the new independent variable η makes the flow more uniform with respect to ξ and therefore allows a larger $\Delta\xi$ to be taken with no loss in accuracy.

A six-point scheme is used to approximate the partial derivatives as seen in Figure 10. All derivatives are written for the location $m + \frac{1}{2}$, n,by the approximations:

$$\left.\frac{\partial f}{\partial \xi}\right|_{m+\frac{1}{2}} = \frac{f^{n}_{m+1} - f^{n}_{m}}{\Delta\xi} \tag{148}$$

$$\left.\frac{\partial f}{\partial \eta}\right|^{n}_{m+\frac{1}{2}} = \frac{1}{2}\left(\frac{f^{n+1}_{m} - f^{n-1}_{m}}{2\Delta\eta} + \frac{f^{n+1}_{m+1} - f^{n-1}_{m+1}}{2\Delta\eta}\right) \tag{149}$$

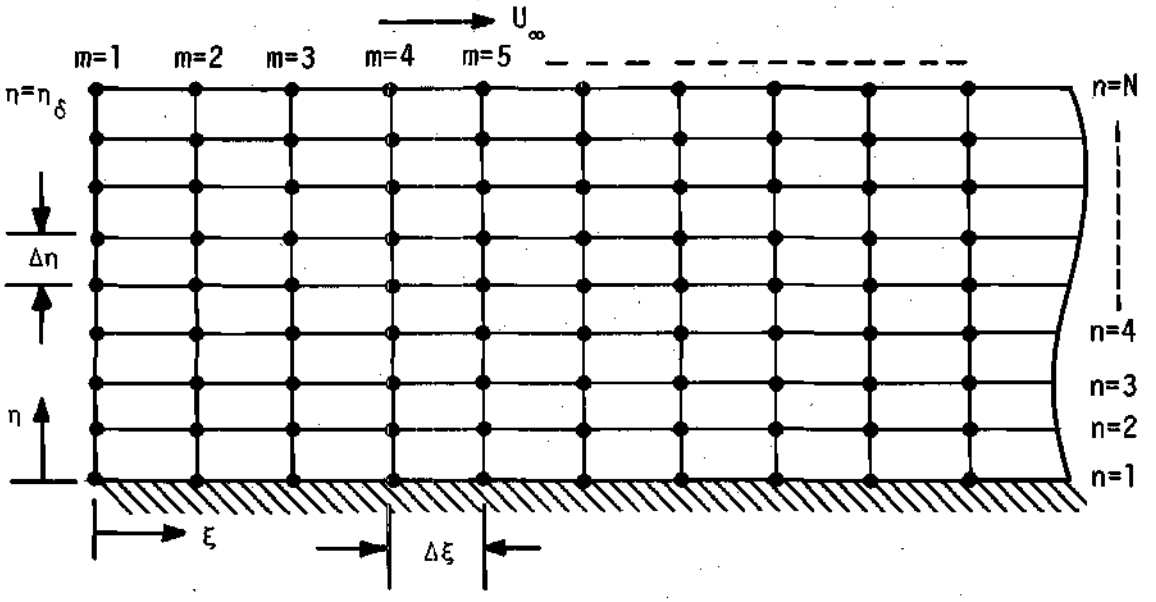

Figure 9. Finite Difference Grid in Boundary Layer

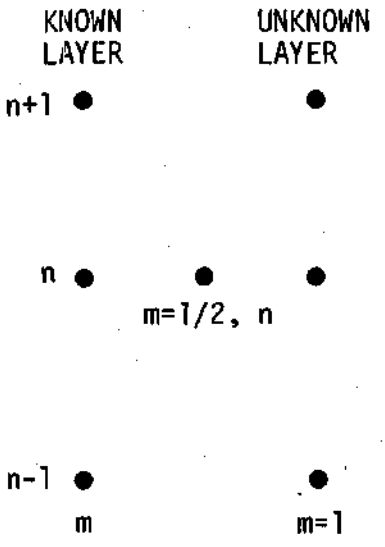

Figure 10. Six Point Grid System in Boundary Layer

$$\left.\frac{\partial^2 f}{\partial \eta^2}\right|^{n}_{m+\frac{1}{2}} = \frac{\left(f^{n+1}_{m+1} - f^{n}_{m+1}\right) - \left(f^{n}_{m+1} - f^{n-1}_{m+1}\right)}{2\Delta\eta^2} + \tag{150}$$

$$\frac{\left(f^{n+1}_{m} - f^{n}_{m}\right) - \left(f^{n}_{m} - f^{n-1}_{m}\right)}{2\Delta\eta^2}$$

Using these approximations in (48) and (50) to evaluate the equations at $m + \frac{1}{2}$, n, the result may be put in the following form.

Momentum Equation:

$$-Am^{n}_{m}\, u'^{n+1}_{m+1} + Bm^{n}_{m}\, u'^{n}_{m+1} - Cm^{n}_{m}\, u'^{n-1}_{m+1} = Dm^{n}_{m} \tag{151}$$

Energy Equation:

$$-Ae^{n}_{m}\, \theta^{n+1}_{m+1} + Be^{n}_{m}\, \theta^{n}_{m+1} - Ce^{n}_{m}\, \theta^{n-1}_{m+1} = De^{n}_{m} \tag{152}$$

where:

$$Am^{n}_{m} = \frac{bm^{n}_{m+1/2}}{4\Delta\eta} + \frac{\ell^{n+1/2}_{m+1}}{2\Delta\eta^2} \tag{153}$$

$$Bm^{n}_{m} = \frac{\ell^{n}_{m+1}}{\Delta\eta^2} + \frac{am^{n}_{m+1/2}}{\Delta\xi} \tag{154}$$

$$Cm^{n}_{m} = -\frac{bm^{n}_{m+1/2}}{4\Delta\eta} + \frac{\ell^{n-1/2}_{m+1}}{2\Delta\eta^2} \tag{155}$$

$$Dm_m^n = \frac{bm_{m+1/2}^n}{4\Delta\eta}\left(u'^{n+1}_m - u'^{n-1}_m\right) + \frac{am_{m+1/2}^n\, u'^n_m}{\Delta\xi} + \qquad (156)$$

$$\frac{\ell_m^{n+1/2}}{2\Delta\eta^2}\left(u'^{n+1}_m - u'^n_m\right) - \frac{\ell_m^{n-1/2}}{2\Delta\eta^2}\left(u'^n_m - u'^{n-1}_m\right)$$

$$Ae_m^n = \frac{be_{m+1/2}^n}{4\Delta\eta} + \frac{\ell_{m+1}^{n+1/2}}{2\Delta\eta^2 Pr} \qquad (157)$$

$$Be_m^n = \frac{ae_{m+1/2}^n}{\Delta\xi} + \frac{\ell_{m+1}^n}{\Delta\eta^2 Pr} \qquad (158)$$

$$Ce_m^n = -\frac{be_{m+1/2}^n}{4\Delta\eta} + \frac{\ell_{m+1}^{n-1/2}}{2\Delta\eta^2 Pr} \qquad (159)$$

$$De_m^n = \frac{ae_{m+1}^n\,\theta_m^n}{\Delta\xi} + \frac{be_{m+1/2}^n\left(\theta_m^{n+1} - \theta_m^{n-1}\right)}{4\Delta\eta} \qquad (160)$$

$$+ \frac{\ell_m^{n+1/2}\left(\theta_m^{n+1} - \theta_m^n\right)}{2Pr\Delta\eta^2} - \frac{\ell_m^{n-1/2}\left(\theta_m^n - \theta_m^{n-1}\right)}{2Pr\Delta\eta^2}$$

$$+ ce_{m+1/2}^n$$

$$am_{m+1/2}^n = \xi_{m+1/2}\, u'^n_{m+1/2} \qquad (161)$$

$$bm_{m+1/2}^n = \xi_{m+1/2}\left(\frac{\psi_{m+1}^n - \psi_m^n}{\Delta\xi}\right) + \frac{\psi_{m+1/2}^n}{2} \qquad (162)$$

$$ae_{m+1/2}^n = am_{m+1/2}^n \qquad (163)$$

$$be^{n}_{m+1/2} = bm^{n}_{m+1/2} - \left(I_e J_y \sqrt{\xi Re_{o_L}}\right)_{m+1/2} \theta^{n}_{e_{m+1/2}} \tag{164}$$

$$ce^{n}_{m+1/2} = -\left(I_e J_y \sqrt{\xi Re_{o_L}}\right)_{m+1/2} \left(\frac{1}{\Delta\eta}\right)\left[\theta^{n}_{m+1/2}\left\{\theta^{n+1}_{e_{m+1/2}} - \theta^{n-1}_{e_{m+1/2}}\right\}\right] + \ell^{n}_{m+1/2}(\gamma-1)\frac{M^{2}_{m+1/2}}{4\Delta\eta^{2}} \tag{165}$$

$$\left(u'^{n+1}_{m+1/2} - u'^{n-1}_{m+1/2}\right)^2 +$$

$$(S_\infty \xi)_{m+1/2} \frac{\gamma-1}{\gamma} \theta^{n}_{m+1/2}\left(\frac{J_y^2 + J_x^2}{\sigma'} - u'\right)^{n}_{m+1/2}$$

Each equation may be written for n equals 2 through N, where $(N-1)\Delta\eta$ is the boundary layer thickness η_δ where the freestream values are reached. For every value of m, this gives N-1 equations for the N-1 unknown velocities, u'^{n}_{m+1}, and N-1 equations for the N-1 unknown temperatures, θ^{n}_{m+1}. All values with subscript m are known because the calculation starts at the leading edge, m=1, where the initial profile is taken and proceeds down the plate layerwise. All values in column m+1 are calculated before m is increased by one and the calculations repeated for the next layer down the plate.

The disadvantage of an implicit finite difference technique is now obvious. Assuming for the moment that the coefficients Am, Bm, Cm, Ae, Be, and Ce are known, which will be discussed later, two systems of (N-1) simultaneous equations, (151) and (152), must be solved

at each value of m for the two sets of N-1 unknowns. The computing time for this solution may dominate any savings due to a larger grid made possible by the implicit technique.

However, the system of N-1 equations for the N-1 unknowns are of a special nature because all the elements of the corresponding matrix vanish except those on three diagonals. A unique method for solving equations of this particular type is discussed by Richtmyer.[50]

This method is developed by looking for coefficients Em_m^n, Fm_m^n, Ee_m^n, and Fe_m^n such that:

$$u'^n_{m+1} = Em_m^n u'^{n+1}_{m+1} + Fm_m^n \tag{166}$$

$$\theta^n_{m+1} = Ee_m^n \theta^{n+1}_{m+1} + Fe_m^n \tag{167}$$

When (166) and (167) are used with (151) and (152) the result is found for n = 2:

$$Em_m^2 = \frac{Am_m^2}{Bm_m^2} \tag{168}$$

$$Ee_m^2 = \frac{Ae_m^2}{Be_m^2} \tag{169}$$

$$Fm_m^2 = \frac{Cm_m^2 u^1_{m+1} + Dm_m^2}{Bm^2_{m+1}} \tag{170}$$

$$Fe_m^2 = \frac{Ce_m^2 \theta^1_{m+1} + De_m^2}{Be^2_{m+1}} \tag{171}$$

and for $3 \leq n \leq N$:

$$Em_m^n = \frac{Am_m^n}{Bm_m^n - Cm_m^n \, Em_m^{n-1}} \tag{172}$$

$$Ee_m^n = \frac{Ae_m^n}{Be_m^n - Ce_m^n \, Ee_m^{n-1}} \tag{173}$$

$$Fm_m^n = \frac{Dm_m^n + Cm_m^n \, Fm_m^{n-1}}{Bm_m^n - Cm_m^n \, Em_m^{n-1}} \tag{174}$$

$$Fe_m^n = \frac{De_m^n + Ce_m^n \, Fe_m^{n-1}}{Be_m^n - Ce_m^n \, Ee_m^{n-1}} \tag{175}$$

Knowing u'^n_m and θ^n_m for all n, then u'^n_{m+1} and θ^n_{m+1} may be found from (166) and (167) as follows.

(1) Find all values of Am, Bm, Cm, Dm, Ae, Be, Ce, and De at m from Equations (153) through (165) by taking all variables which are to be evaluated at m + 1/2 and m + 1 to be equal to their respective values at m.

(2) Find Em_m^n, Ee_m^n, Fm_m^n, and Fe_m^n for $2 \leq n \leq N$ from Equations (168) through (175) by starting at n equals two and stepping n up to N. This direction is necessary since Em_m^n and Ee_m^n are in terms of Em_m^{n-1} and Ee_m^{n-1}, respectively.

(3) Since all the coefficients in (166) and (167) are now known and u'^N_{m+1} and θ^N_{m+1} are given as boundary conditions, n may be stepped down from N in increments of one using (166) and (167) to find u'^n_{m+1} and

θ^n_{m+1} for all values of n. This downward direction is dictated by the fact that u'^n_{m+1} is given in terms of u'^{n+1}_{m+1}.

(4) Good approximations are now available for variables at m+1 and m + 1/2. Therefore, values of Am^n_m, Bm^n_m, Cm^n_m, Dm^n_m, Ae^n_m, Be^n_m, Ce^n_m, and De^n_m are recalculated from (153) through (165) and the above steps (2) and (3) repeated. This recalculation of the coefficients and all boundary layer values continues until the boundary layer values are constant from one iteration to the next. A step is then taken down the plate, m increased by one, and the procedure repeated.

The number of iterations needed at each m is dependent upon the grid size used. A smaller grid may be used with a smaller number of iterations to give the same accuracy as a large number of iterations and a larger grid. In this work, three iterations were used. Experience shows that more iterations than this resulted in no change in the results. The grid size used was:

$$\Delta\xi = 0.04$$

$$\Delta\eta = 0.02$$

The coefficients change very little from one iteration to the next due to the slow variation of the boundary layer properties with ξ.

Since the boundary layer thickness can vary down the plate, a criterion must be used for determining the value of N at each m. After considerable experience it was found that the best criterion to use was:

$$1 - Em_m^n - Fm_m^n < \varepsilon \tag{176}$$

and

$$1 - Ee_m^n - Fe_m^n < \varepsilon \tag{177}$$

The value of ε used was 0.5×10^{-5}. When these criteria were met, N was set equal to n and the velocities and temperatures calculated from that point down to the plate. This was found to be more efficient than checking the difference between θ_{m+1}^{n+1} and θ_{m+1}^{n} at each n as suggested by Brailovskaya and Chudov.[51]

Experience has shown that the finite difference equations are very stable for all values of $\Delta\eta$ and $\Delta\xi$. Even when a large error is introduced into the initial profile, it is damped out very rapidly as one proceeds down the plate. This agrees with the fact that the finite difference equations can be shown to be stable for constant coefficients by means of the Fourier transform.[51] This implicit finite difference approximation has also been used by Blottner on disassociating boundary layers with much success.[52] He, however, did not iterate on the coefficients as is done here. He also encountered no stability problems.

The values of $\Delta\eta$ and $\Delta\xi$ taken on all data calculations were 0.2 and 0.4, respectively. This was judged sufficiently small for convergence, since halving both steps simultaneously produced a maximum change of 1 per cent in the boundary layer profile values. Further reduction from 0.1 and 0.2 for $\Delta\eta$ and $\Delta\xi$, respectively, caused insignificant changes in the profiles.

The procedure for carrying out these calculations was programmed for the Univac 1108 computer in Fortran V at the Rich Electronic Computer Center, Georgia Institute of Technology. The program is shown in Appendix C. The procedure requires a high speed digital computer with efficient programming due to the need to evaluate the Hall current and electrical conductivity at each point in each iteration. As is discussed in Chapter IV, this requires a double trial and error solution of complex Equations (77), (114), (145), (146), and (147).

The coefficients Am, Bm, Cm, Dm, Ae, Be, Ce, and De are evaluated in the main program with Em, Ee, Fm, Fe and Equations (166) and (167) being evaluated in subroutine FD.

CHAPTER VI

RESULTS

Standard Conditions

The results presented in this section are computations performed by the computer program in Appendix C for what will be termed "standard conditions." These were chosen to be realistic, average conditions, but necessarily with some arbitrariness. They are:

$$
\begin{aligned}
M_o &= 1.0 \\
K &= 0.5 \\
P_o &= 3 \text{ atmospheres} \\
T_o &= 2000^\circ K \\
F &= 0.002 \\
L &= 0.3 \text{ meters} \\
\theta_w &= 0.5 \\
S_o(K-1) &= -0.5
\end{aligned}
\tag{178}
$$

The condition for $S_o(K-1)$ insures that the interaction of the magnetic field will be on the order of the initial pressure and will be taken to be one-half throughout this work. If the electrical conductivity

were a constant down the channel, the exit pressure would be the fraction $S_0(1-K)$ of the initial pressure. The computer program uses this quantity to calculate the magnetic field which is given by:

$$B = \frac{S_o P_o}{\sigma_o UL} \tag{179}$$

from the definition of S_o. Solution of this equation is a triple trial and error calculation because B depends on σ_o, which is a function of $j_{\infty o}$, which in turn depends on B. This calculation is carried out in the first section of the main program. Values for B, $j_{\infty o}$, and T_e must be assumed and all three quantities iterated until the equations for σ_o are satisfied, Equation (179) is satisfied, and Ohm's law:

$$j_{\infty o} = \sigma_o UB(K-1) \tag{180}$$

is satisfied.

Holding the ratio of the wall temperature to the free stream temperature constant results in a wall temperature which varies about 20 per cent down the channel. This is a good approximation to practical generators where the electrode wall temperature is generally held constant by external cooling.

Free Stream

The results of the free stream calculation are shown in Figure 11 where all quantities are referenced to their initial values at the entrance denoted by $(\ )_o$. Initial values, at ξ equals zero, for this case are:

$$\begin{aligned} \sigma_o &= 362.2 \text{ mho/m} \\ j_o &= 27.6 \text{ amps/cm}^2 \\ B &= 1.83 \text{ webers} \\ \beta &= 1.67 \end{aligned} \tag{181}$$

It can be seen from Figure 11 that the most influential parameter is the pressure. The reduction in pressure leads to higher electrical conductivities which result in higher currents. This produces an increasing interaction with the magnetic field. The decreasing temperature tends to decrease σ_∞, but the decreasing pressure dominates this effect and σ_∞ increases down the channel. The Mach number increases slightly due to the constant velocity and decreasing temperature.

An assumption of constant electrical conductivity in the free-stream, as Kerrebrock[6] and Hale[14] have done for accelerators, would not be suitable. It creates a question as to the validity of this assumption in their work where the temperature in the free stream is constant, but the pressure and current density vary.

This is the first work, known by the author, showing the influence on the free stream flow of a nonequilibrium electrical conductivity which is a function of pressure, temperature, and current density. The significance of this application in the free stream is that the electrical conductivity increases down the channel due to the dominate influence of the decreasing pressure. The heating of the electrons becomes more efficient at low pressures because there are fewer electrons to heat and fewer gas molecules with which to lose their energy. A decreasing temperature down the channel then, does not reduce the

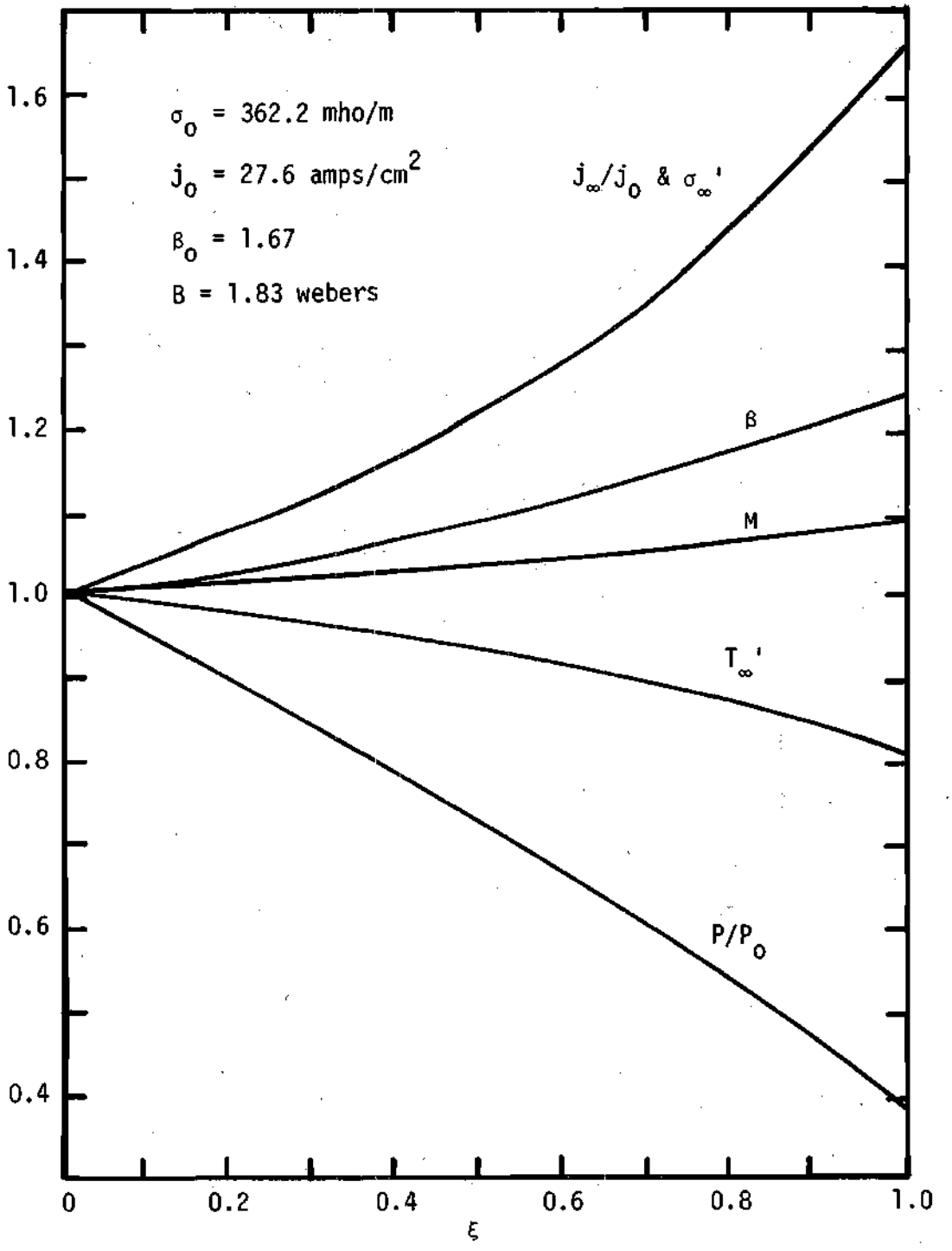

Figure 11. Freestream Flow for "Standard Conditions"

electrical conductivity to a point where the expansion must be stopped due to low efficiencies. It appears that with nonequilibrium heating of the electrons, relatively low exit temperatures may be accomplished.

Boundary Layer Profiles

The calculated boundary layer profiles for u', θ, J_x/J_y, β/β_o, σ', and T_e/T_{e_∞} are shown in Figures 12, 13, and 14 for the "standard" free stream conditions discussed in the previous section. Since a similarity condition was not obtained, the profiles may differ at various axial positions. The plots show the profiles at the entrance, ξ equals zero, and the exit, ξ equals one, for both the anode where electrons carry energy into the boundary layer, and the cathode where electrons carry energy out of the boundary layer. The MHD terms are negligible at the entrance, however, and the profiles are identical for the cathode and anode at the leading edge.

The velocity profile in Figure 12 is nearly a constant with respect to ξ and does not differ significantly from the anode to the cathode. The variation of the u' profile is mostly produced by the decreasing free stream density, which makes ℓ a function of ξ and results in a non-similar condition. For a zero current in the channel the pressure would be constant, the MHD terms would be zero, and the boundary layers would be similar. The MHD terms do not appear explicitly in the momentum equation. They only affect it by changing the temperature profile, which then changes the parameter ℓ. This parameter is the only coupling of the momentum to the energy equation. In view of this result, consideration could be given to decoupling the momentum equation for constant velocity free stream flow with little resulting error.

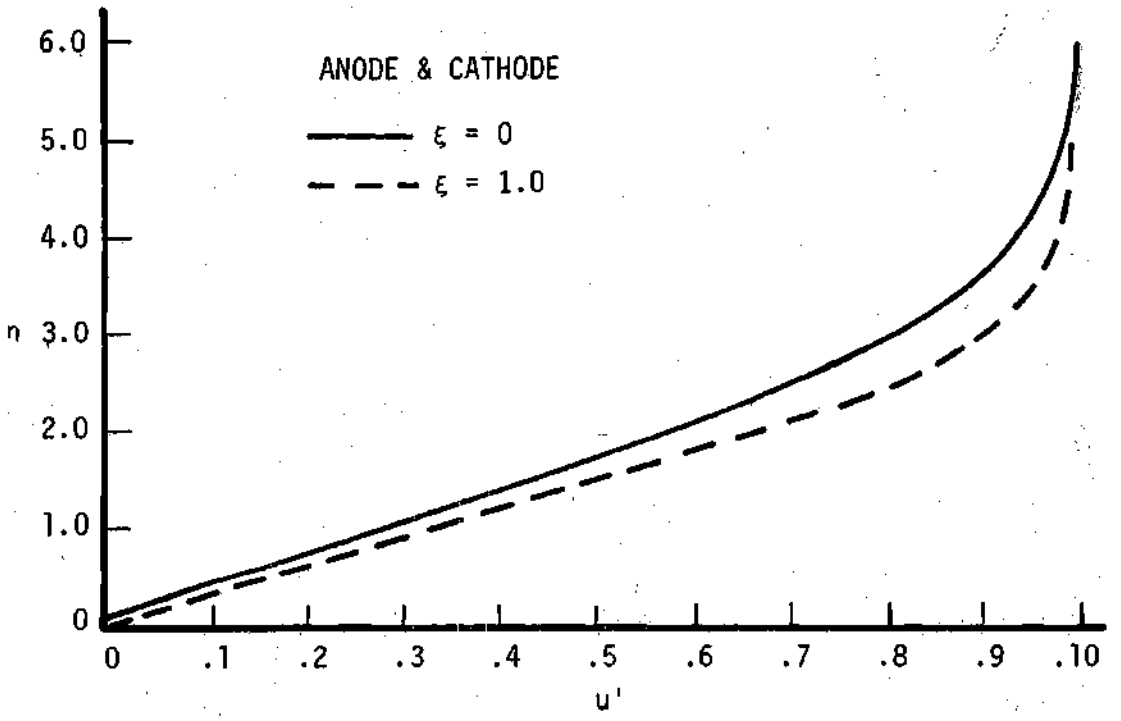

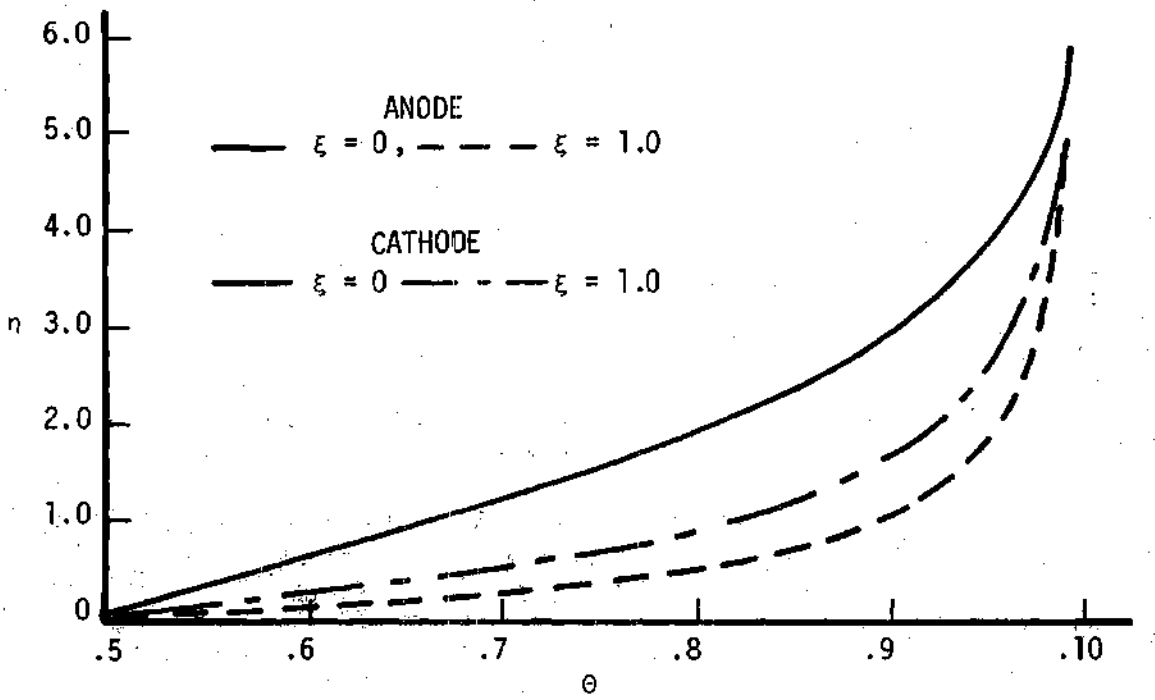

Figure 12. Velocity and Temperature Profiles for "Standard Conditions"

The temperature profiles, also shown in Figure 12, become more severe as the flow progresses down the plate. This is predominately due to the factors ξ and S_∞ which appear in the Ohm heating term in the energy Equation (50). Both factors increase down the plate.

Insight into the origin of these two factors should be understood. Mathematically, the ξ appears due to the transformation from the y to η coordinate. In the y coordinate system, the conductive and convective heat transfer normal to the plate and the viscous heating are much larger at the entrance than the exit because they are dependent upon the gradient in the y direction. However, the Joule heating term, being volume dependent rather than gradient dependent, is approximately constant. This means that the relative size of the Joule heating term increases with ξ. In the transformation to the η coordinate, the size of the gradient dependent terms are decreased at small ξ to make them nearly constant with respect to ξ and, therefore, the size of the Joule heating terms must also be decreased by multiplication with ξ. The small effect of Joule heating near the leading edge may also be understood by realizing that the heat transfer rates are very high in this area, and the addition of a small amount of energy by Joule heating makes little difference in the profiles. However, at larger ξ the heat transfer rates are much smaller and, therefore, the addition of the same Joule heat per unit volume necessitates a larger deviation in the profiles from their non-MHD form. Similar profiles could be obtained only if the Joule heating decreased with ξ at the same rate as the terms which are dependent on the gradient in the η direction and the channel pressure remained constant.

The appearance of S_∞ in the Joule heating term is due to the decreasing pressure and density with increasing ξ. The Joule heating is independent of density and, depositing the same energy per unit volume at high pressure and low pressure, will affect the low density gas much more severely. The extra Joule heat deposited in the boundary layer over that deposited in the free stream will, therefore, affect the boundary layers at the exit more than at the high pressure entrance.

As expected, Figure 12 shows the temperature profile is more severe on the anode than on the cathode because of the convective energy flow of the electrons. The effect is significant as predicted by the value of I_e, discussed in Chapter III, which measures the importance of this effect. The maximum deviation of the temperature profile from anode to cathode is about 10 per cent.

The electrical conductivity profiles in Figure 13 display a rather weak dependence on the reduced gas temperature in the boundary layer. The dependence is seen to be less at the exit than the entrance. This can be explained by looking at the electron temperature in the same figure and noting that it is almost constant through the boundary layer. The electrical conductivity is more dependent on the electron temperature, which controls the ionization, than gas temperature. At high current, low pressure, and high electron temperature, all of which are approached as the flow moves down the channel; the dependence of σ' on T is decreased. These profiles are much more uniform with respect to η than in previous work.[6]

One reason for the uniformity of T_e with respect to η, which creates a more uniform σ', is due to the Hall current. As T_e tends to

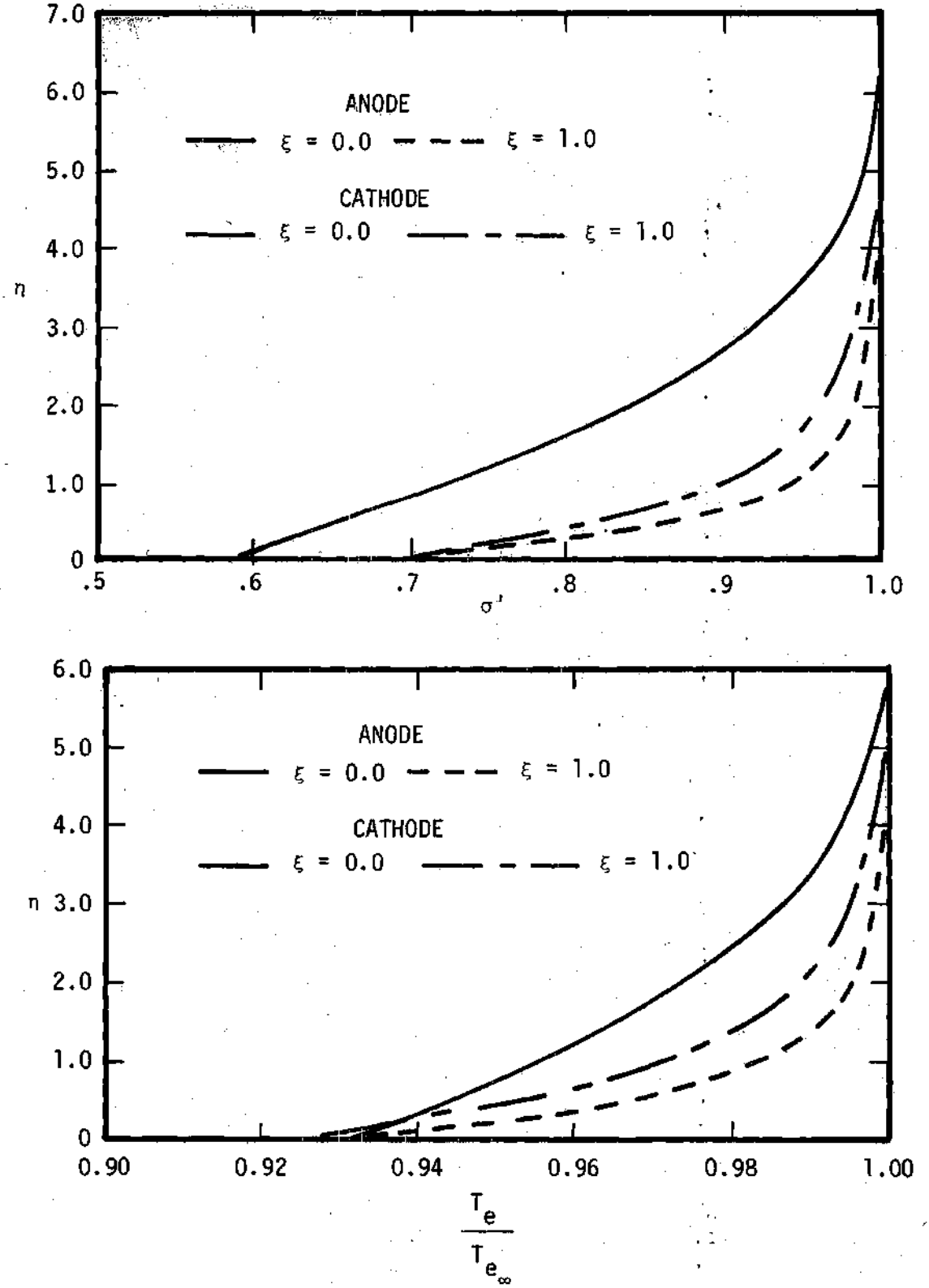

Figure 13. Electrical Conductivity and Electron Temperature Profiles at "Standard Conditions" for Anode and Cathode

decrease in the boundary layer, n_e decreases, which creates a Hall current. This can be seen from Equation (78) for J_x. The J_x in turn increases the total current. This creates more Joule heating and increases the electron temperature.

The Hall parameter and current profiles in Figure 14 show the Hall current to be a maximum at the plate and on the order of 20 per cent of the normal current. Differences between anode and cathode are on the order of 3 per cent and could possibly be neglected. The decreasing value of J_x/J_y down the channel is caused by the higher electron temperatures which occur, creating a more fully ionized condition for the seed gas. This makes the variation of n_e, which creates the Hall current, to be less dependent on T_e. The Hall parameter is seen to have a small deviation through the boundary layer, which decreases with increasing ξ.

Overall Boundary Layer Characteristics

The necessity for calculating the boundary layer profiles is to determine the heat transfer, drag, and electrical loss created by the boundary layers. These quantities are best expressed by the Nusselt number:

$$Nu \equiv \frac{hx}{k} \tag{182}$$

the drag coefficient:

$$C_d \equiv \frac{\mu \left.\frac{du}{dy}\right|_{y=0}}{\rho_\infty U} \tag{183}$$

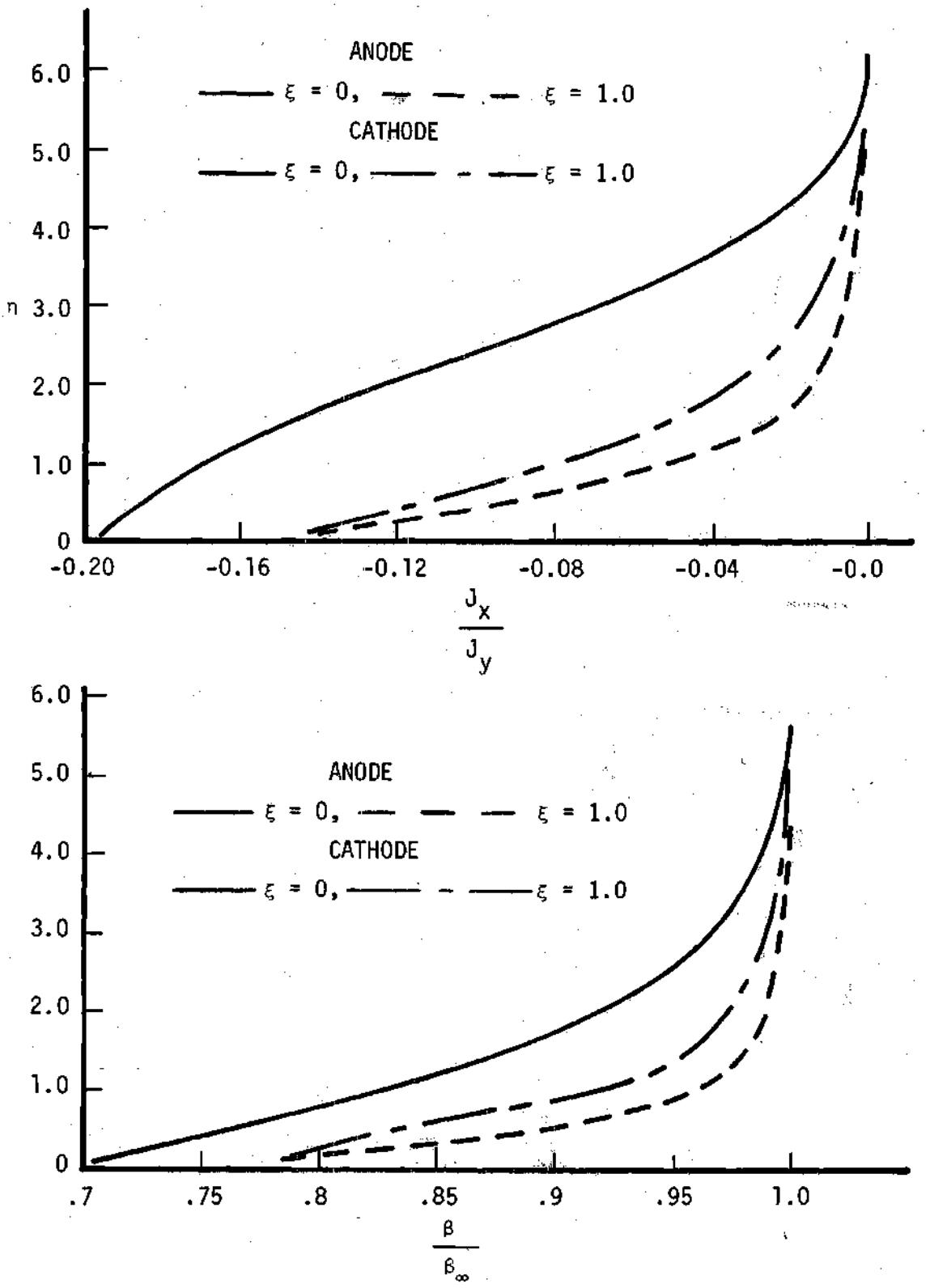

Figure 14. Hall Parameter and Current Profiles at "Standard Conditions" for Anode and Cathode

and the voltage loss displacement thickness:

$$VLDT \equiv \frac{V_{loss}}{E_{y_\infty} L} \tag{184}$$

In order to compare these quantities with conventional boundary layer values for the same free stream velocity and temperature, the values plotted are $\frac{Nu}{\sqrt{Re_x}}$, $C_d\sqrt{Re_o}$, and $VLDT\sqrt{\frac{Re_L}{\xi}}$ where

$$Re_z = \frac{U\rho_\infty Z}{\mu_\infty} \tag{185}$$

These quantities are constant with respect to ξ for constant pressure with no MHD effects. They are shown in Figure 15 for both anode and cathode with the "standard" free stream conditions.

The drag parameter is seen to be very nearly a constant down the channel. This follows from the fact that the velocity profile is coupled weakly with the energy equation.

The Nusselt number is initially at its non-MHD value at the entrance and increases to three times this value at the exit. The maximum difference between the anode and cathode also occurs at the exit where it approaches 25 per cent.

The voltage loss displacement thickness increases slightly down the channel with about 1 per cent deviation between anode and cathode. This displacement thickness is approximately equal to the velocity boundary layer thickness in non-MHD flow. (In this study the velocity boundary layer thickness would be the same as non-MHD flow since the effects on

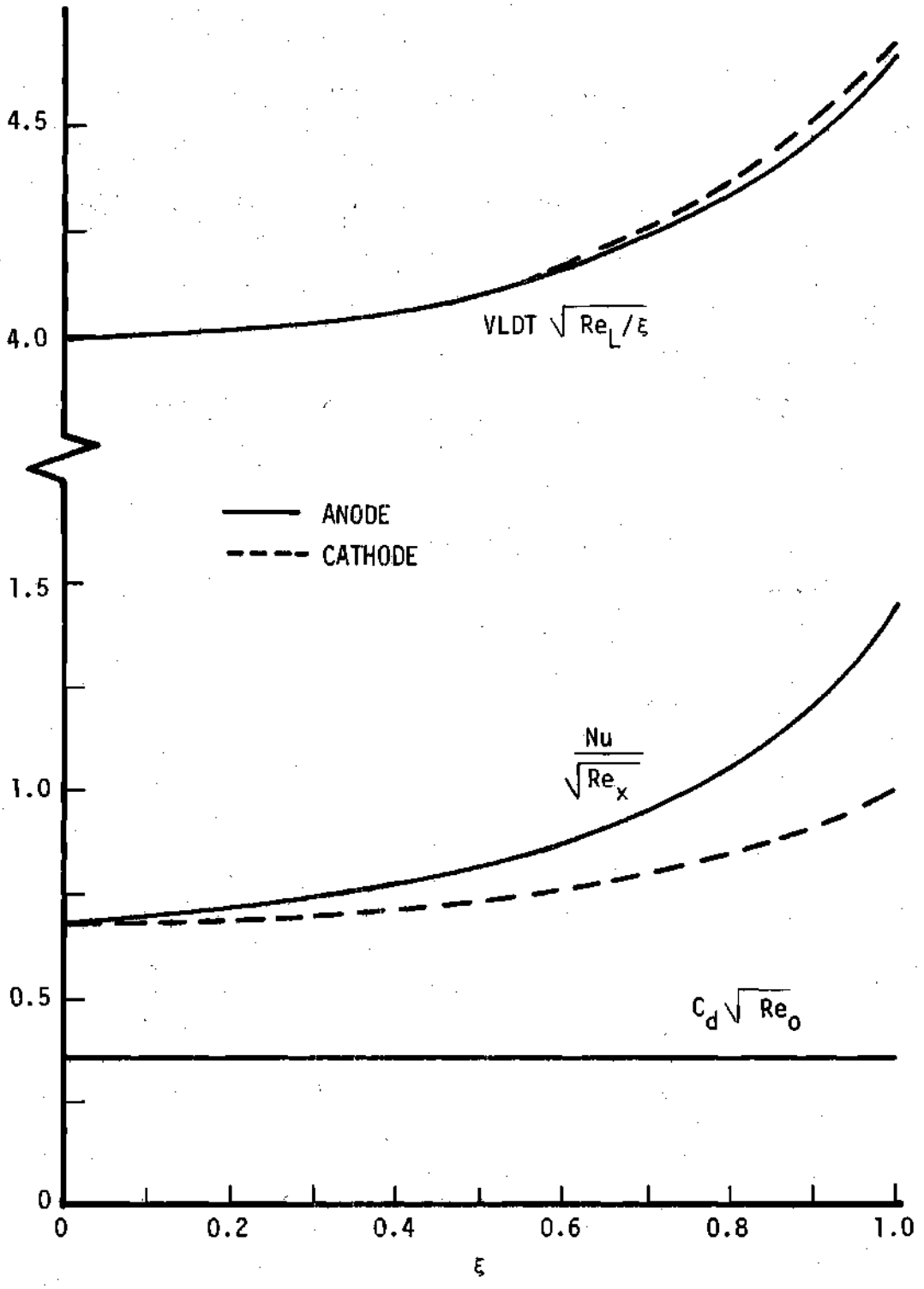

Figure 15. VLDT$\sqrt{Re_L/\xi}$, Nu/$\sqrt{Re_x}$, and $C_d\sqrt{Re_o}$ versus ξ for "Standard Conditions"

u' are negligible.) For typical Reynolds numbers of 10^4 to 10^5, this means that the power loss would usually be very small. For a Reynolds number of 10^5, Figure 15 shows $V_{loss}/E_y L$ to be about 0.02 at the channel exit. The voltage loss due to the boundary layer would then be equal to the voltage generated in the freestream in a distance of 0.02L normal to the electrodes, i.e. the effective generator height would be reduced from the actual value of H to an effective value of (H-0.04L) by losses in anode and cathode boundary layers.

Hall Current Effects

One of the primary motivations for this study was to include the Hall currents to determine their boundary layer effects. (This necessitated a realistic determination of electron temperature, electron density, and electrical conductivity.) As has been discussed in Chapter I, it has been theorized that these Hall currents could lead to large losses[25] and high heat transfer rates. Having obtained results including Hall currents, j_x was set to zero and the boundary layer calculations performed as previously described. The effects of the Hall currents were then determined by comparison of the boundary layer characteristics with and without Hall currents.

The error introduced into the drag coefficient and Nusselt number by neglecting j_x was less than 0.3 per cent. Once the results including Hall currents are studied, this small error would be expected because the total current is:

$$j_T^2 = j_y^2 + j_x^2 \qquad (186)$$

and j_x/j_y is on the order of 0.2. This produces only a 4 per cent increase in j_T^2 and creates a larger electrical conductivity, which tends to reduce Ohm heating.

However, the increase in the boundary layer voltage loss created by the effective field, $\bar{j}_x x \bar{B}$, is significant as shown in Figure 16. The voltage loss displacement thickness is decreased by about 25 per cent when Hall currents are neglected. Since the absolute value is small, this difference should not be of great importance.

The situation proposed by Kerrebrock[25] in which the Hall currents in the boundary layer create a larger electrical conductivity than exists in the free stream, thus shorting out the segmented electrodes and causing large power losses, never arose in this study. When the Mach number and loading parameter were decreased, which increased $-j_x/j_y$, σ' still remained less than one at the wall.

The relative maximum which appears in the σ' vs j curve could be one explanation of this, since j_T would stabilize there. However, when another function was used for σ' which increased continuously with j, the proposed high j_x, with σ' greater than one, never occurred. Therefore, this study concludes that electrode boundary layer shorting does not occur and therefore would not account for the large experimental power losses. This conclusion is substantiated by the good qualitative and quantitative experimental agreement at high current densities, where the shorting phenomena would occur, which Dowdy[29] found with the electrical conductivity model used here.

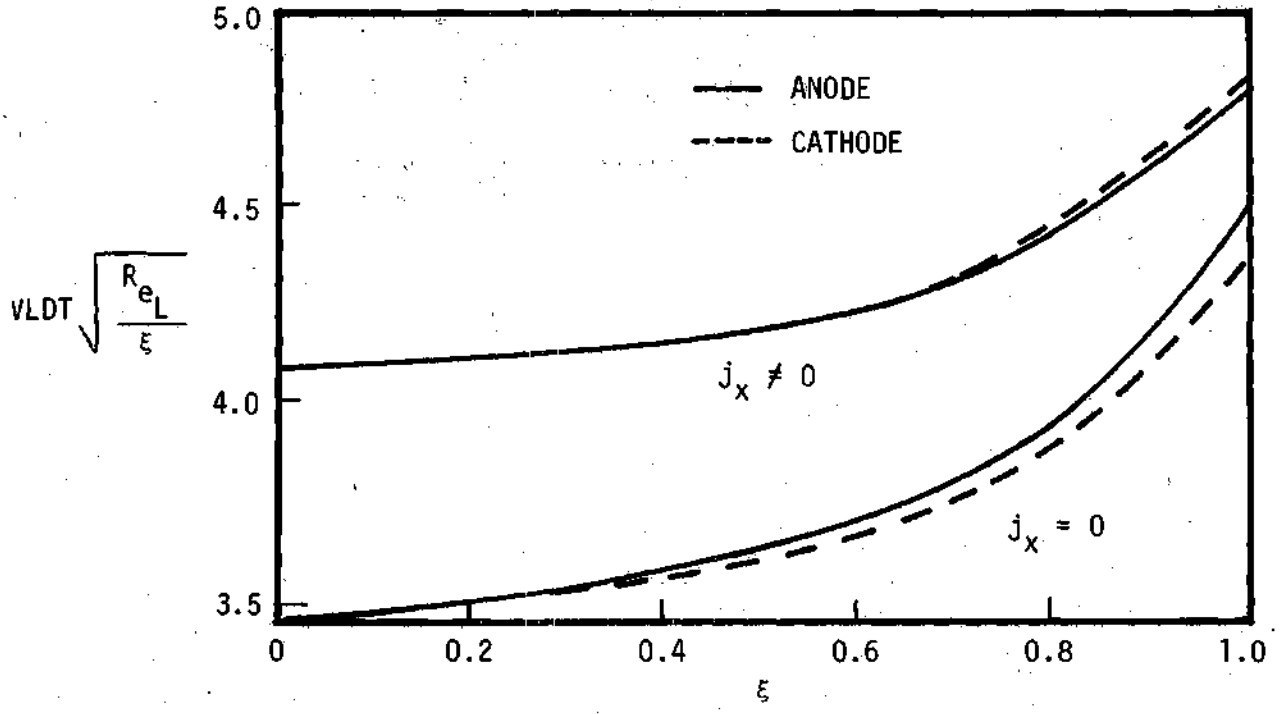

Figure 16. VLDT$\sqrt{Re_L/\xi}$ versus ξ Including and Excluding Hall Currents

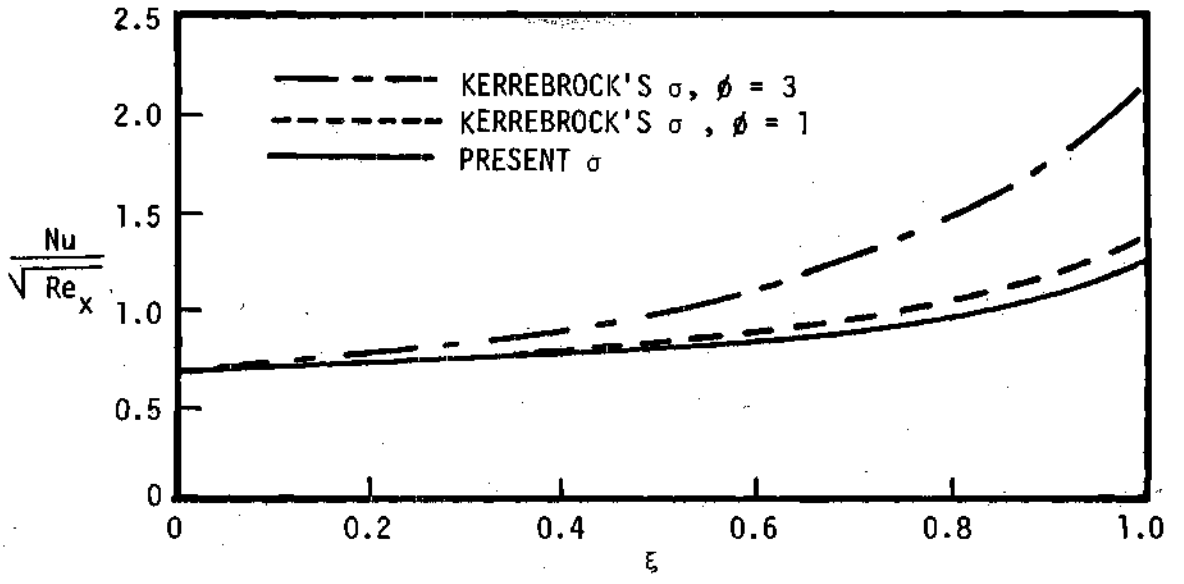

Figure 17. Nu/$\sqrt{Re_x}$ versus ξ for Kerrebrock's σ and Present σ, I_e=0

Effect of Kerrebrock's Electrical Characteristics

In order to determine the effects of using Equations (119) and (120) for calculating the electrical conductivity and Hall parameter in the boundary layer, a subroutine was inserted in the computer program which could be called by the main program and would calculate σ' and j_x from these equations. The free stream flow taken was the same as previously calculated using the electrical conductivity derived in Chapter IV. This was necessary in order to compare boundary layers. The free stream electrical conductivity and Hall parameter were taken as the reference conditions, i.e.,

$$\sigma^*(\xi) = \sigma_\infty(\xi) \tag{187}$$

$$\beta^*(\xi) = \beta_\infty(\xi) \tag{188}$$

Since electron temperatures are not available from this calculation, I_e was set equal to zero for these runs. For comparison purposes, a run was made with the electrical conductivity derived in this work and an I_e of zero. This yielded values which are the average of the previous anode and cathode results.

The calculations were first carried out using:

$$\phi = 3.0$$

$$\alpha = 0.8 \tag{189}$$

as suggested and used by Hale and Kerrebrock[6,14] in their boundary layer work.

The results are shown in Figure 17. Due to very low values of σ' near the wall, around 0.2, very large heat transfer rates were predicted. Values were up to 100 per cent higher than those with the more accurate electrical conductivity. Hall currents at the wall were about one-half j_y, which is also about 100 per cent high.

This suggested that a ϕ of three was too high and should be reduced so that the sensitivity of σ' to T would be less. With ϕ equal to one, the heat transfer predicted is very close to that given by the more accurate expression. This also is shown in Figure 17.

The Hall current for a ϕ of one occurs in the wrong direction and, therefore, was set to zero. As discussed in the previous section, this should not significantly affect the overall results. The voltage loss displacement thickness was essentially the same as the zero Hall current results using the more complex electrical conductivity.

These results indicate that the works of Hale and Kerrebrock[6,14] utilized an expression for σ' which decreases much too rapidly with the gas temperature. The theoretical model used here and the experimental work of Dowdy demonstrate a very slow decrease of the electrical conductivity with the gas temperature, especially at higher current densities.

The parameter α determines the sensitivity of σ' to the current density. However, when Hall currents are neglected, this parameter does not enter into the boundary layer calculation since the current density is constant with respect to η.

Parameter Variations

One disadvantage in using numerical solutions is that specific values must be assigned to various parameters. In this study, the electrical conductivity makes it necessary to specify more parameters than normal. This makes it difficult to generalize results over any range of these parameters. However, since the computing time required to obtain complete boundary layer information for one set of parameter values is about two minutes, the parameters were varied in an attempt to derive results which are more general. Excellent correlation of the drag coefficient and heat transfer was obtained which allows very useful generalizations of the results not before demonstrated.

The seven parameters which were varied are Mach number, channel length, loading factor, entrance pressure, entrance temperature, wall temperature, and seeding fraction. Fifteen runs were made and the parameter values for each is listed in Table 1, along with the symbol used for plotting its results. Run number one used the "standard" conditions discussed in the first part of this chapter.

The value of $S_o(1-K)$ was maintained at one-half for all runs in order to prevent under or over expansion.

Free Stream

The values for the four pertinent free stream variables, $\frac{P}{P_o}$, T_∞', $\frac{j_\infty}{j_{\infty_o}}$, and σ_∞' are given in Table 2 at three positions down the channel. All are equal to one at the entrance. Initial values for σ_o, j_{∞_o}, and B are also listed in this table.

TABLE 1. RUN NUMBERS WITH CORRESPONDING FLOW PARAMETER VALUES AND SYMBOLS

RUN #	SYMBOL	PARAMETERS						
		M	L METERS	K	P_o ATMS.	T_o ^oK	θ_W	F %
1_S	○	1 (STD.)	0.3 (STD.)	0.5 (STD.)	3 (STD.)	2000 (STD.)	0.5 (STD.)	0.2 (STD.)
2_M	▽	0.25	STD.	STD.	STD.	STD.	STD.	STD.
3_M	△	3.0	STD.	STD.	STD.	STD.	STD.	STD.
4_L	△	STD.	0.1	STD.	STD.	STD.	STD.	STD.
5_L	□	STD.	0.5	STD.	STD.	STD.	STD.	STD.
6_K	●	STD.	STD.	0.0	STD.	STD.	STD.	STD.
7_K	●	STD.	STD.	0.75	STD.	STD.	STD.	STD.
8_P	■	STD.	STD.	STD.	1	STD.	STD.	STD.
9_P	▽	STD.	STD.	STD.	5	STD.	STD.	STD.
10_T	▲	STD.	STD.	STD.	STD.	1500	STD.	STD.
11_T	▼	STD.	STD.	STD.	STD.	2500	STD.	STD.
12_W	◤	STD.	STD.	STD.	STD.	STD.	0.3	STD.
13_W	◥	STD.	STD.	STD.	STD.	STD.	0.7	STD.
14_F	▱	STD.	STD.	STD.	STD.	STD.	STD.	0.05
15_F	◹	STD.	STD.	STD.	STD.	STD.	STD.	0.30

Table 2. Freestream Flow with Parameter Variations [$S_o(K-1) = -0.5$]

		RUN NUMBER														
	ξ	1_S	2_M	3_M	4_L	5_L	6_K	7_K	8_P	9_P	10_T	11_T	12_{θ_w}	13_{θ_w}	14_F	15_F
$\frac{P}{P_o}$	0.4	0.79	0.78	0.79	0.79	0.79	0.78	0.79	0.79	0.78	0.78	0.79	0.79	0.79	0.79	0.79
	0.8	0.53	0.50	0.55	0.55	0.53	0.51	0.54	0.56	0.51	0.49	0.56	0.53	0.53	0.55	0.52
	1.0	0.38	0.33	0.41	0.41	0.37	0.38	0.40	0.43	0.34	0.29	0.43	0.38	0.38	0.42	0.36
T'_∞	0.4	0.95	0.95	0.95	0.95	0.95	1.00	0.93	0.95	0.95	0.95	0.95	0.95	0.95	0.95	0.95
	0.8	0.88	0.87	0.89	0.89	0.88	1.00	0.83	0.89	0.88	0.87	0.89	0.88	0.88	0.89	0.88
	1.0	0.83	0.80	0.84	0.84	0.82	1.00	0.76	0.85	0.81	0.78	0.84	0.83	0.83	0.84	0.82
$\frac{J}{J_o}$	0.4	1.16	1.22	1.13	1.13	1.18	1.21	1.14	1.10	1.21	1.26	1.10	1.16	1.16	1.13	1.18
	0.8	1.43	1.65	1.31	1.33	1.49	1.56	1.38	1.24	1.59	1.77	1.26	1.43	1.43	1.30	1.50
$\varepsilon\ \sigma'_\infty$	1.0	1.43	2.11	1.49	1.49	1.79	1.81	1.60	1.35	1.97	2.35	1.39	1.67	1.67	1.37	1.80
σ_o mho/meter		362	221	509	508	304	451	285	481	301	249	476	362	362	405	322
j_{∞_o} amps/cm^2		27.6	10.8	56.8	56.7	19.6	43.6	17.4	18.4	32.5	21.3	33.5	27.6	27.6	29.3	26.1
B weber/m^2		1.83	4.69	0.89	2.68	1.55	1.16	2.92	0.92	2.60	2.38	1.51	1.83	1.83	1.73	1.94

Correlation of these results was not obtained due to the complex variation of σ_∞. It always increases down the channel because of the decreasing pressure, but the rate of the decrease depends on P, T, j_∞, and F in some complex fashion. The faster σ_∞ increases down the channel, the higher the current becomes and the lower the exit pressure.

The general trends which are evident may be listed as follows:

(1) For increasing p, $\partial\sigma_\infty/\partial\xi$ increases.

(2) For increasing T, $\partial\sigma_\infty/\partial\xi$ increases.

(3) For increasing j, $\partial\sigma_\infty/\partial\xi$ decreases.

(4) For increasing F, $\partial\sigma_\infty/\partial\xi$ increases.

By careful investigation of the curves in Figures 5 and 6, these trends may be justified.

These free stream results may be very useful in the design of MHD generators for determining the optimum region of operation as to Mach number, length, pressure, etc.; none of which have been investigated with nonequilibrium conductivities.

The limiting factor introduced by the maximum practical magnetic field would only affect the low Mach number run of 0.25 where B is 4.69 webers/m^2. All other parameters stay well within practical limits.

Anode Boundary Layer Characteristics

The results discussed here are limited to the anode since this is the wall with the most severe heat transfer, and the difference between the two walls has been shown to be only about 25 per cent.

The significant freestream related parameter which changes the magnitude of the boundary layer Ohm heating term is found in Equation (87) to be $S_\infty\xi(K-1)^2$. By use of the definition of S_∞, this parameter

is shown to be approximated by $(P_o/P - 1)(1-K)$ when the average value of σ_∞ is taken.

This parameter is zero at the entrance and increases with increasing ξ. It may then be used in place of the axial coordinate to show the variation of the boundary layer characteristics down the channel. Plots of this nature would allow determination of the heat transfer parameter, and other boundary layer characteristics, at any location in the channel by specifying only the expansion at the position of interest, P/P_o, and the loading factor, K.

Since the parameter $(P_o/P - 1)(1-K)$ controls the importance of the boundary layer Ohm heating term, it seems reasonable to assume that the increase in the heat transfer caused by the MHD effects is related to this parameter. This suggests that instead of plotting $Nu/\sqrt{Re}$ versus $(P_o/P - 1)(1-K)$, one should plot the increase in the heat transfer parameter, $Nu/\sqrt{Re}$, relative to the non-MHD flow value, $Nu/\sqrt{Re}\Big|_{j=0}$; i.e., $\left(Nu/\sqrt{Re} - Nu/\sqrt{Re}\Big|_{j=0}\right)$ versus $(P_o/P - 1)(1-K)$. The value of $Nu/\sqrt{Re}\Big|_{j=0}$ is shown in Figure 18 as a function of Mach number. This is given by the initial profile where the MHD terms are zero and P_∞ is P_o.

The value of $\left(Nu/\sqrt{Re} - Nu/\sqrt{Re}\Big|_{j=0}\right)$ at ξ equals 0.0, 0.4, 0.8, and 1.0 are plotted in Figure 19 versus $(P_o/P - 1)(1-K)$. All fifteen runs shown in Table 1 are plotted. The surprising result is that all data points lie within 10 per cent of a line with a unit slope, except for Run 13 in which the wall temperature was raised from 50 per cent to 70 per cent of the free stream temperature.

This latter deviation is apparently explained by the fact that the decrease in the zero current heat transfer is appreciable, but the

decrease in the Joule heating is very small. This would be a result of the weak dependence of σ on T. Therefore, the heat transfer may possibly not decrease with increasing wall temperature.

The correlation by one curve shown in Figure 19 is extremely good considering it has reduced an eight-dimensional plot to a one-dimensional plot. This is an important result because the variation of $Nu/\sqrt{Re}$ with respect to the eight generator parameters (axial location, Mach Number, loading parameter, entrance pressure, entrance temperature, seeding fraction, wall temperature, or generator length), is shown by a single curve on two plots. One, Figure 19, showing the increase in the parameter relative to its non-MHD value at the same Mach number, and the other, Figure 18, showing the value of $Nu/\sqrt{Re}\Big|_{j=0}$ as a function of Mach number. Without this correlation, a minimum of eight plots would be necessary with several curves on each. Even then the coupling of effects produced by different generator parameters would not be known.

Since the change in the drag coefficient from its similar value is dependent on the temperature profile, it too is plotted with respect to the same parameter, $(P_o/P - 1)(1-K)$. This is shown in Figure 20 where all points lie inside the shaded area. The total change in $C_d\sqrt{Re_o}$ is only on the order of 5 per cent.

The other significant boundary layer characteristic is the voltage loss displacement thickness. Due to a large percentage of this term being solely dependent upon the Hall current, it varies erratically. Its initial value, as well as its variation down the channel, seems to follow no simple pattern, except that its value becomes large when the Hall current is large. To show the data, the initial values at ξ equals

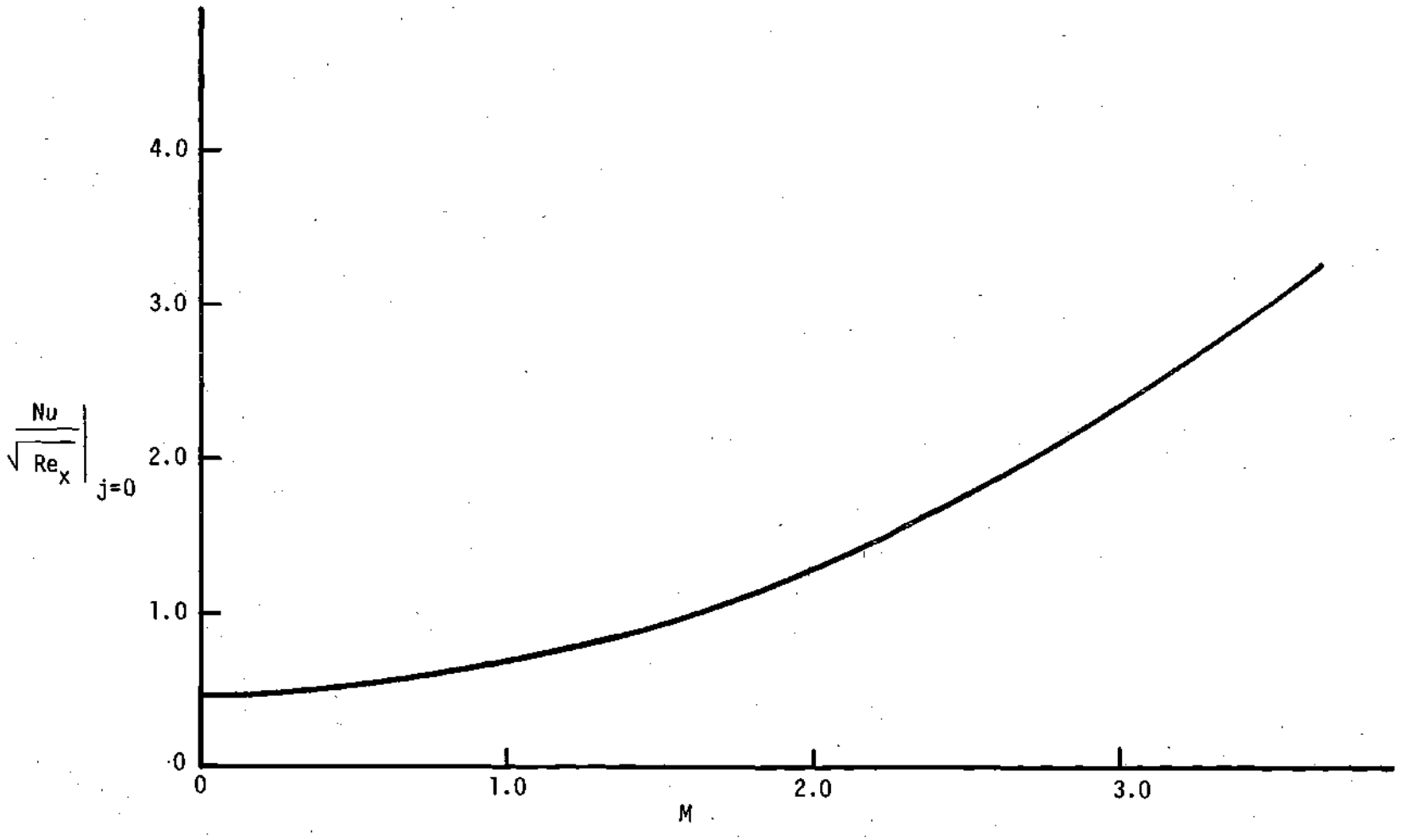

Figure 18. $Nu/\sqrt{Re_x}$ versus Mach Number with no MHD Effects, θ_w=0.5

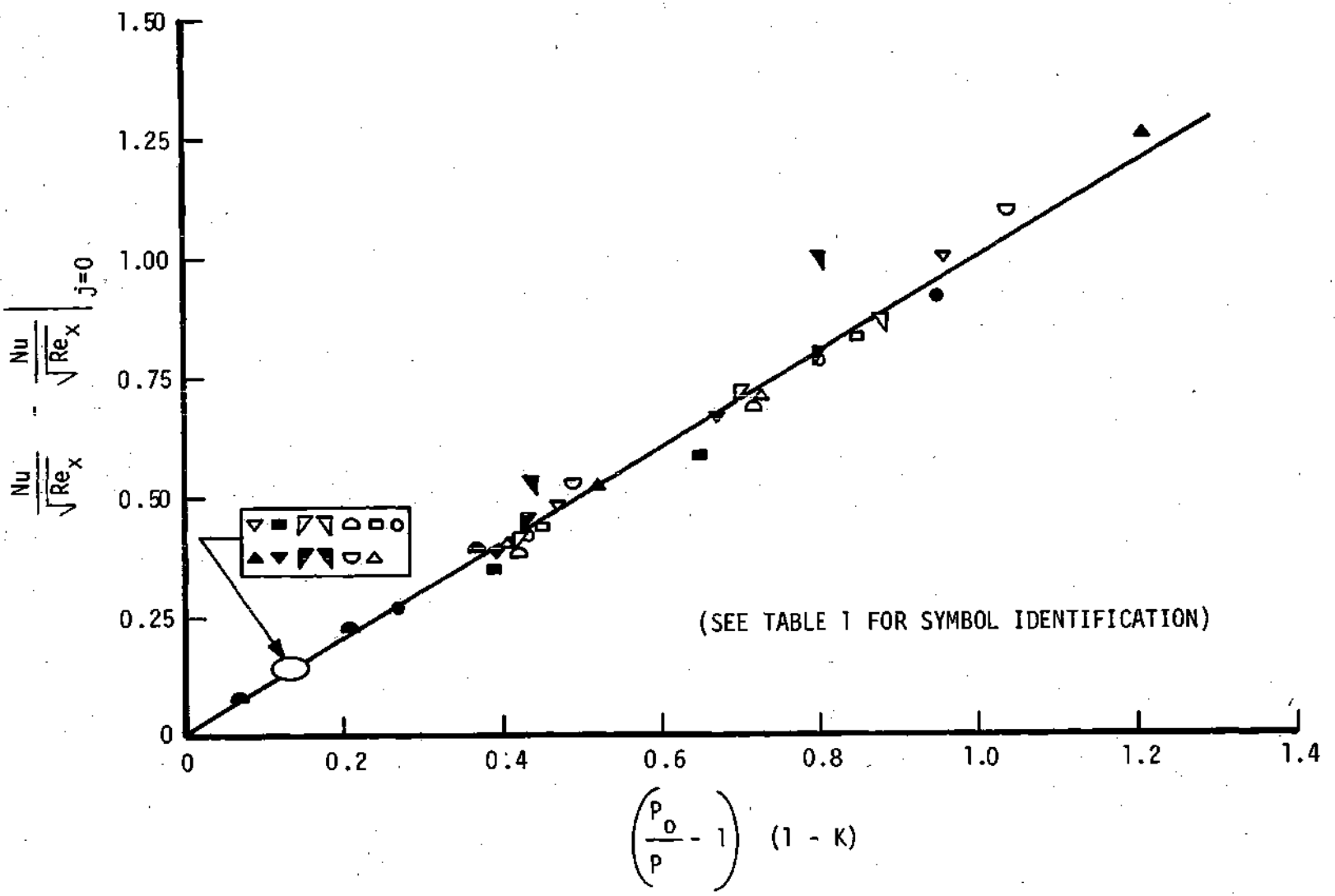

Figure 19. Correlation of Increased Heat Transfer at Anode for Varying Flow Conditions

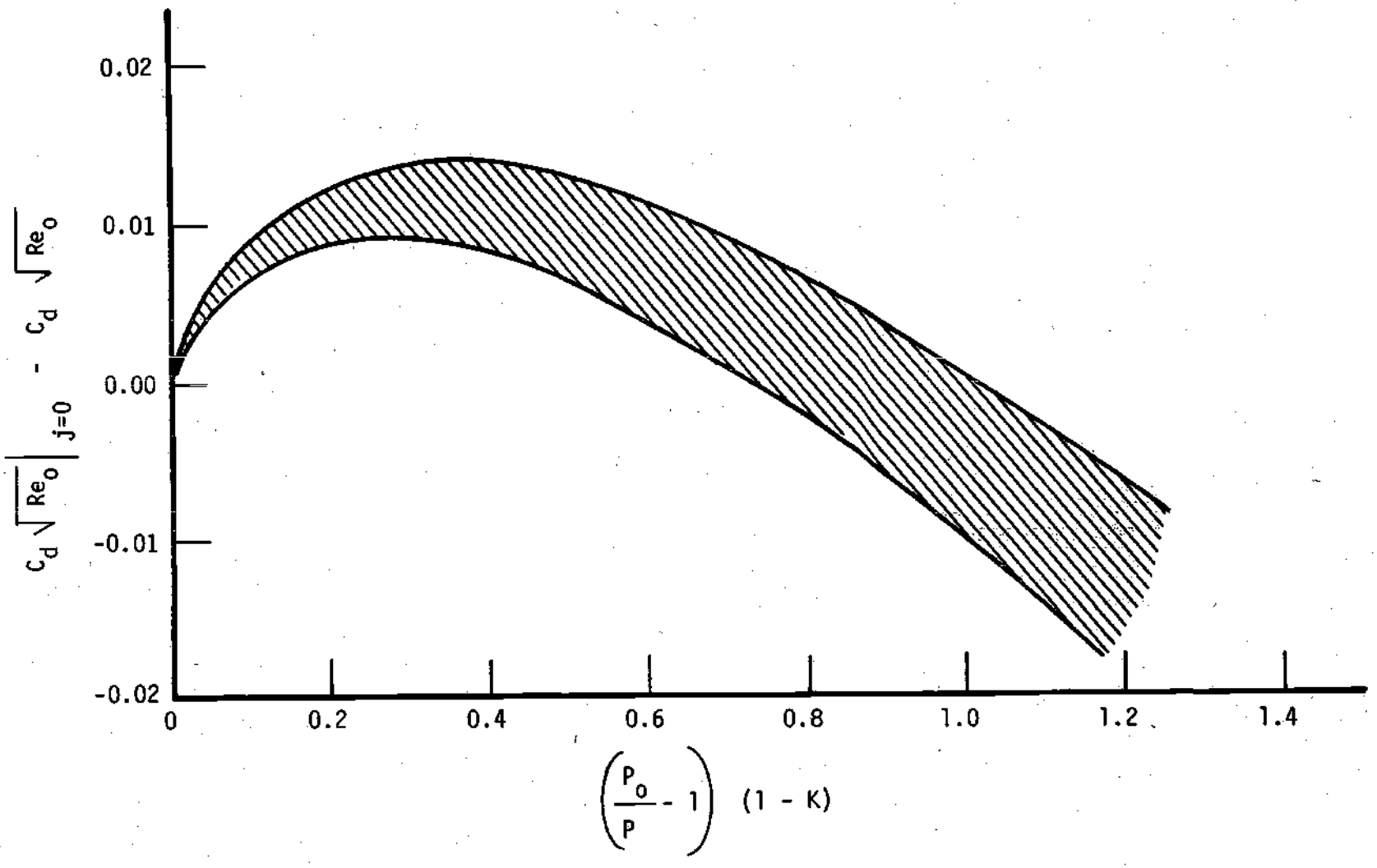

Figure 20. Correlation of Increased Drag Coefficient for Varying Flow Conditions

zero are tabulated in Figure 21 and the variation is shown plotted with respect to $(P_o/P - 1)(1 - K)$. It is very large (11.09) when the magnetic field is large and the lowest value (2.83) occurs for a large seeding fraction. In most of the runs, the exit value is about 120 per cent of the initial value.

The general character of the profiles in the boundary layer changes only with Mach number. The temperature profile has an overshoot for M_o equal to two, along with the electrical conductivity profile. The profiles for u', θ, σ', and J_x/J_y are shown in Figures 22 and 23 for an initial Mach number of three (Run 3_M). The Hall currents are very small for high Mach numbers, due primarily to the low magnetic induction.

Other randomly picked combinations of the free stream parameters were tried to further check the generality of the correlation shown in Figure 19. The only exceptions found were cases where the influence of the relative maximum appearing in the σ vs j curve was felt. From Figure 5, it is apparent that at certain conditions increasing gas temperature may cause the electrical conductivity to decrease. This occurs when the curve for a constant gas temperature dips below a similar curve for a lower gas temperature. This occurs only slightly in Figure 5, but these constant temperature curves are for 2500°K and 1500°K. For temperatures closer together, the crossing of the lines is much more pronounced.

The electrical conductivity profile may make unexpected excursions if conditions are such that the temperature in the boundary layer moves through this reversal region. One such case is shown in Figure 24.

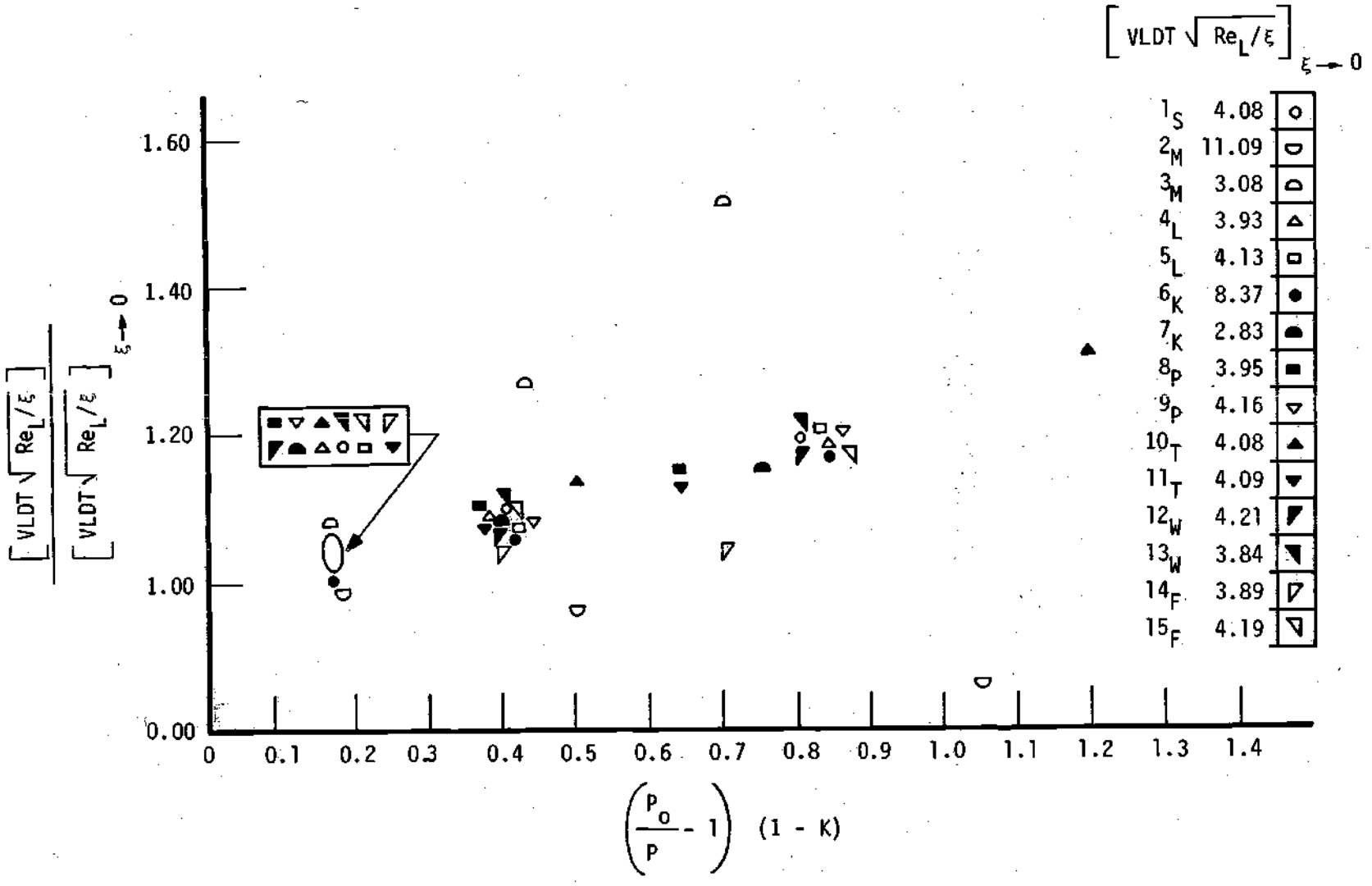

Figure 21. Boundary Layer Voltage Loss Parameter for Varying Flow Conditions

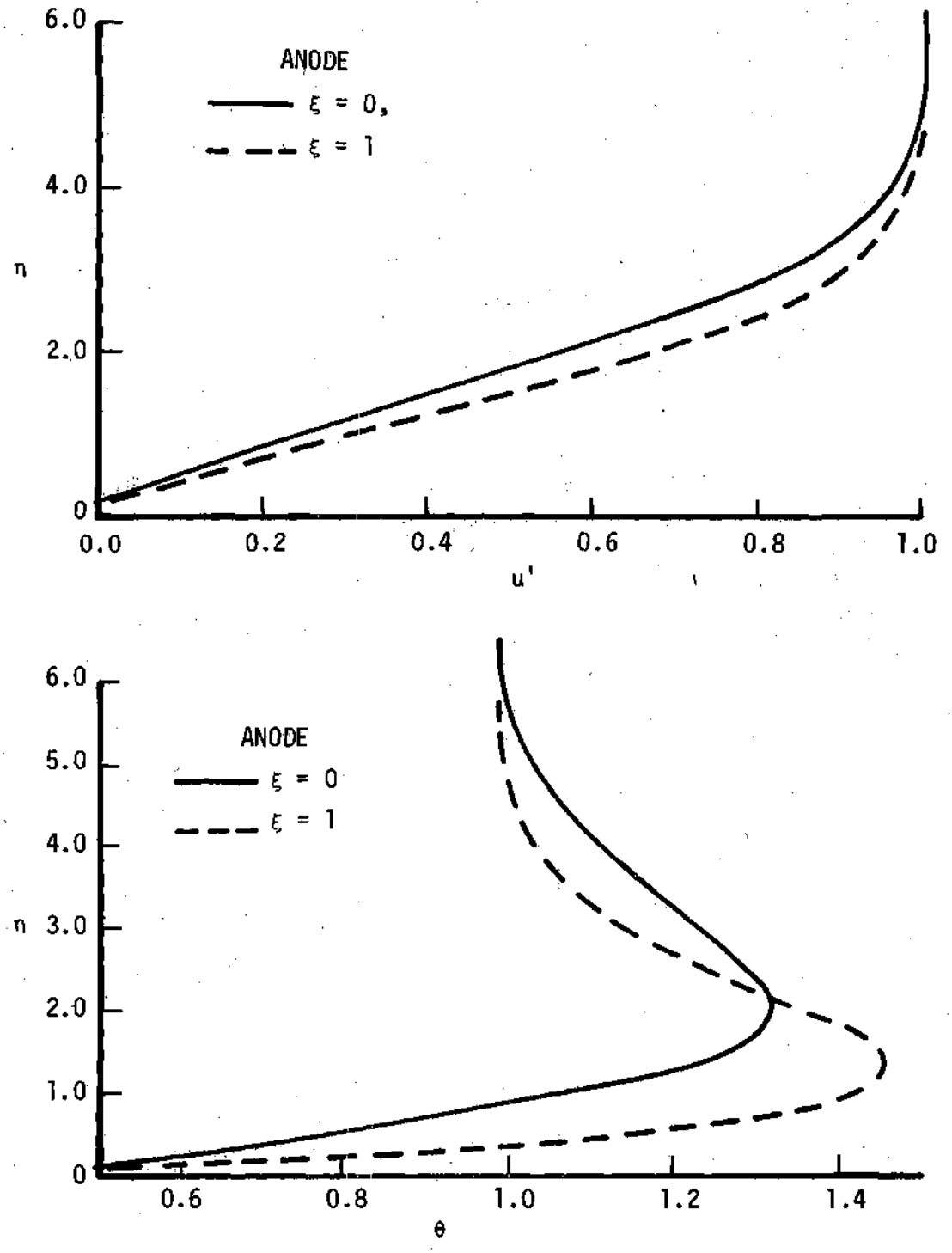

Figure 22. Velocity and Temperature Profiles for a Mach Number of Three (Run 3_M)

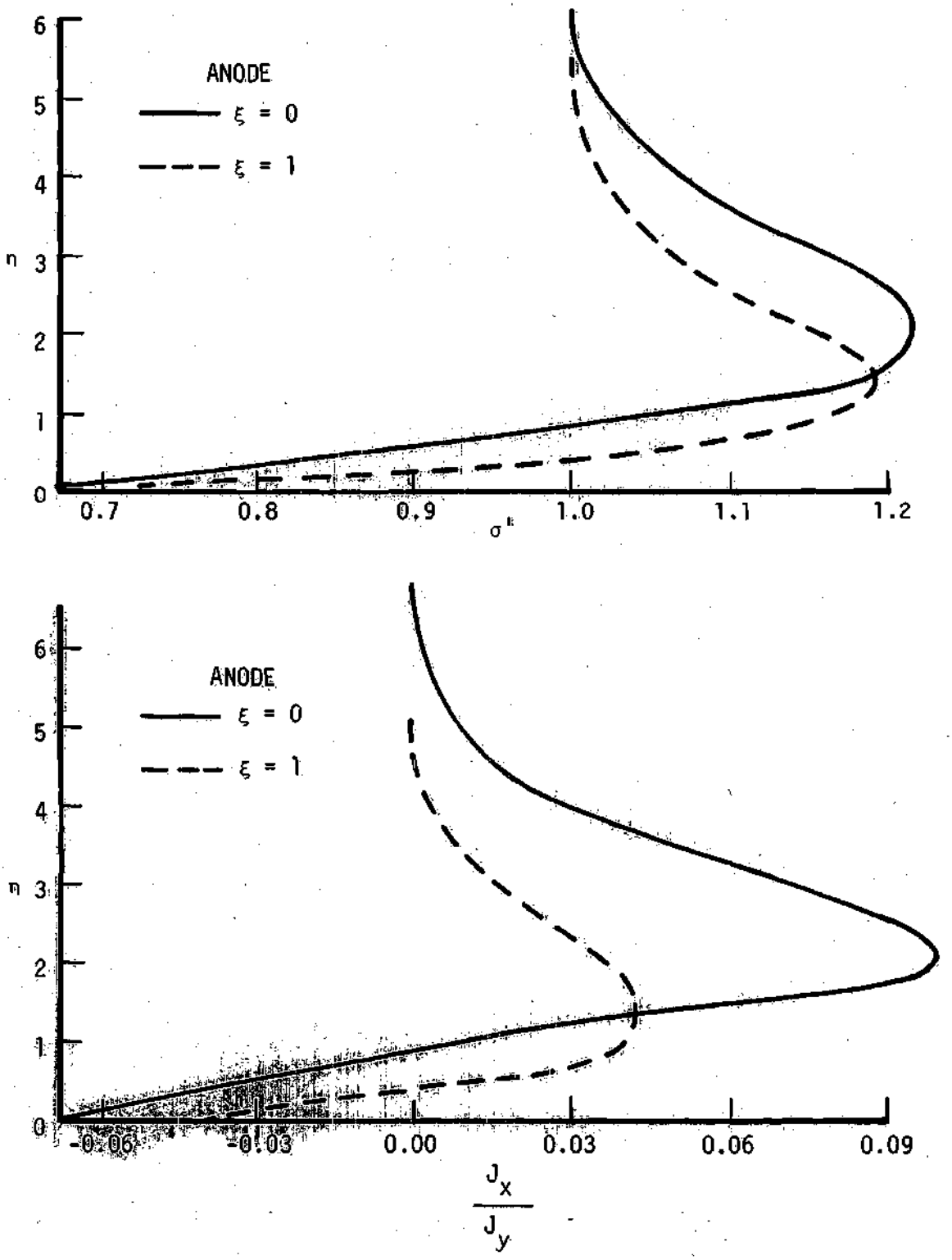

Figure 23. Electrical Conductivity and Hall Current Profiles for a Mach Number of Three (Run 3_M)

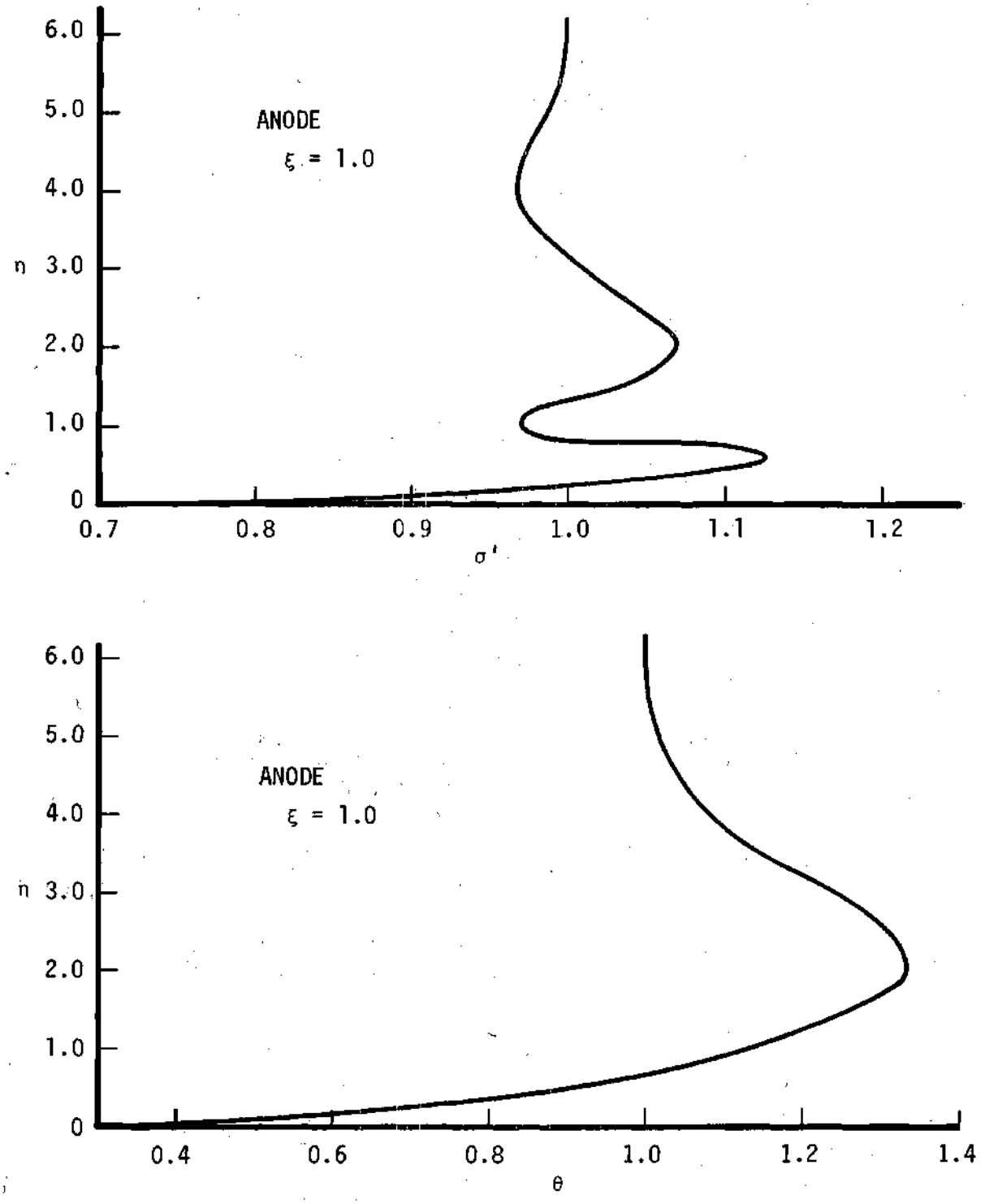

Figure 24. Electrical Conductivity and Temperature Profiles Showing Effects of Relative Maximum in Electrical Conductivity Curve

The conductivity increases with the increasing gas temperature as η increases from zero. Then, due to the dipping of a higher temperature curve under a lower temperature curve, the conductivity decreases with further increase of the gas temperature until the sign of $\partial\sigma/\partial T$ returns to a positive value. The conductivity then follows the temperature profile through the nose of the curve until the temperature again passes through the region where the sign of $\partial\sigma/\partial T$ is negative and the electrical conductivity increases with decreasing temperature. The average boundary layer electrical conductivity in this case is lower then cases where the effect does not occur and therefore causes higher Ohm heating. In this run the data points fall about 200 per cent above the line in Figure 19.

CHAPTER VII

CONCLUSIONS AND RECOMMENDATIONS

Electrical Conductivity

By evaluating the collision integrals in the electron momentum and energy equations using Morse's relations[42] for the energy and momentum exchange between the electrons and atoms, variable collision cross sections,[43] and Sahas' equation for the seed gas and parent gas; a relative maximum may be shown to exist in the σ vs j curve for potassium seeded argon. This is a result of the Ramsauer effect and creates a natural current stability, which has been of some concern.[37] Although the set of equations is relatively complex, computer programming easily overcomes this deficiency to the extent that they may be used in evaluating free stream or boundary layer MHD flow. However, the multiple trial and error solutions must be programmed efficiently.

Free Stream Flow

Calculations of the free stream flow for potassium seeded argon in a constant velocity MHD generator using a realistic nonequilibrium electrical conductivity show an increasing electrical conductivity down the channel to about 170 per cent of its original value. This indicates that problems with low electrical conductivity at the generator exit will not occur as previously thought.

Large electrical conductivities should be possible at high current densities (30-50 amperes/cm^2), and there is no apparent serious

disadvantage in utilizing these high currents. Calculations show that they may be obtained with a Mach number around one and a magnetic induction of less than 20,000 gauss. Low pressures are extremely effective in increasing electron temperatures and conductivities. These pressure effects have not previously been seriously considered.

Optimization of the free stream operating region may be carried out using realistic nonequilibrium electrical conductivity. In order to obtain even qualitative free stream data, a nonequilibrium expression with a pressure dependence included must be used.

Electrode Boundary Layers

The complete Navier-Stokes equations for the electrode, including Hall currents, may be derived and, contrary to previous statements,[23] may be reduced to boundary layer equations by an order-of-magnitude analysis. The pressure gradient normal to the wall acts over a very small distance and does not appreciably change the pressure.

Non-similar MHD boundary layers, including Hall currents, may then be investigated by a numerical solution of the boundary layer equations. This can be carried out using complex, but accurate, variable electrical characteristics. Transformation of coordinates, which produces similar profiles for conventional boundary layers, are highly desirable so that the MHD boundary layer flow field will become more uniform in the axial direction. The initial profile then becomes the conventional similar one.

Implicit finite difference approximations, which produce equations apparently having no stability restrictions, can save significant

computer time that may otherwise be a problem. By employing a method for solving special types of implicit finite difference equations, which all boundary layer equations seem to fall under, the primary disadvantage in implicit techniques is overcome, i.e., no matrix inversions are necessary.

The transformation to a coordinate system producing conventional similar profiles yields a velocity profile for constant velocity free stream flow which is affected very little by the MHD effects.

The thermal MHD effects in the boundary layer are significant and become larger as the flow moves down the channel and the temperature gradients become smaller. The anode has a higher heat transfer than the cathode by about 25 per cent due to the convection of the electrons in the boundary layer. A measure of the significance of this electron convection is given by the parameter I_e, which is $\sigma_\infty BW_A/N_o e\rho_\infty$.

One of the major reasons initially motivating this study was to determine the Hall current effect in segmented electrode boundary layers. This effect was found to be significant only in calculating the boundary layer voltage loss. This loss can be increased by 300 per cent by the Hall currents. However, since the value of a voltage loss without the Hall effect is very small, the increase does not raise its value to a point where it appears to be of practical significance. The reduction in effective height of the generator, i.e., distance between electrodes, created by the boundary layer voltage loss is on the same order as the boundary layer thickness.

The heat transfer and drag coefficient is increased very little by the inclusion of the Hall current, less than 0.3 per cent, and there

is no evidence to support the postulate that the Hall current shorts the segmented electrodes and creates large losses.

Hall currents may then be neglected on the electrode and, if electron energy convection is also negligible, simpler expressions for the electrical conductivity may be used to calculate σ' through the boundary layer. (These simple equations may not, however, be used in the free stream). Kerrebrock and Hale's expression, Equation (119), gives boundary layer characteristics in excellent agreement with those calculated using the more accurate expressions derived in this work. However, a much weaker dependence of the electrical conductivity on the gas temperature must be taken, i.e., lower ϕ in Equation (119), than previously stated.

Since the only insulator wall boundary layer work which includes variable non-equilibrium electrical conductivity[20] uses the higher value of ϕ, the conclusions of that work should be questioned on this as well as other bases. This is particularly true concerning the conclusion that severe shorting along the insulator wall does not occur due to high electrical resistance in the boundary layer. The Hall parameter variation assumed by Hale[14] was found to be totally unsuitable. When calculating Hall effects, electron temperature and density must be computed as is done here.

The increase in $Nu/\sqrt{Re}$ at the electrode wall caused by MHD Joule heating under various operating conditions is correlated extremely well by the parameter $(P_o/P - 1)(1 - K)$. This results in being able to find the heat transfer for any Mach number, axial position, entrance pressure, entrance temperature, loading parameter,

seeding fraction, wall temperature, or generator length from two curves, one for $\left(Nu/\sqrt{Re} - Nu/\sqrt{Re}\Big|_{j=0}\right)$ versus $(P_o/P - 1)(1 - K)$, Figure 19, and the other for $Nu/\sqrt{Re}\Big|_{j=0}$ versus Mach number, Figure 18.

The only exception to this heat transfer correlation is caused by the relative maximum in the σ versus j curve. This phenomenon may create unusual electrical conductivity profiles and cause heat transfer rates to increase by a factor of two or three over those predicted by the correlation. The range of conditions over which this phenomenon occurs is, however, very limited.

All of these comments must be restricted to constant velocity, segmented electrode generator flow using potassium seeded argon as a working fluid operating in the region investigated. Logical extensions into other similar situations, however, would appear to be justified.

Recommendations

Many experimental tasks could be proposed to determine the accuracy of the many aspects which have arisen out of this study. One has already been carried out by Dowdy in determining the existence of the relative maximum appearing in the σ versus j curve.[29] Verification of the original electrical conductivity results in an electric field,[28] with some modifications which have been included here except for radiation, has thereby been accomplished. Similar work should be carried out in magnetically induced fields. Radiation effects should also be studied further. Dowdy's[29] results indicated that they were negligible in his apparatus above 30-40 amperes/cm^2.

Some theoretical work could possibly be done to determine the analytical implications of the excellent correlation of the heat transfer results by the parameter $(P_o/P - 1)(1 - K)$. Coupled with a similar velocity profile, which is shown to be accurate, a much less laborious and more general solution could possibly be forthcoming.

Further analysis on the insulator boundary layer should be carried out along the lines of this study using non-similar profiles, realistic electrical characteristics, and including the Hall currents. This may point out a source of large losses due to shorting along the insulator wall.

An analysis of the voltage loss due to the space charge sheath at the electrodes should also be done. Since the sheath is in a very thin region next to the wall, this could be carried out independently of the boundary layer calculations and possibly demonstrate significant losses.

APPENDIX

APPENDIX A

DERIVATION OF BOUNDARY LAYER FLOW EQUATIONS

Continuity

When the continuity moment of Boltzmann's equation is taken for a species s, the equation is derived:

$$\frac{\partial \rho_s}{\partial t} + \nabla \cdot (\rho_s \bar{w}_o) + \nabla \cdot (\rho_s \bar{V}_s) = \left(\frac{\partial \rho_s}{\partial t}\right)_c \tag{190}$$

where the last term is the loss or addition of species particles caused by collisions. Summing over all species, the collision terms add to zero because when particles are lost from one species, their mass must be gained by the others. This gives:

$$\frac{\partial \rho}{\partial t} + \nabla \cdot (\rho \bar{w}_o) = 0 \tag{191}$$

The last term on the left of Equation (190) adds to zero because of the definition of the diffusion velocity being relative to the mass average velocity of the gas $\bar{w}_o$.

Assuming steady state and two-dimensional flow in the x and y direction only, the continuity equation becomes:

$$\frac{\partial \rho u}{\partial x} + \frac{\partial \rho v}{\partial y} = 0 \tag{192}$$

Momentum

The momentum equation in the arbitrary direction j is given as:

$$\frac{\partial}{\partial t}(\rho_s \bar{w}_{o_j}) + \frac{\partial}{\partial t}(\rho_s \bar{V}_{s_j}) + \nabla \cdot [\rho_s(\bar{w}_o w_{o_j} + \bar{w}_o V_{s_j} + \bar{V}_s w_{o_j})] + (\nabla \cdot \bar{\bar{P}}_s)_j - \rho_{e_s}[\bar{E}_j^* + (\bar{V}_s x \bar{B})_j] = \left[\frac{\partial}{\partial t}(\rho_s \langle w_{s_j} \rangle)\right]_c \tag{193}$$

where ρ_{e_s} is the charge density of species s, $\bar{E}^*$ is defined as:

$$\bar{E}^* = \bar{E} + \bar{w}_o \times \bar{B} \tag{194}$$

and $\bar{\bar{P}}$ is the stress tensor defined by:

$$\bar{\bar{P}}_s = -\begin{bmatrix} \sigma_{x_s} & \tau_{xy_s} & \tau_{xz_s} \\ \tau_{yx_s} & \sigma_{y_s} & \tau_{yz_s} \\ \tau_{zx_s} & \tau_{zy_s} & \sigma_{z_s} \end{bmatrix} \tag{195}$$

The symbol < > denotes the quantity inside is averaged over the velocity distribution. The notation used for the stress is that σ_j is the normal stress on the plane perpendicular to the j axis in the j direction and τ_{ij} is the shear stress on the plane perpendicular to the i axis in the j direction.

Summing Equation (193) over all species in the gas gives:

$$\frac{\partial}{\partial t}(\rho w_{o_j}) + \nabla \cdot (\rho \bar{w}_o w_{o_j}) + (\nabla \cdot \bar{\bar{P}})_j - \rho_e \bar{E}_j^* - (\bar{j} \times \bar{B})_j = 0 \quad (196)$$

where the collision terms again cancel and use has been made of the current density relation to the species diffusion velocity:

$$\bar{j} = \sum_s \rho_{e_s} \bar{V}_s \quad (197)$$

For high current densities, all other diffusion mechanisms are negligible.

In order to obtain a momentum equation in a usable form, a relationship is required which relates the stress tensor $\bar{\bar{P}}$ to strain. Stokes hypothesis[19] is applicable here and used. Since the flow does not vary in the z direction nor have a velocity in that direction, Stokes' hypothesis may be written in two-dimensional form as:

$$\bar{\bar{P}} = -\begin{bmatrix} -p & 0 \\ 0 & -p \end{bmatrix} - \mu \begin{bmatrix} \frac{\partial u}{\partial x} & \frac{\partial u}{\partial y} \\ \frac{\partial v}{\partial x} & \frac{\partial v}{\partial y} \end{bmatrix} - \mu \begin{bmatrix} \frac{\partial u}{\partial x} & \frac{\partial v}{\partial x} \\ \frac{\partial u}{\partial y} & \frac{\partial v}{\partial y} \end{bmatrix} + \frac{2}{3} \begin{bmatrix} \nabla \cdot \bar{w}_o & 0 \\ 0 & \nabla \cdot \bar{w}_o \end{bmatrix} \quad (198)$$

A plasma is customarily defined such that it is initially electrically neutral and the Debye shielding length is small compared to the apparatus.[32] Since the Debye shielding length is the distance over which the ionized gas may be nonneutral, ρ_e may be set to zero

when dealing with an MHD generator in which the definition applies.

Setting ρ_e to zero and using Equations (14), (192), and (198) along with the steady state and two-dimensional assumptions, Equation (196) yields the x and y momentum equations:

$$\rho u \frac{\partial u}{\partial x} + \rho v \frac{\partial u}{\partial y} + \frac{\partial p}{\partial x} - \frac{\partial}{\partial x}\left[\mu\left(2\frac{\partial u}{\partial x} - \frac{2}{3}\nabla \cdot \bar{w}_o\right)\right] \tag{199}$$

$$- \frac{\partial}{\partial y}\left(\mu \frac{\partial u}{\partial y} + \mu \frac{\partial v}{\partial x}\right) - j_y B = 0$$

$$\rho u \frac{\partial v}{\partial x} + \rho v \frac{\partial v}{\partial y} + \frac{\partial p}{\partial y} - \frac{\partial}{\partial x}\left(\mu \frac{\partial v}{\partial y} + \mu \frac{\partial u}{\partial y}\right) \tag{200}$$

$$- \frac{\partial}{\partial y}\left[\mu\left(2\frac{\partial v}{\partial y} - \frac{2}{3}\nabla \cdot \bar{w}_o\right)\right] - j_x B = 0$$

Energy

The species energy equation is:

$$\frac{\partial}{\partial t}\left(\frac{1}{2}\rho_s w_{o_s}^2 + \rho_o \bar{w}_{o_s} \cdot \bar{V}_s + \rho_s e_s + \rho_s e_{s_{chem}}\right) \tag{201}$$

$$+ \nabla \cdot \left[\rho_s \bar{w}_{o_s}\left(\frac{1}{2} w_{o_s}^2\right) + \rho_s \bar{w}_{o_s}(\bar{V}_s \cdot \bar{w}_{o_s}) + \right.$$

$$\left. \rho_s \bar{w}_{o_s}(e_s + e_{s_{chem}}) + \bar{V}_s\left(\frac{1}{2}\rho_s w_{o_s}^2\right) + \bar{w}_{o_s} \cdot \bar{\bar{p}} + \bar{q}_s\right]$$

$$- \rho_{e_s}[\bar{E} \cdot \bar{w}_{o_s} + \bar{E} \cdot \bar{V}_s] =$$

$$- \left[\frac{\partial}{\partial t}\left(n_s \left\langle \frac{1}{2} m_s w_s^2 + \varepsilon_{s_r} + \varepsilon_{s_v} + \varepsilon_{s_c} \right\rangle\right)\right]$$

where $\bar{q}_s$ is energy transfer due to a spatial temperature variation, e is the energy carried by the molecules due to their rotation, vibration and translation, and e_{chem} is the energy due to chemical bonds. When (201) is summed over all species s, it results in:

$$\frac{\partial}{\partial t}\left(\frac{1}{2}\rho w_o^2 + \rho e + \rho e_{chem}\right) + \nabla \cdot \left[\rho \bar{w}_o \left(\frac{1}{2} w_o^2\right)\right. \tag{202}$$

$$\left. + \rho \bar{w}_o (e + e_{chem}) + \bar{w}_o \cdot \bar{\bar{P}} + \bar{q}\right]$$

$$- \rho_e \bar{E} \cdot \bar{w}_o - \bar{E} \cdot \bar{j} = 0$$

Radiation is not included here since energy exchange only due to molecular collisions and motions have been considered.

By use of the continuity equation, the following two relations may be shown:

$$\frac{1}{2}\rho \frac{Dw_o^2}{Dt} = \frac{\partial}{\partial t}\left(\frac{1}{2}\rho w_o^2\right) + \nabla \cdot \rho \bar{w}_o \left(\frac{1}{2} w_o^2\right) \tag{203}$$

$$\rho \frac{D(e + e_{chem})}{Dt} = \frac{\partial}{\partial t}(\rho e + \rho e_{chem}) +$$

$$\nabla \cdot [\rho \bar{w}_o (e + e_{chem})]$$

where $\frac{D}{Dt}$ represents the substantial derivative.

The right sides of (203) and (204) appear in the energy Equation (202) and may be substituted to yield:

$$\rho \frac{D(e + e_{chem})}{Dt} + \nabla \cdot [\bar{w}_o \cdot \bar{\bar{P}} + q] + \tag{205}$$

$$\frac{1}{2} \rho \frac{Dw_o^2}{Dt} - \rho_e \bar{E} \cdot \bar{w}_o - \bar{E} \cdot \bar{j} = 0$$

The x and y momentum Equations (199) and (200) are now multiplied by u and v, respectively, and added to Equation (205). Substituting Stokes' hypothesis, Equation (198), for $\bar{\bar{P}}$, the following is derived:

$$\rho \frac{D}{Dt} (e + e_{chem}) = -p\left(\frac{\partial u}{\partial x} + \frac{\partial v}{\partial y}\right) + \mu \frac{\partial u}{\partial x} \left(2 \frac{\partial u}{\partial x} - \frac{2}{3} \nabla \cdot \bar{w}_o\right) + \tag{206}$$

$$\mu \frac{\partial v}{\partial y} \left(2 \frac{\partial v}{\partial y} - \frac{2}{3} \nabla \cdot \bar{w}_o\right) + \mu\left(\frac{\partial u}{\partial y} + \frac{\partial v}{\partial x}\right)^2 - \nabla \cdot \bar{q} + \bar{w}_o$$

$$\cdot [\rho_e(\bar{w}_o \times \bar{B}) - \bar{j} \times \bar{B})] + \bar{E} \cdot \bar{J}$$

Use has also been made of the definition of $\bar{E}^*$, Equation (194).

For a dense plasma with a current flowing, $\bar{q}$ may be represented by:

$$\bar{q} = \frac{5}{2} \frac{k}{e} \bar{j} T_e - \kappa \nabla T \tag{207}$$

where the first term is the energy carried by the diffusion of electrons and the second is conduction heat transfer.

By using the continuity equation and assuming the perfect gas equation holds:

$$p = \rho RT \tag{208}$$

the following relationship may be shown:

$$p\left[\frac{\partial u}{\partial x} + \frac{\partial v}{\partial y}\right] = \rho R\left[u\,\frac{\partial T}{\partial x} + v\,\frac{\partial T}{\partial y}\right] - u\,\frac{\partial p}{\partial x} + v\,\frac{\partial p}{\partial y} \tag{209}$$

In the pressure and temperature region which an MHD device operates, the perfect gas equation of state is fully applicable.

Using Equations (7) and (15), the last term of (206) may be found to be

$$\bar{j} \cdot \bar{E} = \frac{j_x^2 + j_y^2}{\sigma} + \bar{w}_o \cdot (\bar{j} \times \bar{B}) \tag{210}$$

which demonstrates that the electrical energy extracted from the gas, $\bar{j} \cdot \bar{E}$, is the work which the gas does in flowing against the Lorenz force less the thermal energy given to the gas through Ohmic heating. The sign of the Ohmic heating term is positive with the other two terms being negative.

By use of Equations (207), (209), and (210), the energy Equation (206) may be written:

$$\rho\,\frac{D}{Dt}\,(e + e_{chem}) + \rho R\left(u\,\frac{\partial T}{\partial x} + v\,\frac{\partial T}{\partial y}\right) = \tag{211}$$

$$u \frac{\partial p}{\partial x} + v \frac{\partial p}{\partial y} + \mu \frac{\partial u}{\partial x} \left(2 \frac{\partial u}{\partial x} - \frac{2}{3} \nabla \cdot \bar{w}_o\right) +$$

$$\mu \frac{\partial v}{\partial y} \left(2 \frac{\partial v}{\partial y} - \frac{2}{3} \nabla \cdot \bar{w}_o\right) + \frac{5}{2} \frac{k}{e} \nabla \cdot (T_e \bar{j})$$

$$+ \nabla \cdot (\kappa \nabla T) + \mu \left(\frac{\partial u}{\partial y} + \frac{\partial v}{\partial x}\right)^2 + \frac{j_x^2 + j_y^2}{\sigma} \qquad (211)$$

In order for this equation to be useful, the energies e and e_{chem} must be related to temperature. The quantity e represents the conventional internal energy due to molecular motion and is given by:

$$e = c_v T \qquad (212)$$

where c_v, the specific heat, is assumed a constant. For potassium seeded argon, the fluid which is dealt with here, this is a valid assumption up to 10,000°K.[17,32]

It may be shown that the change in the chemical energy term, e_{chem}, may be neglected with respect to the change in the energy of molecular motion, e. The change in chemical energy is due to ionization and recombination and would appear as a change in percentage ionization of potassium which is a function of temperature, pressure, and current density. Taking a 0.2 per cent seeding rate, the average energy per gas mixture molecule required to reach a full singly ionized state is:

$$E_{chem} = eV_{i_k} f \left(\frac{1}{1 + f}\right) \qquad (213)$$

where:

V_{i_K} = ionization potential for potassium (4.34 volts).

f = seeding fraction by moles.

This gives:

$$E_{chem} = 1.39 \times 10^{-21} \text{ joules/molecule}$$

The average energy per gas mixture molecule due to molecular motion may be approximated by:

$$E_{internal} = \frac{3}{2} kT \tag{214}$$

For a 2000°K gas this gives:

$$E_{internal} = 4.14 \times 10^{-20} \text{ joules/molecule}$$

Therefore, by neglecting e_{chem}, using (212) for e, and the perfect gas relation:

$$c_p - c_v = R \tag{215}$$

the steady flow energy equation may be written from Equation (211) as:

$$\rho c_p \left(u \frac{\partial T}{\partial x} + v \frac{\partial T}{\partial y} \right) = u \frac{\partial p}{\partial x} + v \frac{\partial p}{\partial y} + \tag{216}$$

$$\frac{\partial}{\partial x}\left(\kappa \frac{\partial T}{\partial x}\right) - \frac{5}{2}\frac{k}{e} j_x \frac{\partial T_e}{\partial x} + \frac{\partial}{\partial y}\left(\kappa \frac{\partial T}{\partial y}\right) -$$

$$\frac{5}{2}\frac{k}{e} j_y \frac{\partial T_e}{\partial y} + \mu \left\{ 2\left[\left(\frac{\partial u}{\partial x}\right)^2 + \left(\frac{\partial v}{\partial y}\right)^2\right] + \right.$$

$$\left.\left(\frac{\partial v}{\partial x} + \frac{\partial u}{\partial y}\right)^2 - \frac{2}{3}\left(\frac{\partial u}{\partial x} + \frac{\partial v}{\partial y}\right)^2\right\} + \frac{j_x^2 + j_y^2}{\sigma}$$

Order of Magnitude Analysis

The continuity, momentum, and energy equations (192), (199), (200), and (216) in their present form are very complex. Great simplification can be accomplished for the boundary layer region in large Reynolds number flow. This is possible because many of the terms are negligible compared to others for this condition. Since all practical MHD gaseous generators operate at large Reynold's numbers, this assumption is made. This is also necessary in order to decouple the viscous effects from the free stream region as was done in Chapter II.

One may determine which terms are negligible in this case by an order of magnitude analysis of each term. The MHD effects increase the magnitude of certain terms over that which exists in conventional boundary layers.

All equations will be nondimensionalized by use of the following quantities where $(\ )_\infty$ denotes a characteristic value in the free stream and $(\ )_w$ the wall value.

$$u' \equiv \frac{u}{U}\ ;\quad v' \equiv \frac{v}{U}\ ;\ \xi \equiv \frac{x}{L}\ ,\quad y' \equiv \frac{y}{L}$$

$$\rho' \equiv \frac{\rho}{\rho_o} \; ; \quad \mu' \equiv \frac{\mu}{\mu_o} \; ; \quad P_\infty \equiv \frac{p}{\rho_o U^2} \; ; \quad J_x \equiv \frac{j_x}{\sigma_\infty UB}$$

$$J_y \equiv \frac{j_y}{\sigma_\infty UB} \; ; \quad B' \equiv \frac{B}{B_\infty} \; ; \quad \theta' \equiv \frac{T}{T_o} \; ; \quad \kappa' \equiv \frac{\kappa}{\kappa_o} \tag{217}$$

$$\theta = \frac{T}{T_\infty} \; ; \quad \theta_e \equiv \frac{T_e}{T} \; ; \quad \sigma' \equiv \frac{\sigma}{\sigma_\infty} \; ; \quad w_o' \equiv \frac{w_o}{U}$$

$$S_\infty = \frac{\sigma_\infty U_\infty B_\infty^2 L}{p_\infty} \; ; \quad M = \frac{U}{c} \; ; \quad \nabla' = L\nabla$$

Continuity

Writing the continuity Equation (192) in dimensionless form:

$$\frac{\rho_o U}{L} \left(\frac{\partial \rho' u'}{\partial \xi} + \frac{\partial \rho' v'}{\partial y'} \right) = 0 \tag{218}$$

For large Reynolds numbers the inertial forces are large compared to the viscous forces which restricts the viscous effects to a thin region near the wall and therefore causes y' to be very small in the viscous region under consideration, i.e.:

$$y' \sim \delta << 1 \tag{219}$$

From (218):

$$\frac{\partial \rho' u'}{\partial \xi} = - \frac{\partial \rho' v'}{\partial y'} \tag{220}$$

$$\frac{1}{1} \qquad \frac{1 \cdot v'}{\delta}$$

where the order of magnitude is written under each term. This leads to:

$$v' \sim \delta \tag{221}$$

No simplification is accomplished in the continuity equation but the result that v' is very small may be used to great advantage in the momentum and energy equations.

Momentum Equation

Writing the y momentum Equation (200) in dimensionless form using variables defined in (217) gives for constant free stream velocity:

$$\rho' u' \frac{\partial v'}{\partial \xi} + \rho' v' \frac{\partial v'}{\partial y'} = -\frac{\partial P_\infty}{\partial y'} + \tag{222}$$

$$1 \quad 1 \qquad \frac{\delta}{1} \qquad 1 \quad \delta \qquad \frac{\delta}{\delta}$$

$$\frac{1}{Re_{o_L}} \frac{\partial}{\partial y'} \left[\mu' \left(2 \frac{\partial v'}{\partial y'} - \frac{2}{3} \nabla' \cdot \bar{w}_o' \right) \right] + \frac{1}{Re_{o_L}} \frac{\partial}{\partial \xi} \left(\mu' \frac{\partial u'}{\partial y'} + \mu' \frac{\partial v'}{\partial \xi} \right)$$

$$\delta^2 \quad \frac{1}{\delta} \quad 1 \qquad \frac{\delta}{\delta} \qquad \frac{1}{1} + \frac{\delta}{\delta} \qquad \delta^2 \quad \frac{1}{1} \quad 1 \quad \frac{1}{\delta} \quad 1 \quad \frac{\delta}{1}$$

$$+ \frac{S_\infty P}{\gamma M_o^2 P_o} J_x B'$$

$$\frac{1}{1} \quad 1 \quad 1$$

with the order of magnitude written under each term except for the term $\partial P_\infty / \partial y'$ whose order of magnitude is not known. Since Re is on the

order of 10^4, then $\frac{1}{Re_{o_L}}$ is taken to be on the order of δ^2. The interaction parameter, S_∞, is a measure of the fraction of the pressure potential energy removed and will be of the order of one. The Mach number will also be approximately one.

By inspection of (222) it is seen that all terms except $\partial P_\infty/\partial y'$ and the last term are of the order of δ. Since the last term is of order one then $\partial P_\infty/\partial y'$ must also be of order one and all other terms are negligible which leads to:

$$\frac{\partial P_\infty}{\partial y'} = \frac{S_\infty P_\infty}{\gamma M_o^2 P_o} J_x B' \tag{223}$$

This says that the pressure gradient normal to the plate in the boundary layers is of the same order of magnitude as the axial pressure gradient which is discussed later. However, the pressure inside the boundary layer may be taken equal to the pressure in the free stream. This is seen by looking at the pressure change as one moves from the wall to the free stream at a particular x location. It is given by:

$$P_\infty - P_w = \int_o^\delta \frac{\partial P_\infty}{\partial y'} dy' \sim 1 \cdot \delta \tag{224}$$

which shows the pressure change is small or:

$$P_\infty - P_w \sim \delta \tag{225}$$

This is due to the fact that the Hall current, J_x, only flows in the

boundary layers and $\partial P_\infty/\partial y'$ acts over a very small distance to change the pressure.

Therefore, the y momentum equation gives an expression for the pressure gradient normal to the plate and indicates the pressure in the boundary layer may be taken equal to the pressure in the free stream at the same x value.

Writing the x momentum equation (199) in dimensionless form gives:

$$\rho'\left(u'\frac{\partial u'}{\partial \xi} + v'\frac{\partial u'}{\partial y'}\right) = -\frac{\partial P_\infty}{\partial \xi} + \tag{226}$$

$$1 \quad 1 \quad \frac{1}{1} \qquad \delta \quad \frac{1}{\delta} \qquad\qquad \frac{1}{1}$$

$$\frac{1}{Re_{o_L}}\frac{\partial}{\partial \xi}\left[\mu'\left(2\frac{\partial u'}{\partial \xi} - \frac{2}{3}\nabla'\cdot\bar{w}_o'\right)\right] + \frac{1}{Re_{o_L}}\frac{\partial}{\partial y'}\left[\mu'\left(\frac{\partial u'}{\partial y'} + \frac{\partial v'}{\partial \xi}\right)\right]$$

$$\delta^2 \frac{1}{1} \quad 1 \frac{1}{1} \quad 1 \frac{1}{1} + \frac{\delta}{\delta} \qquad \delta^2 \frac{1}{\delta} \quad 1 \quad \frac{1}{\delta} \quad \frac{\delta}{1}$$

$$+ \frac{S_\infty P_\infty}{\gamma M_o^2 P_o} J_y B'$$

$$\frac{1}{1} \quad 1 \; 1$$

Neglecting terms of order δ:

$$\rho'\left(u'\frac{\partial u'}{\partial \xi} + v'\frac{\partial u'}{\partial y'}\right) = -\frac{\partial P_\infty}{\partial \xi} + \frac{1}{Re_{o_L}}\frac{\partial}{\partial y'}\left[\mu'\frac{\partial u'}{\partial y'}\right] + \frac{S_\infty P_\infty}{\gamma M_o^2 P_o} J_y B' \tag{227}$$

It is seen that if $\frac{1}{Re_{o_L}}$ is larger than δ^2, that the viscous terms dominate the inertial terms.

Energy Equation

When the energy Equation (216) is written in dimensionless form the expression is found for constant free stream velocity:

$$\rho'\left[u'\frac{\partial\theta'}{\partial\xi}+v'\frac{\partial\theta'}{\partial y'}\right]=\frac{M^2}{\gamma-1}\left(u'\frac{\partial P_\infty}{\partial\xi}+v'\frac{\partial P_\infty}{\partial y'}\right) \tag{228}$$

$$1\quad 1\quad \frac{1}{1}\qquad \delta\quad \frac{1}{\delta}\qquad\qquad 1\qquad\qquad 1\quad 1\qquad \delta\quad 1$$

$$+\frac{1}{Re_{o_L}Pr}\left[\frac{\partial}{\partial\xi}\left(\kappa'\frac{\partial\theta'}{\partial\xi}\right)+\frac{\partial}{\partial y'}\left(\kappa'\frac{\partial\theta'}{\partial y'}\right)\right]-$$

$$\delta^2\qquad \frac{1}{1}\quad 1\qquad \frac{1}{1}\qquad\qquad \frac{1}{\delta}\quad 1\qquad \frac{1}{\delta}$$

$$\frac{\sigma_\infty B_\infty W_A}{N_o e\rho_o}\left(J_y\frac{\partial(\theta_e\theta')}{\partial y'}+J_x\frac{\partial\theta_e\theta'}{\partial\xi}\right)+$$

$$\delta\qquad 1\qquad \frac{1}{\delta}\qquad\qquad 1\qquad \frac{1}{1}$$

$$\frac{\gamma-1}{Re_{o_L}}M_o^2\mu'\left(2\left[\left(\frac{\partial u'}{\partial\xi}\right)^2+\left(\frac{\partial v'}{\partial y'}\right)^2\right]+\left(\frac{\partial v'}{\partial\xi}+\frac{\partial u'}{\partial y'}\right)^2\right.$$

$$\delta^2\quad 1\ 1\qquad \frac{1}{1}\qquad\qquad \frac{\delta}{\delta}\qquad\qquad \frac{\delta}{1}\qquad \frac{1}{\delta}$$

$$\left.-\frac{2}{3}\left(\frac{\partial u'}{\partial\xi}+\frac{\partial v'}{\partial y'}\right)^2\right)+S_\infty\left(\frac{\gamma-1}{\gamma}\right)\left(\frac{J_x^2+J_y^2}{\sigma'}\right)\frac{P_\infty}{P_o} \tag{228}$$

$$\frac{1}{1}\qquad \frac{\delta}{\delta}\qquad\qquad 1\quad 1\qquad\qquad \frac{1}{1}$$

where N_o is Avogadro's number and W_A is the atomic mass of the gas.

When terms smaller than one are neglected:

$$\rho' \left[u' \frac{\partial \theta'}{\partial \xi} + v' \frac{\partial \theta'}{\partial y'} \right] = \frac{M_o^2}{\gamma - 1} u' \frac{dP_\infty}{d\xi} \tag{229}$$

$$+ \frac{1}{Re_{o_L} Pr} \frac{\partial}{\partial y'} \left(\kappa' \frac{\partial \theta'}{\partial y'} \right) - \frac{\sigma_\infty B W_A}{N_o e \rho_o} \left[J_y \frac{\partial (\theta_e \theta')}{\partial y'} \right]$$

$$+ \frac{\gamma - 1}{Re_{o_L}} M_o^2 \mu' \left(\frac{\partial u'}{\partial y'} \right)^2 + S_\infty \left(\frac{\gamma - 1}{\gamma} \right) \left(\frac{J_x^2 + J_\infty^2}{\sigma'} \right) \frac{P_\infty}{P_o}$$

Using θ based on T_∞ in place of θ' based on T_o and the free stream energy Equation (5):

$$\rho' \left[u' \frac{\partial \theta}{\partial \xi} + v' \frac{\partial \theta}{\partial y'} \right] = \frac{1}{Re_{o_L} Pr} \frac{\partial}{\partial y'} \left(\kappa' \frac{\partial \theta}{\partial y'} \right) - \tag{230}$$

$$\frac{\sigma_\infty B W_A}{N_o e \rho_o} \left[J_y \frac{\partial (\theta_e \theta)}{\partial y'} \right] + \frac{\gamma - 1}{Re_{o_L}} M^2 \left(\frac{\partial u'}{\partial y'} \right)^2$$

$$+ \frac{S_\infty}{T'_\infty} \frac{P_\infty}{P_o} \left(\frac{\gamma - 1}{\gamma} \right) \left(\frac{J_x^2 + J_\infty^2}{\sigma'} - u' \right)$$

APPENDIX B

ELECTRICAL CONDUCTIVITY COMPUTER PROGRAM

```
-9     FOR    MAIN
       DIMENSION QEA(86),QEK(86),PHI(3)
       DOUBLE PRECISION EXK,EXA,CC,AN,AK,AL,B,C,D,P,Q,DISCR,R,ARG1,ARG2,
      1Y1,RAD,COSP,PHI,TEST,DELTA,COSN
    10 FORMAT (116H           PO       TO          TE           J           SIGM
      1A         NE        HALL/B    R NEUTRALS    R COULOMB  RESISTIVITY)
    11 FORMAT (113H           ATM      DEG K       DEG K      AMP/M2          MHO/
      1M    ELECTRONS/M3 M2/WEBER     OHM-M         OHM-M          OHM-M/)
    20 FORMAT (5(F8.4,F8.1))
   200 FORMAT (F12.1,2F10.0,E12.4,F12.3,E12.4,F10.3,3F12.5)
       PRINT 10
       PRINT 11
       CPI=3.1415926536
       CME=9.1085E-31
       CK=1.3804E-23
       CH=6.6252E-34
       CE=1.6021E-19
       CVKI=4.34
       CVAI=15.68
       CF=.003
       AM=CF+1
       CMA=6.55621E-26
       EO=8.855E-12
       DELTA=2.0943951024
       READ 20,(QEA(L),QEK(L),L=1,86)
       PO=0
       DO 302 K=1,6
       PO=PO+0.5067E5
       POA=PO/1.0133E5
       DO 301 J=1,16
       TO=J*100+1400
       DO 300 I=J,86
       TE=I*100.+1400.
       CC=(2*CPI*(CME/CH)*(CK/CH)*TE)**1.5
       EXK=(CVKI*CE)/(CK*TE)
       EXA=(CVAI*CE)/(CK*TE)
       AK=CC*EXP(-EXK)
       AL=8*CC*EXP(-EXA)
```

```
      AN=PO/(CK*TO)
      B=(AK+AL)*1.E-12
      C=(AK*(AL-AN)+(AN/AM)*(AK-AL))*1.E-24
      D=(-AK*AN*AL)*1.E-36
      P=C-B**2/3
      Q=D-(B*C)/3+(2*B**3)/27
   90 R=(P/3)**3+(Q/2)**2
      IF (DISCR) 90,260,260
      DISCR=-4*P**3-27*Q**2
      ARG1=-Q/2+SQRT(R)
      ARG2=-Q/2-SQRT(R)
      A1=CBRT(ARG1)
      A2=CBRT(ARG2)
  120 Y1=A1+A2
      XNE=(Y1-B/3)*1.E12
      XJ=3*XNE*CE*XNE*CE*(CK/(2.*CMA))
      XJ=XJ*(TE-TO)
      XJ=SQRT(XJ)
      L=L+1
      SEG1=SQRT((B*CK*TE)/(CPI*CME))
      SEG2=(CME*AN)/(XNE*CE*AM*CE)
      SEG3=QEA(L)+CF*QEK(L)
      SEG3=SEG3*1.E-20
      IF (XNE.LT.0.0) GO TO 300
      SEG4=((12*CPI*EO*CK*TE/CE/CE)*SQRT(EO/XNE)*SQRT(CK*TE))/CE
      SEG4=ALOG(SEG4)
      SIGMAR=(4./3.)*SEG1*SEG2*SEG3+(65.3/TE**1.5)*SEG4
      SIGMA=1/SIGMAR
      HALL=SIGMA/XNE/CE
      PRINT 200,POA,TO,TE,XJ,SIGMA,XNE,HALL,SEG7,SEG6,SIGMAR
      GO TO 300
  260 COSP=(-Q/2)/SQRT((-P**3)/27)
      TEST=DATAN(SQRT(1-COSP*COSP)/COSP)
      IF (COSP.LT.0) TEST=3.14159265358979323D+0+TEST
      IF (COSP.EQ.0) TEST=1.57079632679489661D+0
      PHI(1)=TEST/3
      PHI(2)=PHI(1)+DELTA
      PHI(3)=PHI(2)+DELTA
```

```
      RAD=2*SQRT(-P/3)
      DO 299 M=1,3
      COSN=DCOS(PHI(M))
      XNE=(RAD*COSN-B/3)*1.E12
      IF(XNE) 299,299,275
  275 XJ=3*XNE*CE*XNE*CE*(CK/(2.*CMA))
      XJ=XJ*(TE-TO)
      XJ=SQRT(XJ)
      SEG1=SQRT((8*CK*TE)/(CPI*CME))
      SEG2=(CME*AN)/(XNE*CE*AM*CE)
      SEG3=QEA(I)+CF*QEK(I)
      SEG3=SEG3*1.E-20
      SEG4=((12*CPI*EO*CK*TE/CE/CE)*SQRT(EO/XNE)*SQRT(CK*TE))/CE
      SEG5=ALOG(SEG4)
      SEG6=(65.3/TE**1.5)*SEG5
      SEG7=(4./3.)*SEG1*SEG2*SEG3
      SIGMAR=SEG6+SEG7
      SIGMA=1/SIGMAR
      HALL=SIGMA/XNE/CE
      PRINT 200,POA,TO,TE,XJ,SIGMA,XNE,HALL,SEG7,SEG6,SIGMAR
  299 CONTINUE
  300 CONTINUE
  301 CONTINUE
  302 CONTINUE
      END
- XQT    MAIN/CODE
   .6380    402.4   0.6179    402.3   0.6054    402.6   0.5998    403.2   0.6005    404.0
   .6070    404.9   0.6188    406.1   0.6352    407.3   0.6560    408.6   0.6806    409.9
   .7089    411.2   0.7404    412.5   0.7748    413.8   0.8118    415.0   0.8513    416.1
   .8929    417.1   0.9366    418.1   0.9820    418.9   1.0290    419.7   1.0780    420.4
  1.1270    420.9   1.1780    421.4   1.2300    421.7   1.2830    422.0   1.3370    422.2
  1.3920    422.3   1.4470    422.2   1.5030    422.1   1.5600    422.0   1.6170    421.7
  1.6740    421.4   1.7320    421.0   1.7900    420.5   1.8480    420.0   1.9070    419.4
  1.9660    418.8   2.0250    418.1   2.0840    417.4   2.1440    416.6   2.2030    415.8
  2.2630    415.0   2.3220    414.1   2.3820    413.2   2.4410    412.2   2.5010    411.2
  2.5610    410.2   2.6200    409.2   2.6800    408.1   2.7400    407.1   2.7990    406.0
  2.8590    404.9   2.9180    403.8   2.9780    402.6   3.0370    401.5   3.0960    400.3
  3.1560    399.2   3.2150    398.0   3.2740    396.8   3.3330    395.6   3.3920    394.4
```

3.4510	393.3	3.5090	392.1	3.5680	390.9	3.6270	389.6	3.6850	388.4
3.7440	387.2	3.8020	386.0	3.8600	384.8	3.9190	383.6	3.9770	382.4
4.0350	381.2	4.0930	380.0	4.1510	378.8	4.2080	377.6	4.2660	376.4
4.3240	375.2	4.3810	374.0	4.4390	372.9	4.4960	371.7	4.5540	370.5
4.6110	369.3	4.6680	368.2	4.7250	367.0	4.7820	365.9	4.8390	364.7
4.8960	363.6								

APPENDIX C

MHD BOUNDARY LAYER COMPUTER PROGRAM

```
      FOR   MAIN
      DIMENSION U(2,500),THETA(2,500),PHI(2,500),SIGBL(2,500)
     1,THETEC(2,500),JX(2,500),XNEBL(2,500),DFDS(2,500),ETA(500),ELN(500
     2),SIGBLN(2,500),VLDT(1001),NUS(1001),MOREX(1001),NUSJ(1001),
     3HALL(500),YN(500),CD(1001)
      COMMON /FSM/JYEN(1001),SIGEN(1001),TEXN(1001),PN(1001),PO,
     1TO,UO,BW,MS,DX,JYEO,SIGEO,P(1001),TEX(1001),JYEX(1001),SIGEX(1001)
     2,TECFS(1001),TECNFS(1001),MACH(1001),XNEX(1001),HALLO,
     3HALEX(1001)
      COMMON /MFSH/HDUM1
      COMMON /FSMSIG/SIGMA,XNE,TE
      COMMON /SIGHM/CJX
      COMMON /MSPTT/C4,C5K,C5A,C6,C1,C3,CK,AM,CF,QEA(86),QEK(86)
      COMMON /MSIGO/S2DUM1
      COMMON /MFD/ALPHA(500),BETA(500),RL(2,500),EPS(500),DPSI,S3DUM1,
     1S3DUM2
      COMMON /MIP/X2(1000),X3(500),X5(500),PR,THETAW
      COMMON /MIPFD/NMAX,NMP1
      COMMON /MFSIP/GAMMA
      COMMON /WRI/K9
      REAL JYEO,JYEN,JX,JYEX,JYEXH,MACH,MOREX,NUS,KCW,NUSJ,SIGN
      DATA POA/3.0/,TO/2000.0/,CMACHO/1.0/,THETAW/0.5/,EFF/0.5/,
     1CF/0.002/,S/1.0/,RLEN/0.3/
   49 FORMAT (5(F8.4,F8.1))
   60 FORMAT (119H   PSI      MACH      TEX/TO       PN       JY/JYO SIGMAE/
     1SIGMAO VLDT     CD*SR(RE)  NU/SR(RE)  NUJ/SR(RE)    HALL       Y/YN)
   61 FORMAT (1H0,F5.3,7F10.5,F11.5,F12.5,F11.5,F10.5)
   62 FORMAT  (///115H     ETA         YN            U          THETA
     1  PHI        THETEC    SIGMA/SIGMAE    JX/JY     EL/ELEX        HALL/
     2)
   63 FORMAT(F8.2,9F12.5)
   64 FORMAT(1H1,10H      PO =,F4.1,12H ATM    TO =,F6.0,16H DEG K    MA
     1CH =,F4.1,7H    L =,F4.2,16H METER    SIGN =,F4.0,7H    B =,F5.2,
     213H WEBER    S =,F4.1///)
  286 FORMAT (7F15.4)
  287 FORMAT (8E15.6)
      READ 49,(QEA(L),QEK(L),L=1,86)
C   ASSIGNMENT OF CONSTANTS AND INITIAL VALUES
```

```
      K9=0
      DPSI=0.04
      DX=DPSI
      DETA=2.0E-1
      PO=POA*1.0133E5
      BW=2.0
      GAMMA=1.6666667
      PR=0.6665
      UPR=1.
      CE=1.602E-19
      CP=520.3525
      CK=1.3804E-23
      C1=2.12936E14
      C3=1.23843E7
      C4=1.79984E14
      C5K=5.03671E4
      C5A=1.819709E5
      C6=8.1063E-36
      R=208.141
      AM=CF+1
      U0=CMACH0*SQRT(5.*R*T0/3.)
      S3DUM1=4.*DETA
      S3DUM2=S3DUM1*DETA
      DUM1=5.*CK/CP/CE/2.
      DUM2=(GAMMA-1.)*CMACH0*CMACH0
      DUM3=2.*RLEN*(GAMMA-1.)/(GAMMA*U0)
      DUM4=(EFF-1)/EFF
      RM0=0.9377E-8*P0/SQRT(T0)
      KCW=1.51661E-3*SQRT(THETAW*T0)
      DUM5=5.*CK*RLEN/(KCW*CE*2.)
      ROE0=P0/(R*T0)
      JYE0=0.
      MS=(1./DX)
      MSP1=MS+1
      LM=0
      TE=T0
  291 S2DUM1=U0*Bw*(EFF-1.)
C     ITERATION TO FIND MAGNETIC FIELD SUCH THAT INTERATION PARAMETER IS
```

```
    1 PROPER VALUE
      CALL SIGPTO(PO,TO,TE,JYE0)
      SIGE0=SIGMA
      BWC=SQRT(S*PO/SIGE0/RLEN/U0)
      BWER=BWC-BW
      IF (ABS(BWER).LT.0.001) GO TO 288
      IF (LM.EQ.1) GO TO 290
      LM=1
      BWH=BW
      BWERH=BWER
      BW=BW+0.1
      GO TO 291
  290 DBW=-BWER*(BW-BWH)/(BWER-BWERH)
      BWH=BW
      BWERH=BWER
      BW=BW+DBW
      GO TO 291
  288 HDUM1=BW/CE
      HALL0=SIGE0*HDUM1/XNE
      XNEX(1)=XNE
      PRINT 287 PO,TO,U0,BW,S,SIGE0,JYE0,XNE,TE,HALL0
C     SOLVE FOR FREE STREAM FLOW
      CALL FRST(CMACH0,RLEN,EFF,S)
      DO 289 M=1,MSP1
      MOREX(M)=4.0617E-4*TEX(M)*SQRT(TEX(M))/P(M)
      PSI=(M-1)*DX
  289 CONTINUE
C     SOLVE FOR INITIAL PROFILE
      CALL IP(CMACH0,DETA)
      NMAXIP=NMAX
      DO 50 KSIGN=-1,1,2
      SIGN=KSIGN
C       FOR CATHODE SIGN=+1, FOR ANODE SIGN=-1
      NMAX=NMAXIP
      PRINT 64, POA,TO,CMACH0,RLEN,SIGN,BW,S
      PRINT 60
C     INITIALIZE BOUNDARY LAYER VALUES
      PSIMP1=0.
```

```
      NUS(1)=0.
      MP=1
      VLDT(1)=0.
      CJX=0.
      DO 17 N=1,NMAX
      ETA(N)=DETA*(N-1)
      YN(N)=0.
      U(1,N)=X2(N)
      THETA(1,N)=X5(N)
      PHI(1,N)=X3(N)
      TBL=TO*THETA(1,N)
      QJX=CJX
      CALL SIGPTH(PO,TBL,JYE0,TE,QJX,XNEX(1))
      SIGBL(1,N)=SIGMA
      SIGBLN(1,N)=SIGMA/SIGE0
      HALL(N)=HDUM1*SIGMA/XNE
      THETEC(1,N)=TE/TBL
      JX(1,N)=CJX
      ELN(N)=DUM4*(1.+HALL(N)*JX(1,N))/SIGBLN(1,N)+U(1,N)/EFF
      IF (N.EQ.1) GO TO 41
      VLDT(1)=(THETA(1,N-1)*(1.-ELN(N-1))+THETA(1,N)*
     1(1.-ELN(N)))*DETA/2.+VLDT(1)
   41 CONTINUE
      DFDS(1,N)=0.
   17 RL(1,N)=SQRT(1/THETA(1,N))
      NUP=NMAX+100
      DO 42 N=NMAX,NUP
   42 ETA(N)=DETA*(N-1)
      NMAX=NMAX-1
      NMP1=NMAX+1
      M=0
      NUS(M+1)=(THETA(1,2)-THETA(1,1))/(DETA*THETA(1,1)*(1.-THETA(1,1)))
      CD(1)=(U(1,2)-U(1,1))*RL(1,1)/DETA
      F3PSI=0.
      PRINT 61 PSIMP1,MACH(M+1),TEXN(M+1),PN(M+1),JYEN(M+1),SIGEN(M+1),
     1VLDT(M+1),CD(M+1),NUS(M+1),NUSJ(M+1),HALEX(M+1),F3PSI
      PRINT 62
      PHI(2,1)=0.
```

```
      DO 32 N=1,NMAX
   32 PRINT 63, ETA(N),YN(N),U(MP,N),THETA(MP,N),PHI(MP,N),THETEC(MP,N),
     1SIGBLN(MP,N),JX(MP,N),ELN(N),HALL(N)
      PSIM=0.
C    SET CONSTANTS FOR FIXED AXIAL POSITION
   18 M=PSIM/DPSI+1.1
      PSIMP1=PSIM+DPSI
      PSIMPH=PSIM+DPSI/2
      THETA(2,1)=THETAW
      U(2,1)=0.
      SIGEXH=(SIGEX(M)+SIGEX(M+1))/2
      JYEXH=(JYEX(M)+JYEX(M+1))/2
      F1PSI=JYEXH*DUM1*(2.*PN(1)/(PN(M)+PN(M+1)))*(2./(TEXN(M)+TEXN(M+1)
     1))*SQRT(PSIMPH*RLEN/(U0*RM0))
      F2PSI=DUM3*JYEXH*JYEXH*PSIMPH/((P(M)+P(M+1))*SIGEXH)
      F3PSI=SQRT(MOREX(M+1)*PSIMP1/U0/RLEN)
      TEXMH=(TEX(M)+TEX(M+1))/2.
      ITER=0
      MP=1
C    CALCULATE FINITE DIFFERENCE COEFFICIENTS
   19 DO 22 N=2,NMP1
      ALPHA(N)=PSIMPH*(U(1,N)+U(MP,N))/2.
      DFDS(2,N)=(PHI(MP,N)-PHI(1,N))/DPSI
      BETA(N)=PSIMPH*DFDS(MP,N)+(PHI(1,N)+PHI(MP,N))/4.
      IF (MP.EQ.1) GO TO 20
      RL(2,N)=(PN(M+1)/PN(1))*SQRT(1./(THETA(2,N)*TEXN(M+1)))
      GO TO 21
   20 RL(2,N)=RL(1,N)*(PN(M+1)/PN(M))*SQRT(TEXN(M)/TEXN(M+1))
   21 CONTINUE
   22 EPS(N)=0.0
      RL(2,1)=(PN(M+1)/PN(1))*SQRT(1./(THETA(MP,1)*TEXN(M+1)))
      CALL FD(U,UPR)
      DO 23 N=2,NMP1
   23 PHI(2,N)=((U(2,N)+U(2,N-1))/2.)*DETA+PHI(2,N-1)
      DO 24 N=2,NMAX
      ALPHA(N)=ALPHA(N)
      BETA(N)=BETA(N)+SIGN*F1PSI*(THETEC(1,N)+THETEC(MP,N))/2.
      EPS(N)=SIGN*F1PSI*((THETA(1,N)*(THETEC(1,N+1)-THETEC(1,N-1))/
```

```
     1S3DUM1)+THETA(MP,N)*(THETEC(MP,N+1)-THETEC(MP,N-1))/S3DUM1)
      EPS(N)=EPS(N)+((RL(1,N)+RL(2,N))/2.)*DUM2*(TE/TEXMH)*(U(1,N+1)
     1-U(1,N-1))*(U(2,N+1)-U(2,N-1))/S3DUM2
   24 EPS(N)=EPS(N)+F2PSI*(THETA(1,N)+THETA(MP,N))*((1.+JX(1,N)*JX(MP,N
     1))/(SIGBLN(1,N)+SIGBLN(MP,N))-(U(MP,N)+U(1,N))/4.)
C    FIND BOUNDARY LAYER VALUES AT M+1
      CALL FD(THETA,PR)
      DO 30 N=1,NMP1
      TBL=THETA(2,N)*TEX(M+1)
      TECBL=THETEC(MP,N)*TBL
      CALL SIGPTH(P(M+1),TBL,JYEX(M+1),TECBL,JX(MP,N),XNEX(M+1))
      SIGBL(2,N)=SIGMA
      SIGBLN(2,N)=SIGMA/SIGEX(M+1)
      JX(2,N)=CJX
      THETEC(2,N)=TE/TBL
   30 XNEBL(2,N)=XNE
      IF (ITER.EQ.0) MP=2
      IF (ITER.EQ.2) GO TO 26
      ITER=ITER+1
      GO TO 19
   26 HALL(1)=HDUM1*SIGBL(2,1)/XNEBL(2,1)
      YN(1)=0.
      ELN(1)=DUM4*(1.+HALL(1)*JX(2,1))/SIGBLN(2,1)+U(2,1)/EFF
      VLDT(M+1)=0.
      CD(M+1)=SQRT(TEXN(M+1)/THETAW)*(U(2,2)-U(2,1))/DETA
      NUS(M+1)=((THETA(2,2)-THETA(2,1))/(DETA*THETA(2,1)*(1.-THETA(2,1))
     1))*SQRT((PN(M+1)/PN(1))/SQRT(TEXN(M+1)))
      IF (SIGN.GT.0.) GO TO 40
      NUSJ(M+1)=-DUM5*JYEX(M+1)*THETEC(2,1)*THETA(2,1)*F3PS1/
     1(1.0-THETA(2,1))
      GO TO 43
   40 NUSJ(M+1)=0.
   43 DO 31 N=2,NMAX
      HALL(N)=HDUM1*SIGBL(2,N)/XNEBL(2,N)
      ELN(N)=DUM4*(1.+HALL(N)*JX(2,N))/SIGBLN(2,N)+U(2,N)/EFF
      YN(N)=(THETA(2,N-1)+THETA(2,N))*DETA/2.+YN(N-1)
   31 VLDT(M+1)=SQRT((PN(1)/PN(M+1))*SQRT(TEXN(M+1)))*(THETA(2,N-1)*
     1(1.-ELN(N-1))+THETA(2,N)*(1.-ELN(N)))*DETA/2.+VLDT(M+1)
```

```
      PRINT 64, POA,TO,CMACH0,RLEN,SIGN,BW,S
      PRINT 60
      PRINT 61 PSIMP1,MACH(M+1),TEXN(M+1),PN(M+1),JYEN(M+1),SIGEN(M+1),
     1VLDT(M+1),CD(M+1),NUS(M+1),NUSJ(M+1),HALEX(M+1),F3PSI
      PRINT 62
      DO 29 N=1,46,1
   29 PRINT 63, ETA(N),YN(N),U(MP,N),THETA(MP,N),PHI(MP,N),THETEC(MP,N),
     1SIGBLN(MP,N),JX(MP,N),ELN(N),HALL(N)
C    REINITIALIZE VALUES
      PSIM=PSIM+DPSI
      PSIMP1=PSIM+DPSI
      IF (PSIMP1.GT.1.) GO TO 28
      DO 27 N=1,NMP1
      U(1,N)=U(2,N)
      THETA(1,N)=THETA(2,N)
      PHI(1,N)=PHI(2,N)
      JX(1,N)=JX(2,N)
      SIGBL(1,N)=SIGBL(2,N)
      THETEC(1,N)=THETEC(2,N)
      RL(1,N)=RL(2,N)
      DFDS(1,N)=DFDS(2,N)
   27 CONTINUE
      GO TO 18
   28 CONTINUE
   50 CONTINUE
   51 CONTINUE
      END
```

```
      SUBROUTINE IP(CM0,H)
      DIMENSION X1(1000),X4(1000)
      COMMON /MIP/X2(1000),X3(500),X5(500),PR,THETAW
      COMMON /MIPFD/NMAX,NMP1
      COMMON /MFSIP/GAMMA
      DEFINE F1(Y1,Y3,CL)=-Y1*Y3/(2*CL)
      DEFINE F2(Y1,CL)=Y1/CL
      DEFINE F3(Y2)=Y2
      DEFINE F4(PR,CL,CM0,GAMMA,Y1,Y3,Y4)=-PR*Y4*Y3/(2*CL)-(GAMMA-1)*CM0
     1*CM0*Y1*Y1/CL
      DEFINE F5(PR,CL,Y4)=Y4*PR/CL
      DEFINE F6(Y5)=SQRT(1/Y5)
  122 FORMAT (11X,3HETA,11X,3HPSI,13X,1HU,12X,5HTHETA/)
  123 FORMAT (1H ,F15.3,3F15.5)
  124 FORMAT (10X,7HX1(1) =,F7.5,10X,7HX4(1) =,F7.5//)
      X1(1)=0.35
      X2(1)=0.
      X3(1)=0
      X4(1)=0.7
      X5(1)=THETAW
      DEL1=1.E-7
      DEL2=.000001
      L=0
   90 M=1
  100 DUM1=X1(M)
      DUM2=X2(M)
      DUM3=X3(M)
      DUM4=X4(M)
      CL=F6(X5(M))
      D1X1=F1(DUM1,DUM3,CL)*H
      D1X2=F2(DUM1,CL)*H
      D1X3=F3(DUM2)*H
      D1X4=F4(PR,CL,CM0,GAMMA,DUM1,DUM3,DUM4)*H
      D1X5=F5(PR,CL,DUM4)*H
      DUM1=X1(M)+.5*D1X1
      DUM2=X2(M)+.5*D1X2
      DUM3=X3(M)+.5*D1X3
      DUM4=X4(M)+.5*D1X4
```

```
      D2X1=F1(DUM1,DUM3,CL)*H
      D2X2=F2(DUM1,CL)*H
      D2X3=F3(DUM2)*H
      D2X4=F4(PR,CL,CM0,GAMMA,DUM1,DUM3,DUM4)*H
      D2X5=F5(PR,CL,DUM4)*H
      DUM1=X1(M)+.5*D2X1
      DUM2=X2(M)+.5*D2X2
      DUM3=X3(M)+.5*D2X3
      DUM4=X4(M)+.5*D2X4
      DUM5=X5(M)+.5*D2X5
      CL=F6(DUM5)
      D3X1=H*F1(DUM1,DUM3,CL)
      D3X2=H*F2(DUM1,CL)
      D3X3=H*F3(DUM2)
      D3X4=H*F4(PR,CL,CM0,GAMMA,DUM1,DUM3,DUM4)
      D3X5=H*F5(PR,CL,DUM4)
      DUM1=X1(M)+D3X1
      DUM2=X2(M)+D3X2
      DUM3=X3(M)+D3X3
      DUM4=X4(M)+D3X4
      DUM5=X5(M)+D3X5
      CL=F6(DUM5)
      D4X1=H*F1(DUM1,DUM3,CL)
      D4X2=H*F2(DUM1,CL)
      D4X3=H*F3(DUM2)
      D4X4=H*F4(PR,CL,CM0,GAMMA,DUM1,DUM3,DUM4)
      D4X5=H*F5(PR,CL,DUM4)
      X1(M+1)=X1(M)+(D1X1+2*D2X1+2*D3X1+D4X1)/6
      X2(M+1)=X2(M)+(D1X2+2*D2X2+2*D3X2+D4X2)/6
      X3(M+1)=X3(M)+(D1X3+2*D2X3+2*D3X3+D4X3)/6
      X4(M+1)=X4(M)+(D1X4+2*D2X4+2*D3X4+D4X4)/6
      X5(M+1)=X5(M)+(D1X5+2*D2X5+2*D3X5+D4X5)/6
      ETA=H*(M)
      IF (X5(M+1).GE.THETAW) GO TO 103
      X4(1)=X4(1)+0.05
      L=0
      GO TO 90
  103 CONTINUE
```

```
      M=M+1
      GO TO 100
  300 IF (ABS(X2(M+1)-1).LE.DEL2.AND.ABS(X5(M+1)-1).LE.DEL2) GO TO 999
      IF (L.EQ.2) GO TO 408
      IF (L.EQ.1) GO TO 400
      L=1
      X101=X1(1)
      X1(1)=X1(1)+.0001
      X2INFH=X2(M+1)
      X5INFH=X5(M+1)
      GO TO 90
  400 PDX2=X2(M+1)-X2INFH
      PDX5=X5(M+1)-X5INFH
      PDX1=X1(1)-X101
      A1=PDX2/PDX1
      A2=PDX5/PDX1
      L=2
      X401=X4(1)
      X4(1)=X4(1)+.0001
      X2INFH=X2(M+1)
      X5INFH=X5(M+1)
      GO TO 90
  408 PDX2=X2(M+1)-X2INFH
      PDX5=X5(M+1)-X5INFH
      PDX4=X4(1)-X401
      B1=PDX2/PDX4
      B2=PDX5/PDX4
      C1=-X2(M+1)+1+A1*X1(1)+B1*X4(1)
      C2=-X5(M+1)+1+A2*X1(1)+B2*X4(1)
      X1(1)=(C1*B2-B1*C2)/(A1*B2-A2*B1)
      X4(1)=(A1*C2-A2*C1)/(A1*B2-A2*B1)
      L=0
      GO TO 90
  999 CONTINUE
      PRINT 124, X1(1),X4(1)
      NMAX=M+1
      DO 998 MP=1,NMAX
      ETA=(MP-1)*H
```

```
      SUBROUTINE FD(UT,DPR)
      DIMENSION A(500),B(500),C(500),D(500),E(500),F(500),UT(2,500)
      COMMON /MFD/ALPHA(500),BETA(500),RL(2,500),EPS(500),DPSI,S3DUM1,
     1S3DUM2
      COMMON /MIPFD/NMAX,NMP1
      COMMON /MFSIP/GAMMA
  636 FORMAT (E15.6)
  630 FORMAT (20H N GREATER THAN NMAX)
      S3DUM3=S3DUM2*DPR
      N=2
  637 A(N)=BETA(N)/S3DUM1+(RL(2,N+1)+RL(2,N))/S3DUM3
      B(N)=ALPHA(N)/DPSI+(RL(2,N+1)+2.*RL(2,N)+RL(2,N-1))/S3DUM3
      C(N)=-BETA(N)/S3DUM1+(RL(2,N)+RL(2,N-1))/S3DUM3
      D(N)=ALPHA(N)*UT(1,N)/DPSI+BETA(N)*(UT(1,N+1)-UT(1,N-1))/S3DUM1
     1+(RL(1,N+1)+RL(1,N))*(UT(1,N+1)-UT(1,N))/S3DUM3
      D(N)=D(N)-(RL(1,N)+RL(1,N-1))*(UT(1,N)-UT(1,N-1))/S3DUM3+EPS(N)
      IF (N.NE.2) GO TO 638
      E(2)=A(2)/B(2)
      F(2)=(C(2)*UT(2,1)+D(2))/B(2)
      GO TO 639
  638 E(N)=A(N)/(B(N)-C(N)*E(N-1))
      F(N)=(D(N)+C(N)*F(N-1))/(B(N)-C(N)*E(N-1))
      IF (ABS(1.0-E(N)-F(N)).LT.0.000005.AND.(ABS(UT(1,N)-1.0)+
     1ABS(UT(1,N+1)-1.0)).LT.0.001) GO TO 640
  639 N=N+1
      IF (N.LT.NMAX) GO TO 643
      PRINT 630
  643 CONTINUE
      GO TO 637
  640 CONTINUE
      NH=N
      NH1=NH+1
      UT(2,NH1)=1.
      DO 641 N=NH,2,-1
  641 UT(2,N)=E(N)*UT(2,N+1)+F(N)
      DO 642 N=NH,NMP1,1
  642 UT(2,N)=1.
      RETURN
```

```
      SUBROUTINE FRST(CMACH0,RLEN,EFF,S)
      DIMENSION TGK(1001)
      COMMON /FSM/JYEN(1001),SIGEN(1001),TEXN(1001),PN(1001),PO,
     1TO,UO,BW,MS,DX,JYE0,SIGE0,P(1001),TEX(1001),JYEX(1001),SIGEX(1001)
     2,TECFS(1001),TECNFS(1001),MACH(1001),XNEX(1001),HALLO,
     3HALEX(1001)
      COMMON /MFSH/HDUM1
      COMMON /FSMSIG/SIGMA,XNE,TE
      COMMON /MFSIP/GAMMA
      REAL JYEN,JYE,JYE0,JYEX,MACH
  651 FORMAT (5E15.6)
      PON=1/(GAMMA*CMACH0*CMACH0)
      FSDUM1=(GAMMA-1)*EFF/GAMMA
      FSDUM3=EFF-1
      FSDUM2=S*FSDUM3
      MACH(1)=CMACH0
      TGK(1)=1
      TEXN(1)=1.
      PN(1)=PON
      SIGEN(1)=1.
      SIGEX(1)=SIGE0
      JYEN(1)=1.
      HALEX(1)=HALLO
      P(1)=PO
      TEX(1)=TO
      JYE=JYE0
      JYEX(1)=JYE0
      DO 2 M=1,MS
      TGK(M+1)=FSDUM2*DX*SIGEN(M)+TGK(M)
      IF (TGK(M+1).LT.0.01) GO TO 2
      TEXN(M+1)=TGK(M+1)**FSDUM1
      PN(M+1)=TGK(M+1)*PON
      P(M+1)=PN(M+1)*PO*GAMMA*CMACH0*CMACH0
      TEX(M+1)=TEXN(M+1)*TO
      CALL SIGPTO(P(M+1),TEX(M+1),TE,JYE)
      JYEX(M+1)=JYE
      SIGEX(M+1)=SIGMA
      HALEX(M+1)=SIGMA*HDUM1/XNE
```

```
      XNEX(M+1)=XNE
      JYEN(M+1)=JYE/JYE0
      SIGEN(M+1)=SIGMA/SIGE0
      TECFS(M+1)=TE
      TECNFS(M+1)=TE/TEX(M+1)
      MACH(M+1)=CMACH0*SQRT(1./TEXN(M+1))
    2 CONTINUE
      RETURN
      END
```

```
      SUBROUTINE SIGPTH(P,T,JY,ATE,AJX,XNEFS)
      COMMON /SIGHM/CJX
      COMMON /MESH/HDUM1
      COMMON /FSMSIG/SIGMA,XNE,TE
      REAL JY
   10 FORMAT(9E13.5)
      KH=0
      TE=ATE
    1 TJ=JY*SQRT(1.+AJX*AJX)
      CALL SIGPTJ(P,T,TJ,TE)
      CJX=SIGMA*HDUM1*(1./XNE-1./XNEFS)
      ERJX=AJX-CJX
      IF (ABS(ERJX).LT.0.001) GO TO 19
      IF (KH.EQ.1) GO TO 18
      KH=1
      HJX=AJX
      HERJX=ERJX
      AJX=AJX+0.01
      GO TO 1
   18 DAJX=-ERJX*(AJX-HJX)/(ERJX-HERJX)
      HJX=AJX
      HERJX=ERJX
      AJX=AJX+DAJX
      GO TO 1
   19 CONTINUE
      RETURN
      END
```

```
-IT    FOR SIGPTO
       SUBROUTINE SIGPTO(S2P,S2T,S2TEAP,S2J)
       COMMON /MSIGO/S2DUM1
       COMMON /FSMSIG/SIGMA,XNE,TE
       TE=S2TEAP
  347  CALL SIGPTJ(S2P,S2T,S2J,TE)
       S2JH=S2J
       S2J=SIGMA*S2DUM1
       IF (ABS((S2J-S2JH)/S2J).GT.0.0001) GO TO 347
       CONTINUE
       RETURN
       END
```

```
      SUBROUTINE SIGPTJ(S1P,S1T,S1J,TEAP)
      COMMON /FSMSIG/SIGMA,XNE,TE
      COMMON /MSPTT/C4,C5K,C5A,C6,C1,C3,CK,AM,CF,QEA(86),QEK(86)
      COMMON /STJ/LST
      COMMON /WRI/K9
  500 FORMAT(5E15.6)
      LS1=0
      LST=0
      S1TE=TEAP
      IF (S1TE.LT.S1T) S1TE=S1T
      AS1J=ABS(S1J)
      S1DEL=AS1J*1.E-3
      IF (AS1J.LT.1.E-4) S1DEL=1.0E-5
  503 CALL SIGPTT(S1P,S1T,S1TE,S1JC,S1SIG,S1NE)
      S1ERJ=S1JC-AS1J
      IF (ABS(S1ERJ).LT.1.E-8) GO TO 599
      IF (ABS(S1TEH-S1TE).LT.0.5.AND.ABS(S1ERJ).LT.S1DEL) GO TO 599
      IF (LS1.EQ.1) GO TO 506
      LS1=1
      S1TEH=S1TE
      S1ERJH=S1ERJ
      S1TE=S1TE+2.0
      GO TO 503
  506 DS1TE=-S1ERJ*(S1TE-S1TEH)/(S1ERJ-S1ERJH)
      S1TEH=S1TE
      S1ERJH=S1ERJ
      S1TE=S1TE+DS1TE
      IF (S1TE.LT.S1T) S1TE=S1T
      GO TO 503
  599 CONTINUE
      LST=1
      CALL SIGPTT(S1P,S1T,S1TE,S1JC,S1SIG,S1NE)
      TE=S1TE
      SIGMA=S1SIG
      XNE=S1NE
      RETURN
      END
```

```
      SUBROUTINE SIGPTT(PO,TO,TE,XJ,SIGMA,XNE)
      DOUBLE PRECISION EXK,EXA,CC,AN,AK,AL,B,C,D,P,Q,DISCR,RAD,COSP,PHI
     1,TEST,COSN
      COMMON /MSPTT/C4,C5K,C5A,C6,C1,C3,CK,AM,CF,QEA(86),QEK(86)
      COMMON /STJ/LST
      IF (LST.EQ.1) GO TO 600
      TESQR=SQRT(TE)
      CC=(C4*TE)*SQRT(C4*TE)
      EXK=C5K/TE
      EXA=C5A/TE
      AK=CC*EXP(-EXK)
      AL=6*CC*EXP(-EXA)
      AN=PO/(CK*TO)
      B=(AK+AL)*1.E-12
      C=(AK*(AL-AN)+(AN/AM)*(AK-AL))*1.E-24
      D=(-AK*AN*AL)*1.E-36
      P=C-B**2/3
      Q=D-(B*C)/3+(2*B**3)/27
      DISCR=-4*P**3-27*Q**2
      DISCR=SQRT(DISCR)
      COSP=(-Q/2)/SQRT((-P**3)/27)
      TEST=DATAN(SQRT(1-COSP*COSP)/COSP)
      IF (COSP.LT.0) TEST=3.14159265358979323D+0+TEST
      IF (COSP.EQ.0) TEST=1.57079632679489661D+0
      PHI=TEST/3
      RAD=2*SQRT(-P/3)
      COSN=DCOS(PHI)
      XNE=(RAD*COSN-B/3)*1.E12
      XJ=8.1063E-20*XNE*XNE*1.0E-16
      XJ=SQRT(XJ*(TE-TO))
      IF (LST.EQ.0) GO TO 601
  600 I=(TE-1400.)/100.
      FTE=(TE-1400.-100.*I)/100.
      IF (I.GT.86) I=85
      IF (I.GT.86) FTE=1.0
      TQEA=QEA(I)+FTE*(QEA(I+1)-QEA(I))
      TQEK=QEK(I)+FTE*(QEK(I+1)-QEK(I))
      SEG3=TQEA+CF*TQEK
```

```
      SIGMA=(C1*TESQR*PO/(XNE*AM*TO))*SEG3+(65.3/(TE*TESQR))*
     1ALOG(C3*TE*TESQR/SQRT(XNE))
      SIGMA=1./SIGMA
  601 CONTINUE
      RETURN
      END
```

REFERENCES CITED*

1. Selected Papers on New Techniques for Energy Conversion, Dover Publications, Inc. Edited by S. N. Levine, 1966.

2. Reilly, J. P., "Turbulent Boundary Layers on the Insulator Wall of a Two Temperature MHD Channel, Ph.D. thesis, Massachusetts Institute of Technology, Cambridge, Mass., 1962.

3. Shair, F. H., "Theoretical Performance Comparison of Working Fluids in a Nonequilibrium MHD Generator," AIAA J., 2, 11, 1883 (1964).

4. Steg, L., and Sutton, G. W., "The Prospects of MHD Power Generation," Astronautics 5, Aug. 1960, 22.

5. Karlowitz, B., Halasz, D., U. S. Patent 2.210,918 (Aug. 13, 1940).

6. Kerrebrock, J. L., "Non-equilibrium Effects on Conductivity and Electrode Heat Transfer in Ionized Gases," AFOSR-165 TN 4, Daniel and Florence Guggenheim Jet Propulsion Center, Calif. Inst. of Technology (Nov. 1960).

7. Hurwitz, H., Jr., Sutton, G. W., and Tamor, S., "Electron Heating in Magnetohydrodynamic Power Generators," ARS J., Aug. 1962, 1237.

8. Kerrebrock, J. L., and Hoffman, M., "Nonequilibrium Ionization Due to Electron Heating: II Experiments, " AIAA J., 2, 6 (1964).

9. Goldstein, R., Redimond, J., and Oates, G. C., "Electrical Conductivity Measurements in a Faraday Accelerator," AIAA J., 4, 11 (1966).

10. McDaniel, E. W., Collision Phenomena in Ionized Gases, John Wiley and Sons, Inc., New York, 1964.

11. Harris, L. P., and Colime, J. D., "Significance of the Hall Effect for Three MHD Generator Configurations," Trans. of ASME (Journal of Engineering Power), Oct., 1961, 392.

12. Hartmann, J., "Hg-Dynamics I," Math. fys. Medd. 15 (1937).

---

*Abbreviations of journals used herein follows a form employed by the American Institute of Aeronautics and Astronautics Journal.

13. Hwang, C. L., and Fan, L. T., "Bibliography of Hydrodynamic Entrance Region Flow," Engineering Experiment Station, Kansas State Univ., Special Report 67 (1966).

14. Hale, F. J., and Kerrebrock, J. L., "Insulator Boundary Layers in Magnetohydrodynamic Channels," AIAA J. 2, 3, 461 (1961).

15. Dhanak, A. M., "Heat Transfer in Magnetohydrodynamic Flow in an Entrance Section," Trans. ASME Series C: J. Heat Transfer 87, 231 (1965).

16. Hwang, C. L. and Fan, L. T., "Finite Difference Analysis of Forced Convective Heat Transfer in the Entrance Region of a Flat Rectangular Duct," Appl. Sci. Res., Sec. A 13, 401-422 (1964).

17. Hwang, U. P., Fan, L. T., and Hwang, C. L., "Compressible Laminar MHD Flow Inside a Flat Duct with Heat Transfer," AIAA J. 5, 12, 2113-2121 (Dec. 1967).

18. Bush, W. B., "Compressible Flat Plate Boundary Layer Flow with an Applied Magnetic Field," J. Aerospace Sci., 27, 49 (1960).

19. Schlichting, H., Boundary Layer Theory, McGraw-Hill Book Company, Inc., New York, 1960, 4th ed.

20. Hale, F. J., and Kerrebrock, J. L., "Insulator Boundary Layers in Magnetohydrodynamic Channels," AIAA J., 2, 3, 461 (1961).

21. Hale, F. J., "Insulator Boundary Layers in Magnetohydrodynamic Channels," Ph.D. Thesis, Massachusetts Institute of Technology, Cambridge, Mass., 1962.

22. Heywood, J. B., and Moffatt, W. C., "Validity of Integral Methods in MHD Boundary Layer Analysis," AIAA J. 3, 8, 1565 (1965).

23. Kerrebrock, J. L., "Electrode Boundary Layers in Direct Current Plasma Accelerators," J. Aerospace Sci. 28, 8, 631 (1961).

24. Culick, F. E. C., "A Boundary-Layer Problem Associated with Magnetogasdynamic Channel Flow," AIAA J., 1, 11, 2666 (1963).

25. Kerrebrock, J. L., "Segmented Electrode Losses in MHD Generators with Nonequilibrium Ionization--II," Avco-Everett Res. Lab., RR 201.

26. Kruger, C. H. and Viegas, J. R., "Influence of the Ramsauer Effect on Nonequilibrium Electron Temperature," Phys. Fluids 7, 1879-1881 (1964).

27. Kerrebrock, J. L., "Nonequilibrium Ionization Due to Electron Heating: I. Theory," AIAA J. 2, 1072-1080 (1964).

28. Shelton, S. V. and Carlson, W. O. "Variable Collision Cross Section Effects on Electrical Conductivity," AIAA J. 4, 9, p. 1776 (Sept. 1966).

29. Dowdy, M. W., "Electrical Conductivity of Seeded Gases at Moderate Temperatures," Ph.D. Thesis, School of Mechanical Engineering, Georgia Institute of Technology, Dec. 1968.

30. Broadbent, E. G., "A Review of Fluid Mechanical and Related Problems in MHD Generators," Progress in Aeronautical Sciences, Volume 9, Pergamon Press, Oxford, 1968.

31. Brocher, E. F., "The Constant Velocity MHD Generator with Variable Electrical Conductivity," J. Aerospace Science, 29, (1962) p. 626.

32. Campbell, Plasma Physics and Magnetofluid Mechanics, McGraw-Hill Book Company, Inc., N. Y., 1963.

33. Wu, J. C., "On the Finite Difference Solution of Laminar Boundary Layer Problems," Proc. of the Heat Transfer and Fluid Mechanics Institute, 1961, Stanford Press.

34. Tribus, M. Thermostatics and Thermodynamics, D. Van Nostrand Company, Inc., N. Y., 1961, p. 213.

35. Bird, R. B., Stewart, W. E., and Lightfoot, E. N., Transport Phenomena, John Wiley and Sons, Inc., New York, Chapter I.

36. Chapman, S. and Cowling, T. G. The Mathematical Theory of Non-Uniform Gases, Cambridge Univ. Press, London, 1964, p. 322.

37. Kerrebrock, J. L., "Nonequilibrium Ionization Due to Electron Heating: I. Theory," AIAA J., 2, 9, 1072-1080 (1962).

38. Massey, H. S. W., and Burhop, E. H. S. Electronic and Ionic Impact Phenomena, Oxford University Press, London, 1956, p. 12.

39. Kerrebrock, J. L., "Conduction in Gases with Elevated Electron Temperatures," Engineering Aspects of Magnetohydrodynamics, Columbia University Press, New York, 1952, p. 327-346.

40. Ben Daniel, D. J., and Tamor, S., "Nonequilibrium Ionization in Magnetohydrodynamic Generators," G. E. Report No. 62-RL-(2922E), Schenectady, New York, 1962.

41. Shaw, J. K., Kruger, C. H., Mitchner, M., and Viegas, J. R. "Examination of the Validity of the Saha Equation in a Gas Discharge," Electricity from MHD, Proceedings of Symposium on MHD Electrical Power Generation, Salzburg, Austria, July 4-8, 1966, 1, p. 77.

42. Morse, T. F., "Energy and Momentum Exchange Between Non-Equipartition Gases," Physics of Fluids, 6, p. 1420 (1963).

43. Massey, H. S. W. and Burhop, E. H. S., Electronic and Ionic Impact Phenomena, Clarendon Press, Oxford, England, 1952.

44. Kruger, C. H. and Viegas, J. R., Private Communication, Department of Mechanical Engineering, Stanford University, Palo Alto, California.

45. Spitzer, L. and Härm, Physic Review, 89, 977 (1953).

46. Zukoski, E. E., Cool, T. A., and Gibson, E. G., "Experiments Concerning Nonequilibrium Conductivity in a Seeded Plasma," AIAA J., 2, 8, 1410 (August, 1964).

47. Lin, S. C., Resler, E. L., and Kautrowitz, A., "Electrical Conductivity of Highly Ionized Argon Produced by Shock Waves," Journal of Applied Physics, 26, 94 (1955).

48. Sutton, G. W. and Sherman, A., Engineering Magnetohydrodynamics, McGraw-Hill, Inc., New York, 1965, p. 229.

49. Kunz, K. S., Numerical Analysis, McGraw-Hill Book Company, Inc., New York, 1957, p. 188.

50. Richtmyer, R. D., Difference Methods for Initial-Value Problems, Interscience Publishers, Inc., New York, 1964, p. 101.

51. Brailouskaya, I. Yu. and Chudov, L. A. "A Solution of Boundary Layer Equations by the Difference Method," Translation by Foreign Technology Division, WP-AFB, Ohio from Vychislitel'nyye Method i Programmirovaniye; Izdatel' stvo Moskovskogo Universiteta, I, 1962, p. 167-182.

52. Blottner, F. G., "Nonequilibrium Laminar Boundary-Layer Flow of Ionized Air," AIAA J., 2, 11, p. 1921 (November, 1964).

VITA

Samuel Viron Shelton was born in Boynton Beach, Florida on January 26, 1939. He is the younger of two children of the late Homer and Edna Shelton. In December of 1962 he was married to Sharon Hudson of Spartanburg, South Carolina. They now have two girls: Suzanne Hope, born March 12, 1964 and Stacy Marie, born May 15, 1966.

Mr. Shelton attended public school in Palm Beach County, Florida and graduated from Seacrest High School in 1957. That year he entered Georgia Institute of Technology and in 1961 received his Bachelor of Mechanical Engineering, with honor. He immediately entered graduate school with a three-year National Defense Education Act Fellowship to work toward the Ph.D. in Mechanical Engineering.

His thesis work was interrupted in June of 1966 to fulfill his two-year ROTC active duty obligation in the U. S. Army Ordinance Corps. Mr. Shelton was assigned to Jet Propulsion Laboratory in Pasadena, California where he served two years as a research engineer. During this time he worked primarily in the fields of experimental and theoretical gas dynamics and experimental solid propellant combustion research. In June of 1968 he returned to the Georgia Institute of Technology to complete his graduate work.

Mr. Shelton has published several papers in the fields of plasma electrical conductivity, two-dimensional nozzle gas dynamics, solid propellant combustion instability, and wood preservation.

He is a member of Phi Kappa Phi, Pi Tau Sigma, Sigma Xi, and the American Institute of Aeronautics and Astronautics.